FAA-78-15.I

REPORT NO. FAA-RD-78-68,I

VORTEX ADVISORY SYSTEM SAFETY ANALYSIS

Volume I: Analytical Model

J.N. Hallock

U.S. DEPARTMENT OF TRANSPORTATION
RESEARCH AND SPECIAL PROGRAMS ADMINISTRATION
Transportation Systems Center
Cambridge MA 02142

SEPTEMBER 1978

FINAL REPORT

Prepared for

U.S. DEPARTMENT OF TRANSPORTATION
FEDERAL AVIATION ADMINISTRATION
Systems Research and Development Service
Washington DC 20591

Technical Report Documentation Page

1. Report No.	2. Government Accession No.	3. Recipient's Catalog No.
FAA-RD-78-68,I		

4. Title and Subtitle	5. Report Date
VORTEX ADVISORY SYSTEM SAFETY ANALYSIS Volume I: Analytical Model	September 1978
	6. Performing Organization Code
7. Author(s)	8. Performing Organization Report No.
J. N. Hallock	DOT-TSC-FAA-78-15,I
9. Performing Organization Name and Address	10. Work Unit No. (TRAIS)
U.S. Department of Transportation Research and Special Programs Administration Transportation Systems Center Cambridge MA 02142	FA-905/R9111
	11. Contract or Grant No.
12. Sponsoring Agency Name and Address	13. Type of Report and Period Covered
U.S. Department of Transportation Federal Aviation Administration Systems Research and Development Service Washington DC 20591	Final Report Oct. 1977 - Aug. 1978
	14. Sponsoring Agency Code

15. Supplementary Notes

16. Abstract

An analysis was conducted to examine the safety of decreasing landing aircraft separations to three nautical miles between the outer marker and the runway threshold. Such reduced separations would only be used when the Vortex Advisory System indicated that wake vortices would not pose a threat to a following aircraft. Based on state-of-the-art models of vortex and aircraft behavior, the analysis indicates that such reduced interarrival separations may be used safely by Large and Heavy aircraft following Heavies. When the analysis is expanded to include an as-yet unproven cross-winds aloft model, the results indicate that reduced separations may be used by all aircraft regardless of leader/follower aircraft type. Volume I addresses the safety problem from an analytic point of view; Volume II (to be published at a later date) will examine the problem using data collected specifically to verify the analytical model; and Volume III (to be published at a later date) will contain a detailed sensitivity analysis of the model predictions and a critique of the assumptions.

17. Key Words	18. Distribution Statement
Aircraft Wake Vortices Vortices Vortex Advisory System Vortex Transport and Decay	DOCUMENT IS AVAILABLE TO THE U.S. PUBLIC THROUGH THE NATIONAL TECHNICAL INFORMATION SERVICE, SPRINGFIELD, VIRGINIA 22161

19. Security Classif. (of this report)	20. Security Classif. (of this page)	21. No. of Pages	22. Price
Unclassified	Unclassified	160	

Form DOT F 1700.7 (8-72) Reproduction of completed page authorized

EXECUTIVE SUMMARY

The Vortex Advisory System (VAS) was developed as a means for decreasing costly congestion delays in aircraft approach queues at the major airports. The system evolved from the analysis of the behavior of the wake vortices from over 50,000 landing aircraft. It was determined that vortices might present a threat to a following aircraft only during specific wind conditions. Most of the time, however, vortices do not pose a safety problem. The VAS indicates to the controllers when vortices are not a problem; during these times, the interarrival separation standards could be reduced to 3 nautical miles for all aircraft regardless of leader or follower aircraft type.

The vortex behavior data, however, were collected in the region between the middle marker and the runway threshold. Over 82 percent of the landing accidents attributed to wake vortices occurred within this region. The VAS advises when this region is clear of vortices. Although some capacity gains might be realized if the reduced separation standards were used only in this region, the utility of the VAS would increase if the protected region were extended to the outer marker.

Applicable vortex behavior data did not exist; therefore, two programs were undertaken. First, the subject of this volume of the report, an analysis was done to calculate the relative safety of using reduced separations from the outer to middle markers when the VAS indicated that such reduced separations might be used near the runway. Second, the subject of the second volume of the report, data were collected between the outer and middle markers to verify the adequacy of the safety analysis. If data collection alone were to be used to establish safety, many years (and many data-collection sites) would be required to collect sufficient data to verify the safety of the VAS. However, if the data confirmed the analytical predictions of vortex behavior, the analysis herein would demonstrate the safety of using reduced interarrival spacings whenever the VAS indicated such spacings were permitted. Conversely,

if the data did not verify the analysis, the VAS should not be used to reduce spacings between the outer and middle markers.

After reviewing vortex-related accidents and the development and implementation of the VAS, the analytical model of vortex behavior was described. State-of-the-art knowledge of the behavior of vortices, aircraft, and winds aloft was used to formulate the model. At all times, the model was intentionally caused to err on the conservative side. Thus, the risks calculated using this model were proxy estimates of the real stiuation

The risks accepted in the present system using the 3-, 4-, and 5-nautical-mile spacings in effect near the outer marker were calculated. Twelve aircraft were considered as vortex-generating or leading aircraft, and the same 12 were considered as the vortex-encountering or following aircraft: B-747, L-1011, DC-10, B-707H, DC-8H, B-707, DC-8, B-727, DC-9, B-737, Learjet, and PA-28. According to the model, at the current separations, the risk of a hazardous-vortex encounter is zero for Large and Heavy aircraft following other Large and Heavy aircraft and nonzero only for some Small-category aircraft following certain Large and Heavy aircraft. The situations represented by the nonzero risks occur frequently in the current system in the vicinity of the outer marker. Since these situations occur frequently (particularly in VFR conditions) and with nonzero risk of a vortex hazard, these risks were considered to be acceptable--no hazardous-vortex encounters or accidents were known to occur for these situations.

The largest of the nonzero risks was defined as a baseline value. If the chance of a hazardous-vortex encounter for any leader/follower pair were found to be less than, or equal to, the baseline value, the situation would be considered safe.

Risks to be expected when 3-nautical-mile spacings would be permitted were calculated. Operational guidelines were then formulated to maintain risks with VAS-reduced spacings at, or below, the baseline value. These guidelines are: (1) reduced separations to be used only when the VAS indicated that conditions permitted such separations, and (2) precision approaches are required (i.e., no short finals or VOR/localizer approaches). With these guide-

lines, and the verification of the model (Volume II) the risks with VAS-reduced spacings would be no larger than in the current system with the present separation standards.

A brief sensitivity analysis was done to determine if the conclusions of the safety analysis were adversely affected by possible errors in the models and/or parameters. Although the details were altered, the conclusions concerning the safety of VAS-reduced spacings were not changed.

Other evidence was investigated to look for support, or contradiction, of the analytic results. Wake vortex incident reports analyzed by the British Civil Aviation Authority, analysis of vortex-caused accidents, and the current spacings actually flown safely in VFR all lent credence to the results of the calculations: VAS-reduced spacings should be safe.

There were two unresolved issues in the analysis--the model describing cross winds aloft is unproven and its derivation required somewhat inconsistent assumptions, and a possible problem might have been introduced by comparing two conservative estimates of the probability of a hazardous-vortex encounter. Resolution of the former issue will be addressed in Volume II and the consequences (if any) of the latter issue in Volume III. Assuming favorable resolution of these two issues, the analysis indicates the safety of VAS-reduced spacings between the outer and middle markers for all aircraft. The safety of VAS-reduced spacings between the middle marker and touchdown was established by the study of the vortices from over 50,000 landing aircraft.

An alternative analysis was done without recourse to either of the two unresolved issues. Assuming that 50 percent of available roll-control authority was acceptable for countering the rolling motion imposed by a vortex (higher percentages are accepted, or appear to be, with today's separation standards), vortex decay would be the primary mechanism precluding hazardous-vortex encounters between the outer and middle markers. Vortex decay alone, however, does not permit VAS-reduced spacings for following Small aircraft. Vortex decay alone was shown to permit VAS-reduced spacings for Heavy and Large aircraft following Heavies.

PREFACE

The concept of a Vortex Advisory System (VAS) evolved from the analysis of an accumulating wealth of vortex-tracking data. Tens of thousands of tracks demonstrated that the concept was viable; however, all the data were collected between the middle marker and the runway threshold. Before certifying the VAS for an operational test, the Flight Standards Service of the Federal Aviation Administration (FAA) requested that the region between the middle and outer marker be examined to determine its relative safety vortexwise for the use of decreased separations.

Many people contributed to this report. The mathematical model was developed from an unpublished working paper by Alan Bilanin and Coleman Donaldson of Aeronautical Research Associates of Princeton. It is a pleasure to acknowledge their work as well as the able assistance of Berl Winston of the Transportation Systems Center (TSC) who programmed the model and helped to run the numerous cases. I wish especially to thank R. M. Harris of Mitre Corporation; his critical reading of an early draft of this report prompted a complete revision of the document. He derived the cross-wind probability density model presented in Appendix C and made many detailed suggestions for clarifying the model. Agam Sinha of Mitre Corporation pointed out the possible problem of comparing two conservative estimates (Section 5.2), and I wish to thank him for his detailed comments which are reflected in Sections 5.2 and 6.1. I thank R. Craig Goff for supplying the AIDS data which are discussed in Section C.4. Finally, I would like to thank Myron Clark, Joe Tymczyszyn, Jr., Andrew Haines, and Dave Burnham for their suggestions and comments on the final draft of the report.

METRIC CONVERSION FACTORS

Approximate Conversions to Metric Measures

Symbol	When You Know	Multiply by	To Find	Symbol
		LENGTH		
in	inches	2.5	centimeters	cm
ft	feet	30	centimeters	cm
yd	yards	0.9	meters	m
mi	miles	1.6	kilometers	km
		AREA		
in^2	square inches	6.5	square centimeters	cm^2
ft^2	square feet	0.09	square meters	m^2
yd^2	square yards	0.8	square meters	m^2
mi^2	square miles	2.6	square kilometers	km^2
	acres	0.4	hectares	ha
		MASS (weight)		
oz	ounces	28	grams	g
lb	pounds	0.45	kilograms	kg
	short tons (2000 lb)	0.9	tonnes	t
		VOLUME		
tsp	teaspoons	5	milliliters	ml
Tbsp	tablespoons	15	milliliters	ml
fl oz	fluid ounces	30	milliliters	ml
c	cups	0.24	liters	l
pt	pints	0.47	liters	l
qt	quarts	0.95	liters	l
gal	gallons	3.8	liters	l
ft^3	cubic feet	0.03	cubic meters	m^3
yd^3	cubic yards	0.76	cubic meters	m^3
		TEMPERATURE (exact)		
°F	Fahrenheit temperature	5/9 (after subtracting 32)	Celsius temperature	°C

Approximate Conversions from Metric Measures

Symbol	When You Know	Multiply by	To Find	Symbol
		LENGTH		
mm	millimeters	0.04	inches	in
cm	centimeters	0.4	inches	in
m	meters	3.3	feet	ft
m	meters	1.1	yards	yd
km	kilometers	0.6	miles	mi
		AREA		
cm^2	square centimeters	0.16	square inches	in^2
m^2	square meters	1.2	square yards	yd^2
km^2	square kilometers	0.4	square miles	mi^2
ha	hectares (10,000 m^2)	2.5	acres	
		MASS (weight)		
g	grams	0.035	ounces	oz
kg	kilograms	2.2	pounds	lb
t	tonnes (1000 kg)	1.1	short tons	
		VOLUME		
ml	milliliters	0.03	fluid ounces	fl oz
l	liters	2.1	pints	pt
l	liters	1.06	quarts	qt
l	liters	0.26	gallons	gal
m^3	cubic meters	35	cubic feet	ft^3
m^3	cubic meters	1.3	cubic yards	yd^3
		TEMPERATURE (exact)		
C	Celsius temperature	9/5 (then add 32)	Fahrenheit temperature	°F

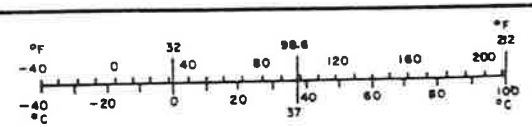

ABBREVIATIONS

p.d.f.	probability density function
A	Airbus
AIDS	Aircraft Integrated Data System
B	Boeing
DC	Douglas Corporation
DEC	Digital Equipment Corporation
DHC	De Havilland (Canada)
FAA	Federal Aviation Administration
GWVSS	Ground Wind Vortex-Sensing System
IFR	Instrument Flight Rules
ILS	Instrument Landing System
KLM	Koninklijke Luchtvaart Maatschappij (Royal Dutch Airline)
L	Lockheed
LDV	Laser-Doppler Velocimeter
MAVSS	Monostatic Acoustic Vortex-Sensing System
MM	Middle Marker
NASA	National Aeronautics and Space Administration
NTSB	National Transportation Safety Board
OM	Outer Marker
PA	Piper Aircraft
PAVSS	Pulsed Acoustic Vortex-Sensing System
TSC	Transportation Systems Center
VAS	Vortex Advisory System
VFR	Visual Flight Rules
VOR	Very-High-Frequency Omnidirectional Range
WVAS	Wake Vortex Avoidance System.

$\bar{R}$	one-minute running average of the wind magnitude (knots)
T	temperature of air in the core of a vortex (^{o}F)
T_{∞}	ambient air temperature (^{o}F)
U	speed of vortex-encountering aircraft (feet/sec)
U_i	East/West component of wind, $R_i \sin\theta_i$ (knots)
$\bar{U}$	one-minute average of East/West component of wind (knots)
v	swirling velocity of vortex, $\Gamma/2\pi R$ (feet/sec)
$v(r)$	velocity field of a vortex (feet/sec)
v_D	initial descent speed of vortices (feet/sec)
v_T	maximum aileron-induced wingtip velocity (feet/sec)
V	speed of vortex-generating aircraft (feet/sec)
V_i	North/South component of wind, $R_i \cos\Theta_i$ (knots)
$\bar{V}$	one-minute average of North/South component of wind (knots)
$V_{\text{line vortex}}$	swirl velocity of a line vortex (feet/sec)
V_{Doppler}	measured Doppler vertical velocities (feet/sec)
$\bar{w}$	wind vector (knots, degrees clockwise from North)
w_c	magnitude of the aloft cross wind, $\lvert w_y \rvert$ (knots)
w_x	x-component of wind aloft, head wind (knots)
w_y	y-component of wind aloft, cross wind (knots)
W	wind run, distance vortices translate due to cross wind (feet)
W_t	gross weight of aircraft (pounds)
x	head-wind axis, $\alpha+180^{o}$
y	cross-wind axis, $\alpha+90^{o}$; lateral displacement of aircraft about ILS localizer beam (feet)
y_o	lateral position of center of hazardous-encounter cross section (feet)
$\bar{y}$	mean lateral position of aircraft about ILS localizer beam (feet)
z	vertical displacement of aircraft about ILS glide-slope beam (feet)

z_o	vertical position of center of hazardous-encounter cross section (feet)
$\overline{z}$	mean vertical position of aircraft about ILS glide-slope beam (feet)
α	runway heading (degrees clockwise from North)
Γ	circulation or strength of a vortex (ft^2/sec)
Γ_{int}	intercept of Γ_o line with Γ' axis (ft^2/sec)
Γ_o	initial circulation of a vortex (ft^2/sec)
Γ_∞	total circulation about a vortex (ft^2/sec)
Γ'	effective strength or circulation of a vortex (ft^2/sec)
$\dot{\Gamma}$	time rate of change of the circulation (ft^2/sec^2)
ϵ	x-projection of ellipse E given cross wind, w_c
θ	"from" wind direction (degrees clockwise from North)
θ_i	wind direction sampled two times per second (degrees clockwise from North)
$\overline{\theta}$	one-minute running average of the wind direction (degrees clockwise from North)
μ	mean wind speed aloft (knots)
π	3.14159265...
ρ	air density in the core of a vortex ($slugs/ft^3$)
$\rho(r)$	density field of a vortex ($slugs/ft^3$)
ρ_∞	ambient air density ($slugs/ft^3$)
σ	standard deviation of the aloft cross wind (knots)
σ_y	standard deviation of lateral displacement of aircraft about the mean location (feet)
σ_{ye}	lateral deviation of the vortex-encountering aircraft (feet)
σ_{yg}	lateral deviation of the vortex-generating aircraft (feet)
σ_z	standard deviation of vertical displacement of aircraft about the mean location (feet)
σ_{ze}	vertical deviation of the vortex-encountering aircraft (feet)
σ_{zg}	vertical deviation of the vortex-generating aircraft (feet)

σ_D	standard deviation in the descent distance of vortices (feet)
σ_H	Pythagorean sum of the horizontal deviations (feet)
σ_V	Pythagorean sum of the vertical deviations (feet)
σ_W	standard deviation in the wind run (feet).

1. INTRODUCTION

All aircraft generate trailing wake vortices as a consequence of generating lift; however, the potential danger of encountering these wake vortices has only recently become apparent. Aircraft wake vortices now constitute one of the major problems confronting the air traffic control system.

Before 1970, landing aircraft were required to maintain at least 3-nautical-mile separations under Instrument Flight Rule (IFR) conditions. The separation standard was based primarily on radar-operating limits, and to a lesser extent, on runway-occupancy limitations. There were no separation standards imposed because of vortex considerations.

With the introduction of the wide-body jets and the increasing number of aircraft operations at the major airports, the wake vortex problem has taken on increasing importance. The vortices from large aircraft can present a hazard to smaller aircraft which inadvertently encounter the vortices; the following aircraft can be subjected to rolling moments which exceed the roll control authority of the aircraft, to a dangerous loss of altitude, and to possible structural failure. The probability of a vortex encounter is greatest in the terminal area where Small, Large, and Heavy aircraft operate on the same flight paths in close proximity, and where recovery from an upset may not be possible because of the low aircraft altitude.

Accordingly, the solution implemented by the Federal Aviation Administration (FAA) in March 1970 was to increase the separation standards behind the Heavy jets (a Heavy jet has a maximum certificated takeoff weight of 300,000 pounds or more) evolving by 1973 to 4 nautical miles for a following Heavy aircraft, and to 5 nautical miles for a following non-Heavy aircraft. The standards were revised in November 1975 by requiring the addition of an extra nautical-mile separation at threshold for following aircraft with a maximum certificated takeoff weight of less than 12,500 pounds

behind a Large or Heavy aircraft. These increased separations led to additional delays, and decreased the capacity and efficiency of the airport system.

One technique that has been developed to regain some of the lost capacity is the use of a Vortex Advisory System (VAS). The system indicates to controllers when the separation standards can be reduced to 3 nautical miles regardless of the leader or follower aircraft type. The VAS has evolved from the examination of tens of thousands of vortex tracks and the correlation of vortex behavior with the ambient winds.

All the vortex-tracking data have been recorded in the middle marker to runway threshold region. Over 82 percnet of the landing accidents attributed to wake vortices have occurred within this region (Ref. 1). The use of the VAS advises when this region is clear of vortices. Although some capacity gains may be realized if only this region is permitted to use the reduced separation standards, the utility of the VAS increases if the protected region can be extended to the outer marker.

Since applicable data did not exist, two approaches were undertaken. First, the subject of this volume of the report, a probability analysis was done to calculate the relative safety of reduced separations out to the outer market when the VAS indicated that reduced separation would be permitted near the runway. Such an analysis was undertaken as it was expected that the conditions that permitted reduced separations inside the middle marker would also permit reduced separations to be used inside the outer marker. The second approach, the subject of the second volume of this report, concerns the gathering of appropriate data to verify the claims of the probability analysis.

The method employed in the probability analysis is to use the best data available which describe vortex and aircraft behavior in the approach region to calculate the chance of a vortex encounter. At all times, the model is deliberately caused to err on the conservative side. To give meaning to small probability values, the numbers are interpreted by comparing with a known safe situation.

In general, the probabilities calculated in this report have been overestimated in absolute terms, but the relative values of the calculated probabilities should not be affected.

Section 2 reviews the history of vortex-related accidents to put the FAA wake vortex program into proper perspective. The most frequent type of vortex-related accident involves one aircraft on approach following another aircraft landing on the same runway. Most of these accidents have occurred within the middle marker and with interarrival separations less than 3 nautical miles.

Section 3 describes the development and embodiment of the VAS with particular reference to the Chicago O'Hare system. The key to the VAS is a wind criterion which has evolved from the analysis of over 50,000 aircraft landings. Whenever the surface wind exceeds a defined wind criterion, IFR interarrival spacings may be safely reduced to a uniform 3 nautical miles; whenever the surface wind does not exceed the wind criterion, the separations remain unchanged at the vortex-based 3, 4, 5, or 6 nautical miles. The analysis of the over 50,000 vortex tracks is the foundation for the safety of the VAS in the runway threshold to middle-marker region.

The vortex encounter model is derived in Section 4. State-of-the-art knowledge of the behavior of vortices, aircraft, and winds is used to construct an analytical model for calculating the probability of a hazardous-vortex encounter between the outer and middle markers. By intent, the model is both as general as possible and conservative. The development of the model mixes rigorous mathematics with many engineering approximations. Sufficient data exist to permit constructing defensible descriptions of vortex and aircraft behavior. Imperfect knowledge of the correlation between cross winds aloft and VAS-measured winds has led to a very mathematical, and sometimes inconsistent, description of the winds; limited data and observations seem to support the description, but the measurements to be discussed in Volume II are required for verification.

Section 5 contains the safety analysis for the outer to middle marker region, both the logic and the results, encompassing all

aircraft categories (Heavy, Large, and Small). It is shown that interarrival separations may be set at a uniform 3 nautical miles in IFR whenever the VAS indicates that reduced separations may be employed. Aircraft, however, must be restricted to precision straight-in approaches from the outer marker. A possible problem is indicated concerning the comparison of conservative estimates; the analysis of this problem is extensive and is deferred to Volume III along with a more detailed sensitivity analysis. Assuming successful resolution of the problem and validation of the wind model, the analysis in Section 5 shows why 3-nautical-mile separations can be safe vortexwise regardless of the category of the leader and follower aircraft.

There are 2 main unresolved issues--the cross-wind aloft model and the possible problem related to the comparison of conservative estimates. In Section 6, the scope of the VAS is reduced to apply only to Large and Heavy aircraft landing behind Heavy aircraft. Here, the safety of 3-nautical-mile separations is discussed without using either of the 2 unresolved issues.

Sections 2, 3, and 4 are not dependent on material in other sections. Sections 5 and 6 refer often to Section 4. Depending on the interest of the reader, Sections 2 and 3 may be skipped. If the details of the vortex encounter model are accepted; Sections 4.1.1, 4.1.2, and all of 5 and 6 contain the material necessary for understanding why it is claimed that the VAS will permit safe 3-nautical-mile separations between the outer and middle markers.

Section 7 summarizes briefly the alternative safety analyses discussed in Sections 5 and 6. Both analyses use the same model for a vortex hazard. If a maximum roll-control input of 50 percent of the full roll-control authority of an aircraft to counter a vortex swirling flow is acceptable (assuming the worst case of an axial vortex encounter with a very slowly decaying vortex), then 3-nautical-mile separations between outer and middle markers may be used for Large and Heavy aircraft following Heavies. To extend the VAS to include Small aircraft, two unresolved

issues have been introduced into the analysis (wind model and possible problem of comparing conservative probability estimates). If favorably resolved (Volume II and III), then the VAS can be used for all aircraft as is shown in Section 5.

2. WAKE VORTEX ACCIDENTS

Of the approximately 45,000 aviation accidents that occurred during the 10-year period of 1964-1973 in the conterminous United States, wake vortices were cited by the National Transportation Safety Board (NTSB) as a cause or factor in 147 accidents. Some of the 147 accidents may not be genuinely vortex-related; analyses subsequent to the issuance of the NTSB reports question the role of vortices in at least 63 of these accidents. Of the remaining 84 probable vortex-related accidents, 27 resulted in fatalities. Reference 1 describes a study of the vortex-related accidents, and categorizes these accidents by the flight phases of the vortex-generating aircraft and the accident aircraft, their relative runways of operation, and other pertinent factors.

Examination of the vortex-related accidents provides historical perspective to the wake vortex program. The discussion below follows closely the summary of Ref. 1 published in Ref. 2. The statistics herein update Refs. 1 and 2 to reflect recent findings concerning two of the accidents.

2.1 OVERALL STATISTICS

During the period of 1964-1973, the NTSB classified an average of 15 accidents per year as being vortex-related; 3 accidents per year resulted in fatalities (Ref. 1). Single-aircraft accidents, by comparison, occurred at an annual rate of 4510 with 540 fatal. Vortex-related accidents constituted only 0.33 percent of all single-aircraft accidents. Twenty-seven of the 147 accidents were fatal and resulted in 55 fatalities (Fig. 1). There were 88 landing accidents (21 fatal and 43 fatalities), 28 takeoff accidents (4 fatal and 9 fatalities), and 31 in-flight accidents (2 fatal and 3 fatalities). Twenty-six of the 31 in-flight accidents were crop dusters (1 fatal and 1 fatality) involved in agricultural activities in close proximity to the ground.

Eliminating the apparently vortex-unrelated accidents and the in-flight crop-duster accidents leaves 64 landing accidents

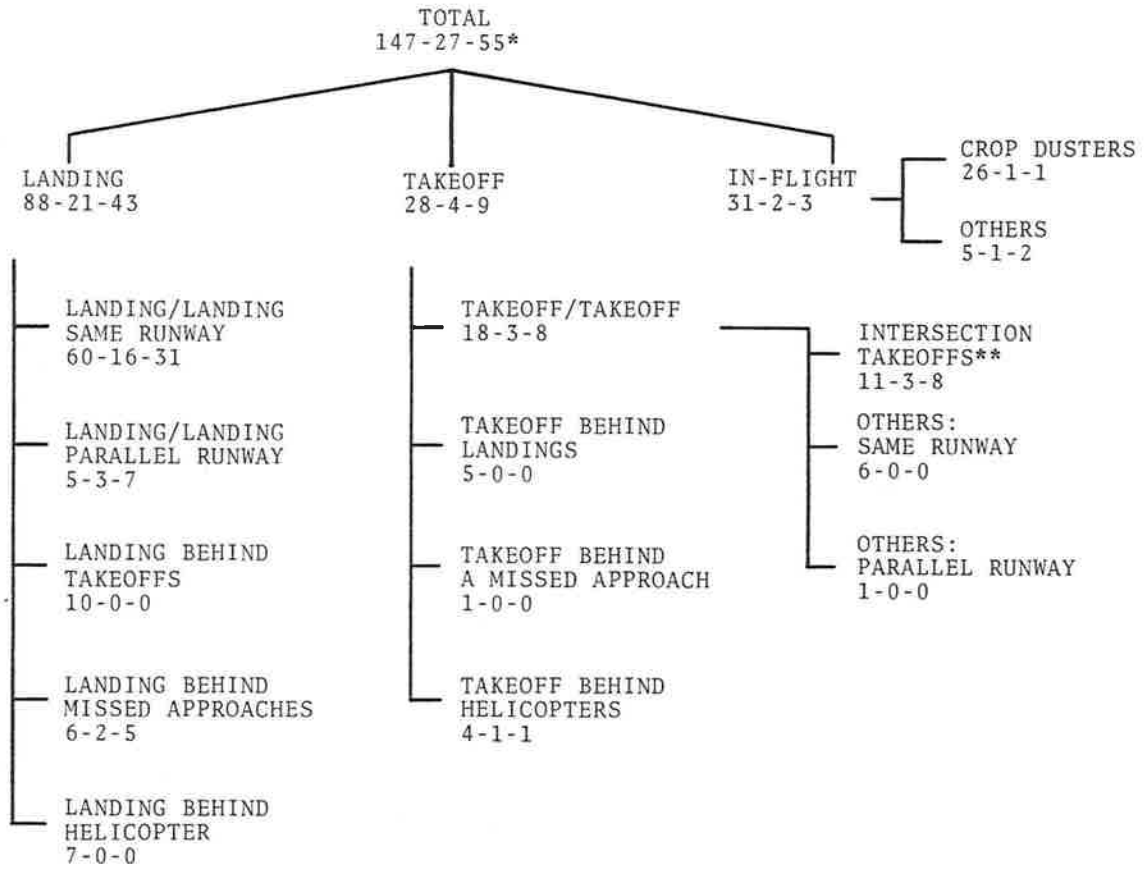

* ACCIDENTS - FATAL ACCIDENTS - FATALITIES, RESPECTIVELY

** NO ACCIDENTS OR FATALITIES IN THIS CATEGORY AFTER THE ESTABLISHMENT OF THE 3-MINUTE SEPARATION RULE IN 1969

FIGURE 1. BREAKDOWN OF NTSB'S VORTEX-RELATED ACCIDENTS FOR THE TEN-YEAR PERIOD 1964-1973

(16 fatal and 33 fatalities), 18 takeoff accidents (3 fatal and 8 fatalities), and 2 in-flight accidents (1 fatal and 2 fatalities). The probable vortex-related accidents are 84, 20 fatal with 43 fatalities (Fig. 2).

Approximately five-sixths of the landing accidents and three-quarters of the takeoff accidents occurred at controlled airports. For the ten-year period of 1964-1973, the vortex-related accident rate at towered airports was less than 1 per 3-million landings and less than 1 per 10-million takeoffs. The air carrier rate was less than 1 per 40-million operations for both landings and takeoffs.

General aviation aircraft weighing less than 12,500 pounds have been the primary victims of the vortex problem. The general aviation aircraft seems to be almost as vulnerable to the vortices of aircraft weighing more than 100,000 pounds as to the vortices of aircraft weighing more than 300,000 pounds (Ref. 1).

There have been only two-probable vortex-related air-carrier accidents: a DC-9 landing accident (a training flight behind a DC-10) at Fort Worth, Texas; and a DHC-6 (Twin Otter) takeoff accident at Kennedy International Airport, Jamaica, New York. The latter, however, was an intersection-takeoff accident involving an aircraft weighing less than 12,500 pounds.

The study of the NTSB data base indicated that all the probable vortex-related landing accidents occurred when the aircraft separations were less than the separation standards (Ref. 1). The only probable vortex-related landing accident that occurred under Instrument Flight Rules (IFR) was an in-flight vortex encounter where both aircraft were conducting missed approaches.

2.2 LANDING/LANDING: SAME RUNWAY ACCIDENTS

The most frequent type of vortex-related accident involved an aircraft on approach following another landing aircraft landing on the same runway. Fifty-seven such accidents occurred behind conventional aircraft (45 probable), and 7 occurred behind landing helicopters (all probable). This category thus accounts for more

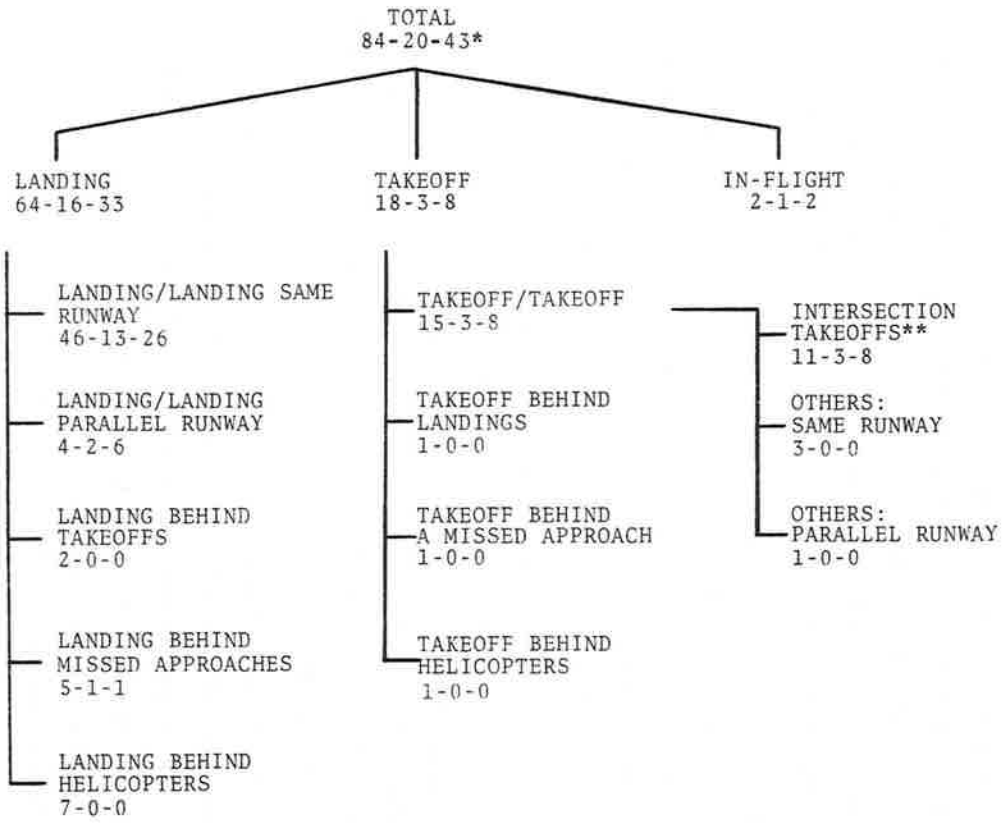

NOTE: ALL IN-FLIGHT CROP-DUSTER ACCIDENTS HAVE BEEN EXCLUDED FROM THIS SET.

* # ACCIDENTS - # FATAL ACCIDENTS - # FATALITIES, RESPECTIVELY

** NO ACCIDENTS OR FATALITIES IN THIS CATEGORY AFTER THE ESTABLISHMENT OF THE 3-MINUTE SEPARATION RULE IN 1969.

FIGURE 2. BREAKDOWN OF PROBABLE VORTEX-RELATED ACCIDENTS FOR THE TEN-YEAR PERIOD 1964-1973

than 82 percent of the vortex-related landing accidents, and about 76 percent of all-probable vortex-related accidents. Since the Vortex Advisory System (VAS) seeks to minimize delays by decreasing landing/landing separations during certain wind conditions, the vortex-related landing/landing accidents are examined in greater detail. Only the fixed-wing aircraft-caused accidents are considered below.

2.2.1 Encounter-Point Statistics

Table 1 presents the encounter-point statistics. For the probable vortex-related landing accidents, 33 percent of the vortex encounters took place after the victim aircraft had crossed the runway threshold, 54 percent between the runway threshold and the middle-marker region, and the remaining 13 percent occurred more than 1 nautical mile from the runway threshold. Thus, 87 percent of the landing accidents occurred within the region of the middle marker.

The accidents outside the region of the middle marker seem to be rather random encounters occurring because a small aircraft is approaching low and with poor lateral navigation. In this manner, the small aircraft manages to encounter vortices even when the vortices have been blown away from the extended runway centerline.

Comparatively few accidents resulted from vortex encounters at high altitudes. This may be partially explained as higher encounter altitudes provide space in which the aircraft can recover.

2.2.2 Aircraft Types Involved

Figure 3 shows a landing weight histogram for accident aircraft involved in landing accidents behind fixed-wing aircraft landing on the same runway. It is clear that small general aviation aircraft is the primary victim of the vortex problem. About 85 percent of the accident aircraft weighed less than 4000 pounds, while almost 97 percent weighed less than 11,000 pounds.

TABLE 1. VORTEX ENCOUNTER-POINT STATISTICS FOR LANDING ACCIDENTS BEHIND CONVENTIONAL AIRCRAFT LANDING ON THE SAME RUNWAY

ENCOUNTER LOCATION	ALL ACCIDENTS FROM NTSB DATA BASE			AFTER ELIMINATION OF ACCIDENTS UNRELATED TO THE VORTEX PROBLEM		
	NO. OF ACCIDENTS-FATAL ACCIDENTS-FATALITIES-SERIOUS INJURIES-OCCUPANTS, RESPECTIVELY	PERCENTAGE	CUMULATIVE PERCENTAGE	NO. OF ACCIDENTS-FATAL ACCIDENTS-FATALITIES-SERIOUS INJURIES-OCCUPANTS, RESPECTIVELY	PERCENTAGE	CUMULATIVE PERCENTAGE
After Touchdown	4-0-0-0-14	7	7	NONE	0	0
After Threshold But Before Touchdown	18-2-5-3-34	30	37	15-2-5-3-26	33	33
0-500 Ft From Runway	8-1-2-0-13	13	50	6-1-2-0-11	13	46
500-1500 Ft From Runway	13-3-7-3-25	21	71	12-3-7-3-24	26	72
1500-3500 Ft From Runway	7-4-5-6-13	12	83	7-4-5-6-13	15	87
3500 Ft-1 Mile From Runway	NONE	0	83	NONE	0	87
More Than 1 Mile From Runway	10-6-12-4-48	17	100	6-3-7-3-12	13	100
TOTAL	60-16-31-16-147	100	100	46-13-26-15-86	100	100

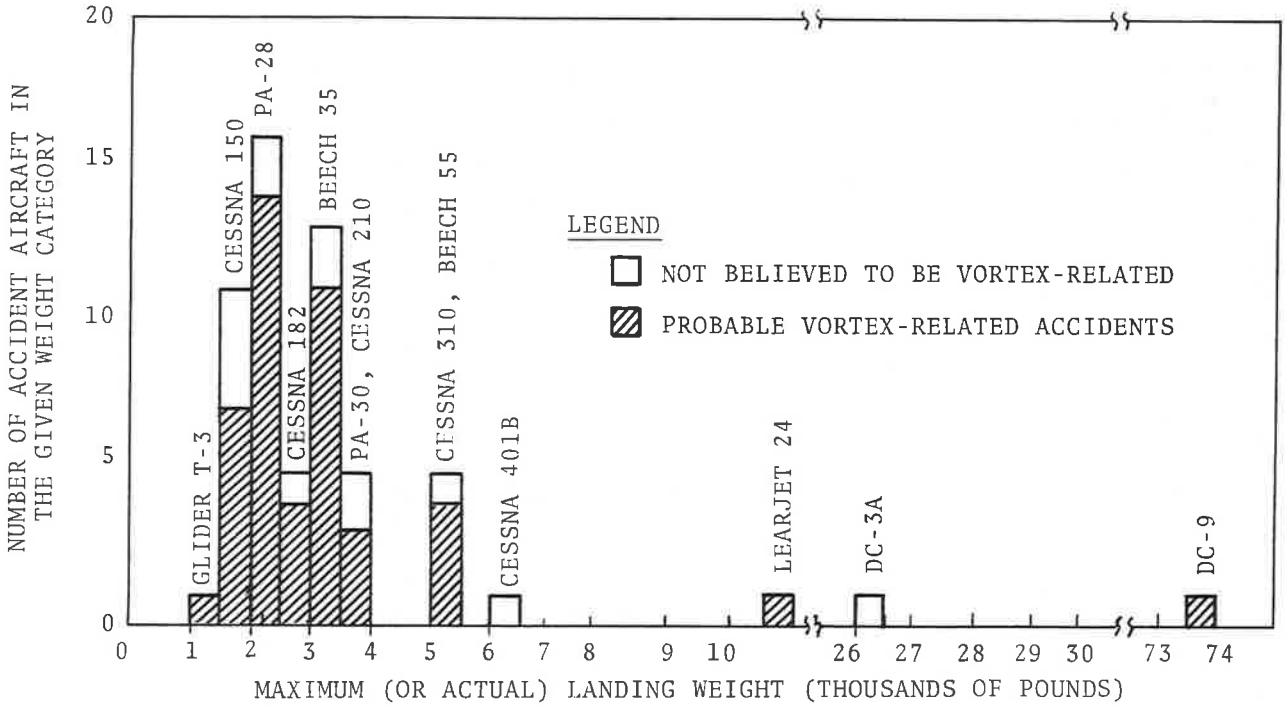

FIGURE 3. LANDING WEIGHT HISTOGRAM FOR ACCIDENT AIRCRAFT DURING LANDING ACCIDENTS BEHIND LANDINGS ON THE SAME RUNWAY

As for the vortex-generating aircraft which caused these accidents, the largest number of accidents (12) were attributed to B-707's, followed by 6 accidents attributed to B-727's. Figure 4 indicates the weights of the vortex-generating aircraft. More than 90 percent of the accidents have been caused by non-Heavy air-carrier aircraft weighing less than 300,000 pounds; this may not be significant given the relatively few Heavy aircraft compared to the many non-Heavy air-carrier aircraft during the period of this analysis. Some accidents have even been attributed to vortices from aircraft weighing less than 25,000 pounds.

2.2.3 Reported Wind Conditions

Approximately two-thirds of the accidents occurred under wind conditions of 5 knots or less. Some accidents in the NTSB data base did occur with winds higher than 10 knots; most of these accidents, however, were found to be unrelated to the vortex problem.

2.3 HISTORICAL PERSPECTIVE

The preponderance of vortex-related accidents for landing aircraft occurred between the middle-marker location and the runway threshold. Accordingly, the United States program on aircraft wake vortices (Ref. 2) concentrated on the middle marker to threshold region to develop a Wake Vortex Avoidance System (WVAS) as an integral part of the Upgraded Third Generation Air Traffic Control System (Ref. 3). The Vortex Advisory System (VAS) concept evolved from the analysis of approximately 50,000 vortex tracks, and is proposed as an interim measure to decrease delays at the major hub terminals.

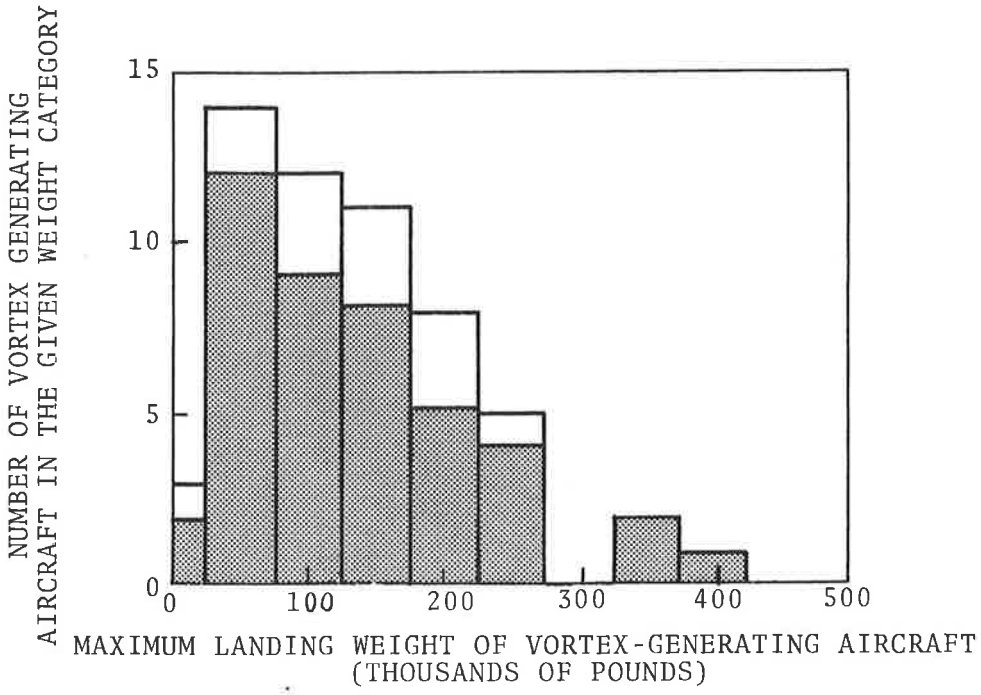

LEGEND

NOT BELIEVED TO BE VORTEX-RELATED

PROBABLE VORTEX-RELATED ACCIDENTS

NOTE: "UNIDENTIFIED JETS" NOT INCLUDED IN THIS HISTOGRAM

FIGURE 4. LANDING WEIGHT HISTOGRAM FOR VORTEX-GENERATING AIRCRAFT DURING LANDING/LANDING ACCIDENTS ON THE SAME RUNWAY

3. VORTEX ADVISORY SYSTEM

Trailing vortex wakes of large aircraft can pose a hazard to smaller following aircraft. As a result, large separation distances have been imposed to maintain safety. (Separation distances, in this report, refer to the interarrival spacings between aircraft imposed during final approach under Instrument Flight Rules.) Under the sponsorship of the FAA, the TSC has collected an abundant amount of information about vortices. Analysis of the extensive data on vortex behavior as a function of meteorological conditions has indicated that there are wind conditions during which vortices do not pose a threat to a following aircraft (Refs. 2, 4, and 5).

3.1 VORTEX DATA COLLECTION

After limited tests had been conducted at Boston's Logan International Airport, the John F. Kennedy International Airport became the first extensive test site for the study of vortex behavior. The purpose was to evaluate two vortex-sensing systems, the Ground Wind Vortex-Sensing System (GWVSS) and the Pulsed Acoustic Vortex-Sensing System (PAVSS). Each system consists of sensors (propeller anemometers or acoustic radars) strategically placed on lines perpendicular to the extended runway centerline. The instrumentation (two GWVSS lines and one PAVSS line) was set up in the middle-marker to runway-threshold region of runway 31R. In addition, a meteorological tower was erected to monitor simultaneously the winds. Reference 2 describes the test site and the operation of the vortex-sensing systems.

At the time the Kennedy site was being established, the Air Traffic Service of the FAA requested that the Instrument Flight Rules (IFR) and vortex separations applied under IFR be checked to ascertain their adequacy for protecting airliners from an inadvertent vortex encounter. Because of the expected limited traffic using runway 31R, it was decided to instrument a second runway. Since Kennedy did not have adequate real estate for the vortex-tracking equipment in the middle-marker area of the other runways,

a second airport was selected--Denver's Stapleton International Airport. The choice of Stapleton was prompted by: (1) available real estate in the middle-marker region of runway 26L; (2) the different climate of Denver, Colorado, as compared with Jamaica, New York; and (3) the chance to record aircraft types which do not frequent Kennedy (e.g., the B-737). Two GWVSS, one PAVSS, and two meteorological towers were set up at Stapleton (Ref. 2).

Data collection began at Kennedy in July 1973, and at Stapleton in August 1973. By November 1973, at which time the Stapleton site was closed, vortices from 10,000 aircraft had been monitored (3100 at Kennedy and 6900 at Stapleton). The data demonstrated that under IFR, current vortex separations were indeed adequate for preventing a vortex encounter. In fact, the data indicated that for most of the time the separations were unnecessarily restrictive (Ref. 2).

For the next 2-½ years, the Kennedy site was used as it was originally intended--an operational site for testing and evaluating vortex sensors.

Since June 1970, almost 400 unsolicited reports of possible vortex encounters (incidents) were received by air traffic control officers at the London Heathrow International Airport. Consequently, the British Civil Aviation Authority instituted a program to gather information on vortex behavior under operational conditions, and on the effect of a wake vortex encounter by civil aircraft (Ref. 6). The majority of reported incidents occurred at or near Heathrow and on final approach. No accidents were recorded however. In some cases, the encounter took place very near to the ground. Incidents were reported from a wide variety of aircraft pairs (leader/follower), and it was found that the heaviest jets (B-747 and L-1011) were cited in 40 percent of all reported incidents, even though they constituted only about 12 percent of all traffic at Heathrow during peak periods (Refs. 7 and 8). After consideration of the incident reports and consultation with the appropriate operations groups, the approach-separation distance for lighter aircraft following a wide-body jet in the United Kingdom

was increased in March 1974 from five to six nautical miles.

There has been close liaison between the British Civil Aviation Authority and the FAA on wake vortex research for some years. They jointly agreed in late 1973 that it would be beneficial if equipment similar to that tested at Stapleton and Kennedy were installed at Heathrow. The test program would afford the opportunity to expand substantially the vortex track and meteorological data base under new and varied environmental conditions, to correlate reported vortex incidents with measured vortex and meteorological conditions, and to track vortices from aircraft rarely seen in the United States (e.g., Trident, Viscount, and A-300).

The equipment (two GWVSS, one PAVSS, and two meteorological towers) was emplaced between the middle-marker and runway-threshold area of runway 28R, and became fully operational in May 1974. Data collection continued through June 1975. A total of 12,950 landings was monitored (Refs. 4 and 5).

As a result of the Heathrow tests, the correlation between the ambient meteorology and vortex behavior was underscored (Refs. 4 and 5). It was noted that it would be safe to use decreased separations often; thus, the concept of the VAS evolved. The concept of the VAS consists of measuring the wind in the approach region, comparing the wind velocity with a wind criterion, and indicating to the air traffic controller when separations could be safely decreased.

Tests were continued at Kennedy to assist in the design of the VAS and to study the decay of vortices in the terminal area. Portions of the tests began in the fall of 1975, but the full tests began in March 1976 and continued to the close of the Kennedy site in January 1977. Over 4700 aircraft passages were monitored in the March 1976 to January 1977 time frame.

The decay of vortices was studied at Kennedy using a Monostatic Acoustic Vortex-Sensing System (MAVSS) (Refs. 9 and 10). The analysis of the data led to a revision of the separation standards for aircraft with a maximum certificated gross takeoff weight of less than, or equal to, 12,500 pounds (classified as

Small aircraft by Air Traffic Control) following Large (Large--aircraft of more than 12,500 pounds maximum certificated takeoff weight up to 300,000 pounds) and Heavy aircraft. The new separation rules, applied at the runway threshold, were promulgated in November 1975; few vortex-related accidents have occurred since then. The present IFR landing separation requirements are: three nautical miles for any aircraft following a Small aircraft and for Large and Heavy aircraft following a Large aircraft; four nautical miles for a Small following a Large and for a Heavy following another Heavy; five nautical miles for a Large following a Heavy; and six nautical miles for a Small following a Heavy.

The primary purpose of the tests at the Chicago O'Hare International Airport was the evaluation of the VAS concept. The middle-marker region of runways 32L, 14R, and 27R were each instrumented with a GWVSS line. Outputs from the VAS were compared with actual vortex behavior measured by the three GWVSS lines. Between July 1976 and September 1977, over 22,500 aircraft landings were monitored. In September 1977, the development tests of the VAS were terminated; an upgraded VAS for operational use is now being implemented at O'Hare.

Analysis of vortex behavior from over 50,000 aircraft landings showed that a wind-rose criterion could be used to determine when separations may be reduced uniformly to three nautical miles between the middle marker and threshold regardless of leader/follower aircraft type (Refs. 2, 4, and 5). Most of the time, vortices in the middle-marker to touch-down region either transport away from the extended runway centerline or decay to an innocuous level. The few cases when a vortex persisted near the extended runway centerline for a time commensurate with, or in excess of the three-nautical-mile standard, were studied in great detail. It was observed that the measured one-minute averaged winds could be used to predict when vortices would not persist near the extended runway centerline. Whenever the wind exceeds the wind-rose criterion, uniform three-nautical-mile spacings may be used with safety vortexwise inside the middle marker (the region where the vortex data were collected). Not one of the vortices from the more than

50,000 aircraft would have posed a safety problem inside the middle marker if all interarrival spacings were three nautical miles during the times when the wind exceeded the wind-rose criterion. Therefore, it is asserted that the safety of the VAS has been demonstrated for the middle-marker to runway-threshold region. For details about this data collection and analyses, see Refs. 2, 4, and 5.

3.2 VORTEX ADVISORY SYSTEM DESIGN

The VAS was designed to use a wind-rose criterion. The system compares the measured wind magnitude and direction (with respect to each runway heading) with the wind criterion. The result of the comparison is indicated via a simple display; a green light means that three-nautical-mile spacings may be used for landing aircraft; and a red light means that the normal three, four, five, or six-nautical-mile spacing should be used under IFR depending upon the respective aircraft types. No vortex tracking sensors are used.

The VAS consists of four major subsystems: (1) a meteorological subsystem for the measurement of the winds; (2) a data-processing subsystem for the processing of the wind data, and, using the VAS algorithm, for determining when spacings between interarrival aircraft may be reduced; (3) a data-display subsystem for the display of separation requirements and wind conditions to the air traffic controllers; and (4) a performance-monitoring and data-recording subsystem for maintenance and archival purposes.

3.2.1 Meteorological Subsystem

The meteorological subsystem consists of a network of instrumented towers placed about the airport perimeter. In concept, each runway end would have a single 50-foot tower approximately halfway between the runway threshold and the middle marker and about 1000 feet to one side (to prevent vortex impingement on the tower disturbing the meteorological measurements). The proximity of runway thresholds, however, can often permit the placement of a single tower to serve two (or more) runways. Seven towers are used in

the O'Hare system to provide wind data on 12 runway ends.

Each 50-foot tower is instrumented with 3 sets of wind magnitude and direction sensors, one sensor at the 50-foot height and the remaining two at 47 feet. The redundancy provided by a triple-sensor installation greatly increases system reliability, insuring acquisition of valid wind data and detection of sensor failures.

The instrumentation transmitting the meteorological data from each tower to a central facility consists of a multiplexer which sequentially samples the sensor outputs, and a line modem which serializes the data and transmits them over a wire pair to receivers in the control tower. A 16-channel, 12-bit multiplexer is used. The multiplexer operates under the control of the modem which commands the scan rate. The modem operates in a lines-switching mode at a crystal controlled 5440-Hz bit rate. In addition to the six multiplexer channels used to read the three wind speed-and-direction outputs, four channels are used to monitor the status of the tower electronics by monitoring a precision-voltage reference and power-supply outputs.

Tower electronics are housed in an environmental enclosure mounted near the base of each tower. Since lightning strikes are a major problem in this type of installation, extra care was taken to insure against lightning damage. All input and output signal lines are protected with transient arrestors. The input 60-Hz power line is regulated, and contains a separate transient arrestor. Standard FAA control lines are used to transmit the data from each meteorological tower to the control tower.

3.2.2 Data-processing Subsystem

The serial data stream from each meteorological tower is received by a modem which converts the input into parallel 16-bit words representing the output of each channel sampled by the tower instrumentation. The output from each receiving modem is input to a microprocessor (one for each meteorological tower). The microprocessors sample the wind data at a two samples/second rate. The sampled wind magnitude (R_i) and wind direction (θ_i) are used to

compute a one-minute running average ($\overline{R}$ and $\overline{\theta}$) by the following scheme: for each sample, compute $U_i = R_i \sin\theta_i$ and $V_i = R_i \cos\theta_i$; then, compute $\overline{U}$ and $\overline{V}$ using a running 128-sample average, and compute $\overline{R} = (\overline{U}^2 + \overline{V}^2)^{1/2}$ and $\overline{\theta} = \tan^{-1}(\overline{V}/\overline{U})$. A 1-minute average (actually a 64-second average) was chosen since the average life of a vortex was found to be 1 minute (Refs. 2 and 5).

The microprocessor also performs the functions of failure detection and gust computation. The sampled R_i and θ_i from each sensor on a tower are compared at the end of each sampling interval (½ second), and must agree to within 3 knots and 20 degrees, respectively; if they do not agree, at least one of the sensors is assumed to have failed. Normally, the 50-foot sensor data are selected; if a 50-foot R_i or θ_i fails, the microprocessor switches to the 47-foot R_i or θ_i which is not in the wind shadow of the tower. Failure of at least two R_i's or θ_i's to agree for eight successive samples (4 seconds) causes a tower-failure signal to be generated. The microprocessor calculates the wind-gust magnitude using a sliding 32-second interval. Within each 32-second interval the sampled wind magnitude is averaged using a 4-sample running average. Momentary peaks due to high-frequency gusts, which would not affect aircraft operations, are filtered out by the 4-sample running average. Any measured peak must be at least 9 knots above $\overline{R}$ to be considered a gust, and the gust value is the peak value observed during each sliding 32-second interval.

In addition to outputs of $\overline{R}$, $\overline{\theta}$, and gust (if any), the microprocessor outputs system status words to indicate which specific failure (if any) is detected. Failure indications are displayed on the system-maintenance console, thereby providing maintenance personnel with the means to effect rapid repairs.

The microprocessor also contains the VAS wind-criterion algorithm in look-up table form for determining the separation standard: the 3/4/5/6 nautical miles or 3 nautical miles for all aircraft. The VAS wind criterion is the inner of the two concentric ellipses in Fig. 5. The inner ellipse has major and minor axes of 12.5 and 5.5 knots, respectively; the outer ellipse, 14.5

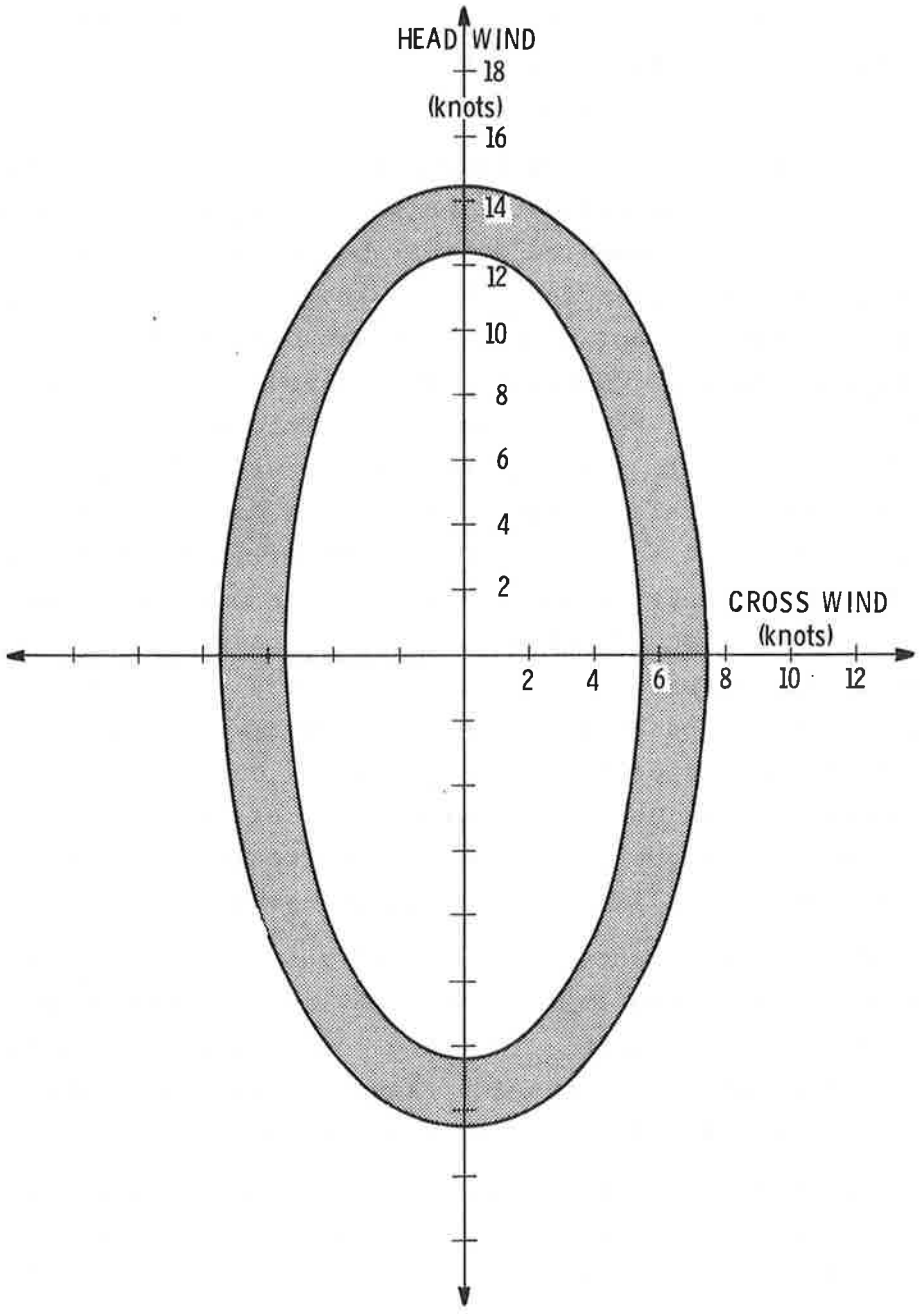

FIGURE 5. THE VAS WIND CRITERION

and 7.5 knots, respectively. The major axes are aligned in the direction of the runway. If the averaged wind vector is on or inside the inner ellipse, the 3/4/5/6-nautical-mile separations are indicated. If the averaged wind vector is on or outside the outer ellipse, the uniform 3-nautical-mile separation is indicated. The region between the two ellipses serves as a buffer zone to prevent rapid changes between the 3/4/5/6- and the 3-nautical-mile separation indications. If the averaged wind vector is on or inside the inner ellipse, the wind must increase so as to reach the outer ellipse before the 3-nautical-mile separations are indicated. If the averaged wind vector is on or outside the outer ellipse, the wind must decrease so as to reach the inner ellipse before the 3/4/5/6-nautical-mile separations are indicated.

3.2.3 Data-Display Subsystem

Two types of displays are used in the VAS, a system-monitor display and a runway-monitor display.

3.2.3.1 System-Monitor Display

The system-monitor display is intended for use by the tower-cab and IFR-room supervisors. The display indicates in summary form the winds measured by all the meteorological towers. The primary function of the display is to provide an overview of the wind conditions across the airport enabling the supervisor to select an operating configuration which will maximize traffic flow.

3.2.3.2. Runway-Monitor Display

The runway-monitor display is intended for use by a controller responsible for traffic on a single runway. The controller selects the specific runway via a set of thumbwheel switches. The controller also indicates if arrival or departure winds are desired, e.g., enter A32L for arrivals on runway 32L, and D32L for departures from 32L. The display thereafter accepts data with the corresponding label from the data bus. Thus, if A32L is entered, wind parameters measured at the tower near the approach end of runway 32L are displayed, while a D32L entry causes wind parameters measured

at the tower near the approach end of runway 14R to be displayed.

Separations are indicated by a red or green light and are indicated only when an arrival runway is selected. A red light means that 3/4/5/6-nautical-mile separations need to be maintained during IFR; a green light means that all 3-nautical-mile separations may be used. The dimensions of the VAS wind criterion (inner ellipse of Fig. 5) have been defined to permit aircraft at or within the middle marker to safely land if the VAS suddenly transitions from green to red.

3.2.4 Performance-monitoring and Data-recording Subsystem

To facilitate maintenance of the VAS, a system maintenance panel indicates the status of the various components and if repairs are needed. All the data output by the VAS are recorded on nine-track digital tape. This tape contains a complete record of all VAS operations for use in system diagnostics and to meet FAA operational requirements for a record of all air traffic control operations.

4. VORTEX ENCOUNTER MODEL

The wind criterion employed by the VAS ensures that vortices will not pose a problem to a landing aircraft between the middle marker (MM) and touch down when the green light is on. Permitting separations to decrease below the 4-, 5-, and 6-nautical-mile standards inside the MM will contribute to minimizing delays. However, significant improvements in minimizing delays can be realized if the coverage of the VAS-protected region can be extended to the outer marker (OM). Measurements have been made of vortex behavior between the MM and OM; Volume II of this report addresses a comprehensive vortex data collection program in this region.

The objectives of this section are to derive a general model for calculating the probability of a hazardous vortex encounter between the OM and the MM and to determine the applicability of the VAS green light to this region. The intent is to be as general as possible, so that the results may be applied at any airport. Limitations of the model (i.e., anomalous vortex behavior, terrain effects, etc.) will be delineated herein or in the appendices. However, the model is based on state-of-the-art knowledge of how vortices, aircraft, and winds behave.

Two independent conditions must be met for a hazardous vortex encounter to occur. First, the trailing vortex system must be sufficiently strong to be hazardous to the vortex-encountering or following aircraft, and second, the following aircraft must encounter the vortices of the leading or vortex-generating aircraft. Thus, two probabilities are defined, the probability that a vortex is hazardous, P_h, which is related to the strength of the trailing vortex system and to the size and control characteristics of the vortex-encountering aircraft; and the probability of encountering the vortices, P_e, which is related to the flight paths of the two aircraft and to the motion of the vortex system. The probability of a hazardous vortex encounter, P_{he}, is then

$$P_{he} = P_h P_e. \tag{1}$$

4.1 PROBABILITY OF A VORTEX ENCOUNTER

4.1.1 Definition of Vortex Encounter

Before deriving an analytic expression for the probability of a hazardous vortex encounter, it is necessary to define what is meant by an encounter. Although the definition is simple and by no means complete or unique, it does take into account a practical criterion for a hazardous vortex encounter to occur. This criterion is that the swirling velocities of the vortex induce velocities on the wing of the vortex-encountering aircraft in excess of the roll velocities which result with full aileron deflection. In other words, a hazardous condition exists when the vortex induces roll rates exceeding the roll control authority of the vortex-penetrating aircraft. Analysis of flight test (Refs. 11 and 12) and simulation (Refs. 13 and 14) results has verified that the criterion agrees with pilot assessment of a hazardous vortex encounter. To be conservative in the model, a more stringent criterion shall be used: a hazardous condition is defined to exist when the vortex-induced roll rate exceeds some fraction f (to be defined, but less than 1) of the roll control authority of the vortex-encountering aircraft. Since the aircraft are in trail, only the worst case of an axial vortex encounter is considered herein.

The vortex wake at a distance behind an aircraft is, in general, comprised of two counterrotating vortices spaced a distance b_o apart. Sufficiently far from the center of each vortex, the swirling velocity v is described by

$$v = \frac{\Gamma}{2\pi R}, \tag{2}$$

where Γ is the circulation or strength of the vortex, and R is the distance from the center of the vortex. Inside the circle of radius R, the swirling velocities are larger than v although the swirling velocity is zero at the center of the vortex. Define R_o as the radius at which the swirl velocity equals the fraction f of

the maximum aileron-induced wingtip velocity v_T:

$$R_o = \frac{\Gamma}{2\pi f v_T}. \tag{3}$$

R_o defines a cross section, such that if the wingspan of an aircraft is embedded in the circle of radius R_o, the fraction f of the roll-control authority of the aircraft is exceeded. Thus, for a potentially hazardous vortex encounter the vortex tangential velocity at R_o must be greater than or equal to fv_T.

For a vortex-encountering aircraft of maximum roll capability p and wingspan b_e,

$$v_T = \frac{pb_e}{2} = \left(\frac{pb_e}{2U}\right)U, \tag{4}$$

where $pb_e/2U = \hat{p}$ is the maximum non-dimensional roll rate and U is the airspeed of the vortex-encountering aircraft. Thus,

$$R_o = \frac{\Gamma}{2\pi f \hat{p} U} \tag{5}$$

defines a hazard radius about each vortex dependent on vortex strength, maximum non-dimensional roll rate, fraction of the maximum aileron-induced wingtip velocity imparted to counter the vortex-swirling velocity, and airspeed.

For commercial jetliners, the maximum tip velocity for full aileron deflection is, at a minimum, six percent of the flight speed; for general-aviation-type aircraft, the maximum tip velocity is at least eight percent of the flight speed. (The maximum non-dimensional roll rate is the product of the aileron-and-spoiler control effectiveness and the maximum aileron-and-spoiler deflection angles divided by the roll-damping coefficient (Ref. 15). Ailerons and spoilers for new commercial jetliners are designed so that $\hat{p}$ is at least 0.06.)

Inside a circle of radius R_o, the characteristic vortex-

swirling velocities are larger than the maximum wingtip velocities attainable with the fraction f of the roll capability of the vortex-encountering aircraft. If the wingspan of the vortex-encountering aircraft is smaller than $2R_o$, the aircraft can be entirely immersed in a swirling flow whose tangential velocity exceeds the fraction f of the aircraft's roll authority. On the other hand, if the wingspan is larger than $2R_o$, vortex-induced swirl velocities cannot exceed the fraction f of the roll authority of the aircraft. Thus, the condition for a potentially hazardous vortex encounter is that

$$R_o \geq b_e/2. \tag{6}$$

According to the model then, a potentially hazardous vortex encounter can occur only if $R_o \geq b_e/2$, and if a following aircraft is fully located within the circle defined by R_o. The probability of a potential hazard is:

$$P_h = \begin{cases} 1 & R_o \geq b_e/2, \\ 0 & R_o < b_e/2. \end{cases} \tag{7}$$

The encounter is either hazardous ($P_h = 1$) or it is not ($P_h = 0$). To be conservative "soft" or partial encounters are considered to be hazardous. $P_h = 0$ includes encounters of little or no concern, and $P_h = 1$ includes cases which are serious as well as many which are of little concern. Thus, $P_{he} = P_h P_e$ is defined as zero when the hazard radius R_o decays below $b_e/2$, and is finite for a specific following aircraft when R_o exceeds $b_e/2$. Note that $P_{he} = 0$ does not preclude a vortex encounter, it means that an encounter is not hazardous.

4.1.2 Vortex Decay

The hazard posed by a vortex primarily involves the vortex strength. The strength or circulation of a vortex decays with distance behind the vortex-generating aircraft, and the decay is

influenced by many factors. Close behind the aircraft, the initial dispersion of the wake is governed by configuration, which includes geometry (particularly flap and engine placement) and thrust and flap settings.

While the initial vortex-decay rate is configuration-sensitive, ultimately the decay rate must be determined by self-decay of the vortex pair coupled with atmospheric shear, turbulence, and stratification. While there is some understanding of the turbulent mechanisms involved in dissipation of vortices, no theories which can reliably predict the decay of an aircraft wake are available today. Theories do exist for describing the onset of either of the two catastrophic decay modes: sinuous instability or vortex-linking (Ref. 16) and vortex-bursting (Ref. 17). The predicted times are generally within a factor of two of the observed times for both breakup by linking and by bursting. Atmospheric turbulence is the mechanism that causes catastrophic decay to occur. To be conservative in the model, the catastrophic decay modes (which occur most of the time) will be ignored; only the slowest decay mode (viscous decay) will be considered.

Decay by eddy viscosity involves extremely calm atmospheric conditions, when linking or bursting may not be occurring, but there is still sufficient aircraft-generated turbulence to cause eventual vortex erosion. Aircraft in a "dirty" configuration (gear and flaps down) generate turbulence which is added to the wake permitting eddy-viscosity decay of the wake. Considering only this mode of decay establishes an outer limit or upper bound on the life of a vortex.

Eddy-viscosity-caused decay of the vortices behind "dirty" aircraft is illustrated in Figure 6 (Ref. 18). The sources of the data are the ground-based measurements taken by TSC at Kennedy International Airport (Ref. 10), NASA/FAA flight test measurements using probing aircraft (Fig. 25 of Ref. 19), and NASA towing-tank results (Ref. 20). Although the definition of vortex strength differed for the different data sources, the major results would not differ if other definitions were used.

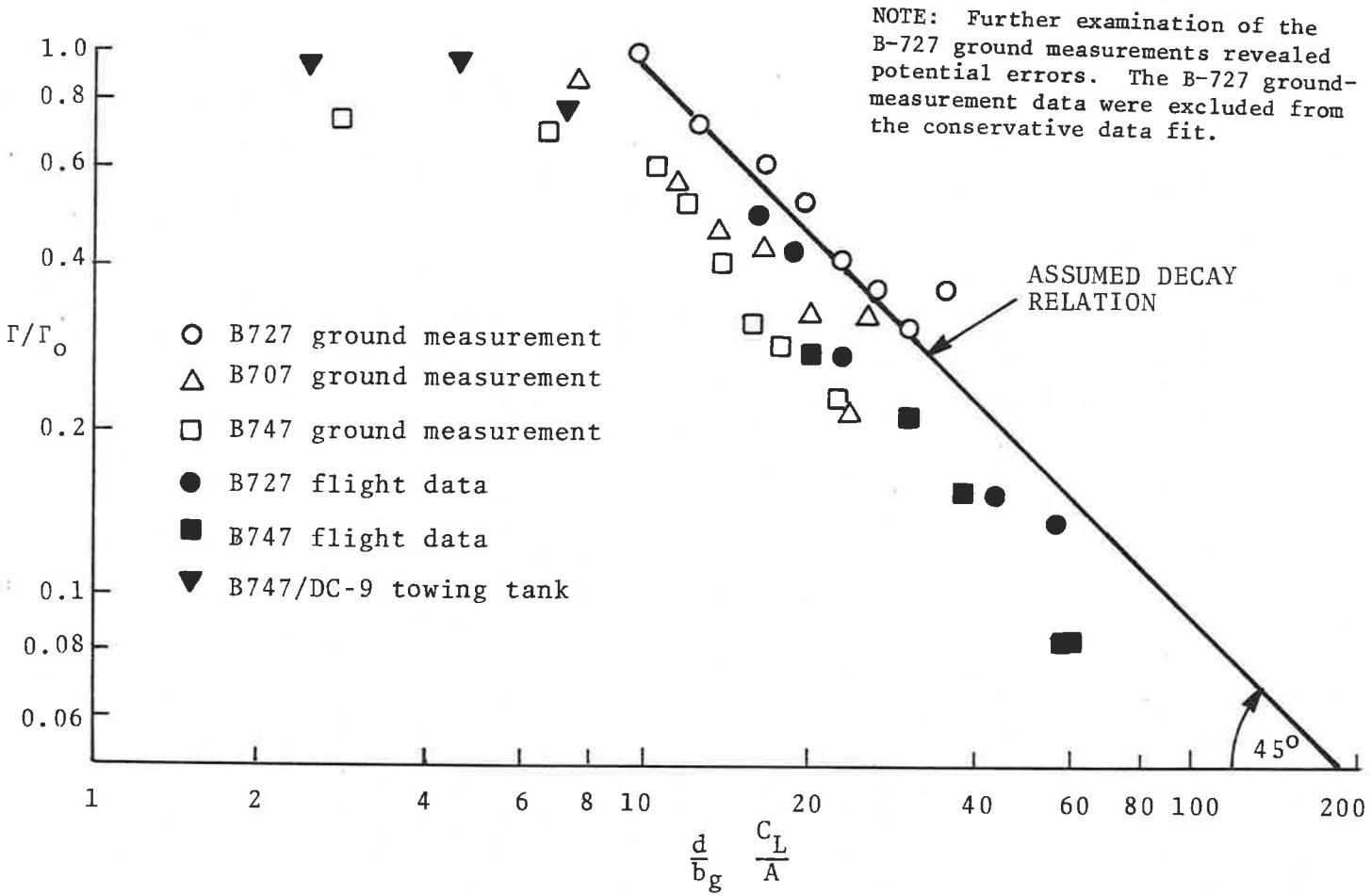

FIGURE 6. WAKE STRENGTH DECAY FOR LANDING AIRCRAFT AS A FUNCTION OF DOWNSTREAM DISTANCE

The figure shows that non-dimensionalizing the circulation by an effective initial circulation Γ_o and non-dimensionalizing distance d behind the vortex-generating aircraft by its wingspan b_g, its lift coefficient C_L, and its aspect ratio A, cause the data points to coalesce fairly well. It is remarkable that such diverse measurements indicate similar decay. Beyond dC_L/b_gA of 9.58 (corresponding to the region beyond about 50 span lengths), the data fit is

$$\frac{\Gamma}{\Gamma_o} = 9.58 \left(\frac{d}{b_g} \frac{C_L}{A}\right)^{-1}. \tag{8}$$

In this region, the eddy viscosity acts to diffuse the vorticity causing wake dissipation to proceed as d^{-1} or $(\text{time})^{-1}$. Earlier, when Γ/Γ_o is essentially constant, aircraft configuration effects are acting to diffuse vorticity so that decay can subsequently occur.

The shape of the curve in Figure 6 showing constant Γ at short distances and thereafter a $(\text{time})^{-1}$ dependence is the same as found for the core circulation of a B-747 in landing configuration measured by a laser Doppler velocimeter (Fig. 5 in Ref. 21). The "break" for the laser measurements occurred at about 33 span lengths, somewhat closer to the vortex-generating aircraft than the "break" shown in Figure 6. Other investigators (several papers in Ref. 22) have found slightly different shaped curves or noted decay to be stronger near the ground, but the main feature of constant circulation followed by decay appears consistent with all observations.

Figure 6 shows that circulation is reduced to 20 percent of its initial magnitude by $dC_L/b_gA = 50$, about 250 span lengths back (A/C_L is about 5 for most landing aircraft during the approach). For a B-747 at approach speed, this is about 8 nautical miles back at a time of 205 seconds. For a B-727 at approach speed, this is about 4.4 nautical miles back at a time of 131 seconds. If the ambient turbulence is light or greater, catastrophic decay through

linking or core-bursting will occur before these times. However, only eddy-viscosity decay will be assumed in the model to insure that the model is conservative. The hazard radius, R_o, thus becomes

$$R_o = \frac{\Gamma}{2\pi f\hat{p}U},$$

$$= \frac{1.52\ \Gamma_o}{f\hat{p}U}\left(\frac{d}{b_g}\ \frac{C_L}{A}\right)^{-1},$$

$$= \frac{1.52\ \Gamma_o}{f\hat{p}U}\left(\frac{d}{5\ b_g}\right)^{-1},$$

$$= \frac{7.6\ \Gamma_o\ b_g}{f\hat{p}Ud} \qquad \text{for } \frac{dC_L}{b_g A} \geq 9.58. \tag{9}$$

As the distance behind the vortex-generating aircraft, d, increases, the hazard radius R_o decreases. Recalling equation (6),

$$\frac{7.6\ \Gamma_o\ b_g}{f\hat{p}Ud} \geqslant \frac{b_e}{2} \tag{10}$$

is required for a potentially hazardous vortex encounter. Thus, $P_h = 1$ (and $P_{he} > 0$) only when

$$d \leqslant \frac{15.2\ \Gamma_o\ b_g}{f\hat{p}Ub_e}, \qquad \text{for } \frac{dC_L}{b_g A} \geq 9.58. \tag{11}$$

When the solution to equation (11) yields $d < 9.58\ (C_L/b_g A)^{-1}$ then R_o can never exceed $b_e/2$ at any distance, thus there is no distance at which a potentially hazardous encounter can occur, and

$$d = 0. \tag{12}$$

Measurements (Refs. 2, 21, and various papers in 22) show that the circulation or strength of a vortex increases with the spatial extent about a vortex up to an ultimate value Γ_∞; the radius at which Γ_∞ is attained is denoted by r_∞. If the vortex field is sampled (such as by an aircraft wing) with a probe with $r<r_\infty$, only a portion of Γ_∞ will be experienced. Given two aircraft with different wingspans, as long as $b_e < 2r_\infty$, the strength of the vortex experienced by the aircraft with the larger wingspan will be greater than for the smaller wingspan. Various radial dependencies have been claimed by researchers (Ref. 2); a linear variation with b_e for Γ is adopted herein as it is consistent with strength data measured using real aircraft (Refs. 10, 21, and 23) rather than aircraft models in towing tanks (Refs. 2 and 17).

Equation (11) requires an estimate of the initial strength Γ_o of a vortex (strength before the onset of decay). The initial strength Γ_o of the vortices as would be experienced by an encountering aircraft of wingspan b_e is shown in Appendix A to have the form

$$\Gamma_o = mb_e + \Gamma_{int} , \tag{13}$$

where m and Γ_{int} are two curve-fitting parameters; values of m and Γ_{int} are tabulated in Appendix A. Equation (11) may now be rewritten ($dC_L/b_gA \geq 9.58$),

$$d \leq \frac{15.2}{f\hat{p}U} \frac{b_g}{b_e} (mb_e + \Gamma_{int}). \tag{14}$$

When $dC_L/b_gA < 9.58$, equation (12) is valid (i.e., no hazard).

The NTSB data base (Section 2) indicated that to the extent separation data were available all the probable vortex-related landing accidents occurred when the separations were less than the respective separation standards. To determine an upper bound for the fraction f of the maximum roll-control authority, the distance d was set equal to the respective separation standard. The

standards that pertain to the OM location were used (3, 4, and 5 nautical miles), not those for the runway threshold location (3, 4, 5, and 6 nautical miles). Table 2 shows the 12 aircraft considered along with their landing speeds and wingspans. Table 3 shows the upper bound on the fraction of roll-control authority required to neutralize the vortex-swirl velocity. The largest f is 0.756, and occurred for the PA-28 following the DC-8.

In the spirit of being conservative, f will be set equal to one-half the maximum value found in Table 3 (f = 0.5 x (0.756) = 0.378). No further justification is offered; an f = 0.378 means that only one-half of the maximum roll authority required to safely fly the current separation standards is expected to be conservative.

Using f = 0.378 and equation (14) (or equation (12), if necessary), the distances at which the hazard radius becomes smaller than the semispan can be calculated. These distances are given in Table 4. Ignoring for the moment the Small-category aircraft (PA-28 and Learjet), the only calculated distances in excess of 3 nautical miles are for the B-727, B-737, and DC-9 following the B-747. Except for these cases, separation standards could be set at 3 nautical miles between the OM and MM with or without a VAS. (Recall that the accidents are confined to the ground-effect region inside the MM.) Note that the DC-9 must be 2.54 nautical miles behind the DC-10 to reduce the probability of hazard to zero. The DC-9 accident at Dallas-Fort Worth Greater Southwest International Airport occurred with the DC-9 about 2 nautical miles behind the DC-10.

So far the model has only considered vortex decay. To show that 3 nautical miles is safe behind the B-747 when VAS is used, the model must now be expanded to consider both vortex motion with the wind and vortex descent. It is very important to note, however, that vortex decay alone does permit decreased separation standards for most aircraft pairs outside of ground effect.

TABLE 2. AIRCRAFT PARAMETERS

Aircraft Model	Landing Speed (ft/sec)	Wingspan (ft)
B-707/120B	232.3	130.9
B-727/100	205.8	108.0
B-737/100	197.0	93.0
B-747/200B	238.0	195.7
DC-8/20	222.0	142.3
DC-9/20	189.6	93.3
DC-10/30	232.3	165.3
L-1011/200	241.1	155.3
B-707/320B	232.3	145.8
DC-8/62	210.2	148.4
PA-28/180	110.0	30.0
Learjet-25	154.0	35.6

TABLE 3. MAXIMUM FRACTION OF ROLL-CONTROLL AUTHORITY REQUIRED TO COUNTERACT VORTEX-SWIRLING FLOWS WHEN THE AIRCRAFT ARE SPACED AT THE CURRENT SEPARATION STANDARD

Lead Aircraft	Trail Aircraft											
	B-747	DC-10	L-1011	DC-8H	B-707H	DC-8	B-707	B-727	DC-9	B-737	Learjet	PA-28
B-747	0.219	0.234	0.229	0.266	0.242	0.205	0.200	0.240	0.275	0.265	0.413	0.646
DC-10	0.150	0.160	0.157	0.183	0.167	0.141	0.138	0.167	0.192	0.185	0.295	0.463
L-1011	0.145	0.155	0.152	0.176	0.160	0.136	0.132	0.159	0.182	0.176	0.274	0.428
DC-8H	0.138	0.147	0.144	0.168	0.153	0.129	0.126	0.152	0.174	0.168	0.264	0.414
B-707H	0.128	0.138	0.135	0.157	0.143	0.121	0.119	0.143	0.165	0.159	0.256	0.403
DC-8	0.167	0.181	0.179	0.208	0.190	0.201	0.198	0.244	0.284	0.275	0.475	0.756
B-707	0.174	0.185	0.181	0.210	0.191	0.202	0.197	0.235	0.268	0.259	0.390	0.606
B-727	0.142	0.151	0.148	0.172	0.156	0.165	0.161	0.192	0.219	0.211	0.316	0.491
DC-9	0.091	0.097	0.095	0.111	0.101	0.107	0.105	0.127	0.146	0.141	0.227	0.351
B-737	0.079	0.084	0.083	0.096	0.087	0.092	0.090	0.108	0.124	0.119	0.185	0.289
Learjet	0.018	0.020	0.020	0.037	0.022	0.023	0.023	0.029	0.034	0.032	0.061	0.098
PA-28	0.021	0.023	0.023	0.026	0.024	0.025	0.024	0.029	0.033	0.032	0.049	0.077

TABLE 4. MINIMUM DISTANCE IN NAUTICAL MILES REQUIRED TO REDUCE THE VORTEX HAZARD TO ZERO

Lead Aircraft	Trail Aircraft											
	B-747	DC-10	L-1011	DC-8H	B-707H	DC-8	B-707	B-727	DC-9	B-737	Learjet	PA-28
B-747	2.31	2.47	2.42	2.71	2.56	2.81	2.64	3.18	3.64	3.51	5.47	8.54
DC-10	1.58	1.64	1.61	1.79	1.70	1.86	1.75	2.11	2.41	2.33	3.62	5.66
L-1011	1.53	1.70	1.67	1.87	1.76	1.94	1.83	2.21	2.54	2.44	3.91	6.13
DC-8H	1.46	1.56	1.53	1.71	1.62	1.78	1.67	2.01	2.31	2.22	3.50	5.47
B-707H	1.36	1.46	1.43	1.60	1.51	1.66	1.57	1.90	2.19	2.11	3.39	5.33
DC-8	1.32	1.44	1.42	1.60	1.51	1.65	1.57	1.94	2.25	2.17	3.77	6.00
B-707	1.38	1.47	1.44	1.60	1.52	1.67	1.56	1.87	2.13	2.05	3.10	4.81
B-727	1.13	1.20	1.18	1.31	1.24	1.36	1.28	1.52	1.74	1.67	2.51	3.90
DC-9	0.00	0.77	0.76	0.85	0.80	0.88	0.83	1.01	1.16	1.12	1.80	2.83
B-737	0.00	0.00	0.00	0.76	0.00	0.00	0.00	0.86	0.98	0.95	1.47	2.29
Learjet	0.00	0.00	0.00	0.00	0.00	0.00	0.00	0.00	0.00	0.00	0.49	0.78
PA-28	0.00	0.00	0.00	0.00	0.00	0.00	0.00	0.00	0.00	0.00	0.39	0.61

4.1.3 Encounter Probability

The probability of a hazardous encounter is the product of the probability that the vortex is hazardous, P_h (1 if $R_o \geq b_e/2$), and the probability of encountering that hazardous vortex, P_e. This section computes the probability of encounter for the following aircraft where encounter is defined as being fully immersed within the hazard region defined by R_o.

Figure 7 shows the encounter region in the cross plane of the approach path. The origin is taken as the nominal location of the generator aircraft at the time of its passage through the cross plane. Normally this would be the point at which the glide path intercepts the cross plane, as shown in the figure. The lateral displacement from the origin is denoted by y and vertical by z, as shown. Navigation errors of the generator aircraft are assumed to be independent Normally distributed with standard deviations σ_{yg} and σ_{zg}, respectively, statistically defining the generation point of the vortex pair.

The follower aircraft, as shown in Figure 7 intercepting the cross plane, may be on a different nominal flight path from that of the generator. The mean lateral and vertical displacements of the follower describing this flight path are labeled L and G, respectively. These are also assumed independent Normally distributed with standard deviations σ_{ye} and σ_{ze}.

The position of the center of the vortex pair is a function of descent rate, cross wind, and the time since the passage of the generator. W and D are the resultant mean lateral and vertical transport components, with standard deviations σ_W and σ_D. (The evaluation of these parameters will be considered further in the next sections.) In addition to the variance associated with the transport mechanism, the position of the vortex pair is also subject to the variance in the navigation of the generator, thus the total lateral and vertical variances are:

$$\sigma_y^2 = \sigma_{yg}^2 + \sigma_W^2 \qquad (16)$$

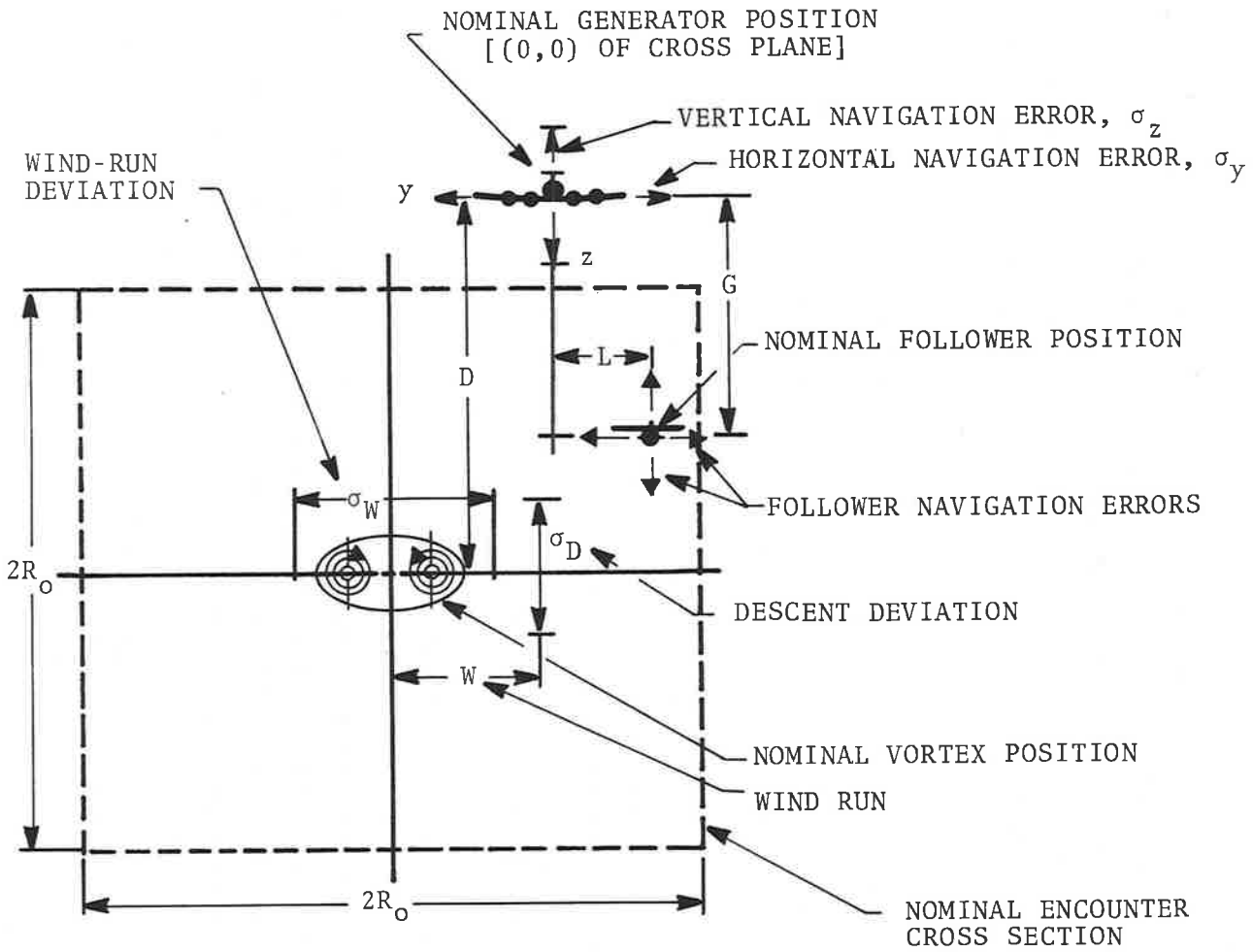

FIGURE 7. ENCOUNTER GEOMETRY IN PLANE PERPENDICULAR TO FLIGHT PATH

$$\sigma_z^2 = \sigma_{zg}^2 + \sigma_D^2 \quad . \tag{17}$$

With the locations of the center of the vortex pair and the follower aircraft thus defined, the encounter can be defined statistically and its probability calculated. Section 4.1.1 defined a possibly hazardous encounter to be that condition where the entire wingspan of the encounter aircraft is within the vortex hazard cross section. Two distinct cases must be evaluated depending upon the relationship of R_o to b_o, the spacing between the two vortices ($b_o = \pi b_g/4$):

1. $R_o >> b_o$ -- hazard radius much larger than the separation between the two vortices. In this case the hazard cross section can be considered to be a single circle of radius R_o located at the center of the vortex pair.

2. $R_o \sim b_o$ -- hazard radius of the same magnitude or smaller than the separation between the two vortices. In this case the hazard cross section can best be considered to be two distinct circles of smaller hazard radius (corresponding to the strength and circulation of the single vortex).

These two cases are illustrated in Figure 8.

For the hazard potential to exist, the wingspan of the follower must lie fully within the R_o circle. The hazardous encounter cross section is defined by the geometric pattern mapped out by fitting a wingspan b_e inside the circle. If $2R_o < b_e$, the cross section is zero. Otherwise, if the center of the encounter cross section is located at (y_o, z_o), the center of the vortex-encountering aircraft must lie on the y-axis between $y_o + (R_o - b_e/2)$ and $y_o - (R_o - b_e/2)$ and on the z-axis between $z_o \pm (R_o^2 - b_e^2/4)^{1/2}$ for the aircraft to be completely engulfed within a circle of radius R_o. Figure 9 shows the geometry. For mathematical convenience, let the hazardous encounter cross section be the rectangle (see

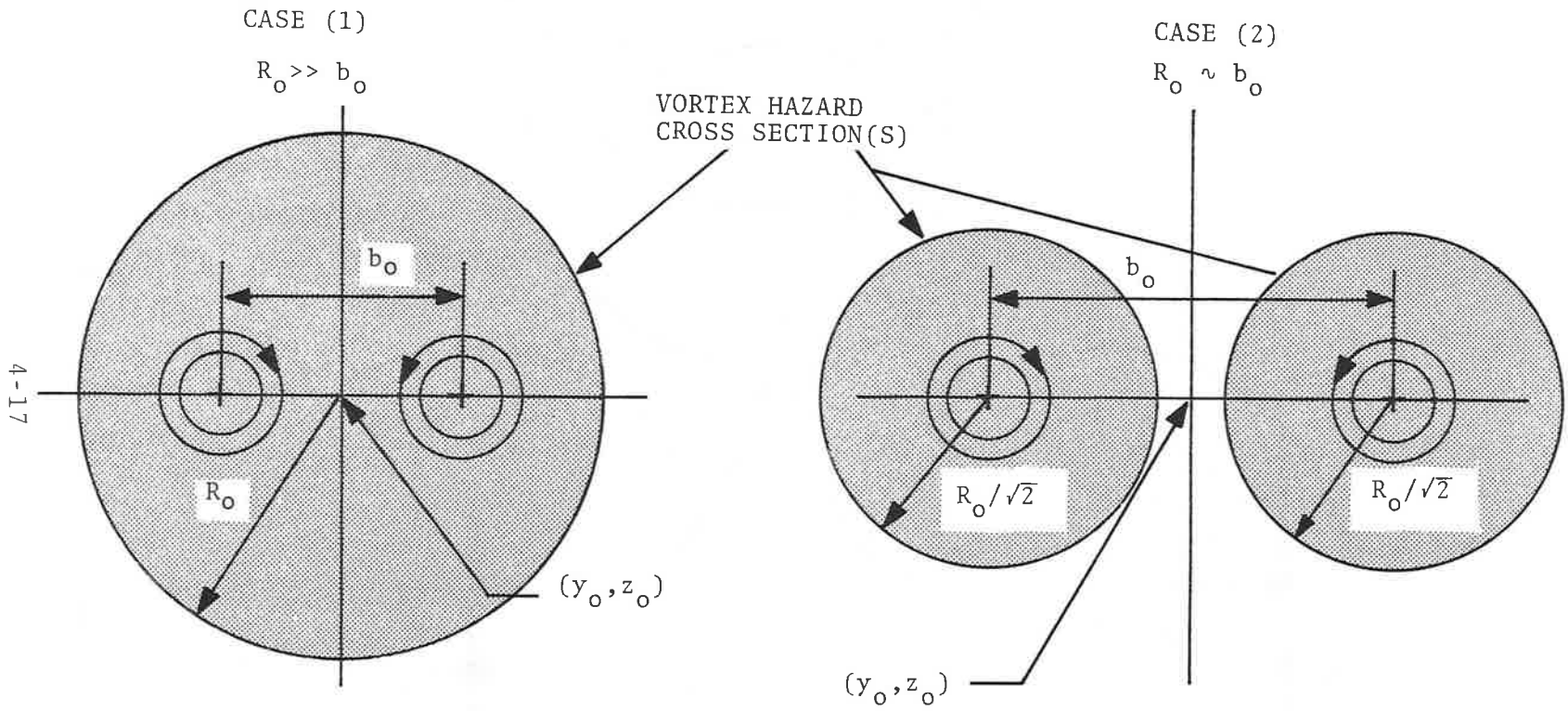

FIGURE 8. VORTEX HAZARD CROSS SECTIONS

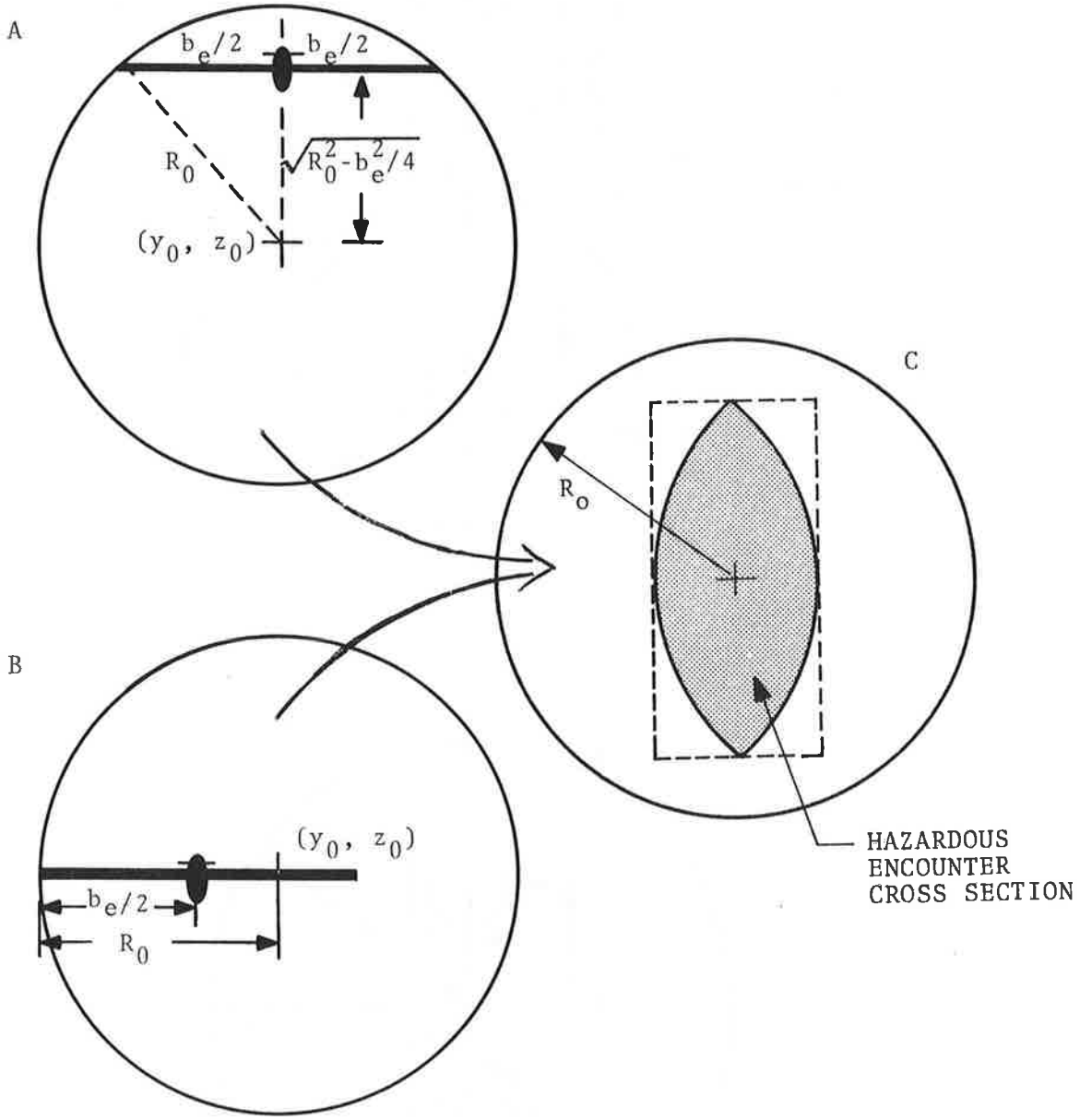

FIGURE 9. BOUNDS ON THE HAZARDOUS-ENCOUNTER CROSS SECTION

Figure 9) of height $2(R_o^2 - b_e^2/4)^{\frac{1}{2}}$ and width $2(R_o - b_e/2)$ rather than the smaller ellipse-like shape (a conservative approximation).

The net mean position of the hazardous encounter cross section relative to the follower aircraft is

horizontal: $W - L$

vertical: $D - G$.

The net variance in that position is

$$\text{horizontal:} \quad \sigma_H^2 = \sigma_{yg}^2 + \sigma_{ye}^2 + \sigma_W^2 \tag{18}$$

$$\text{vertical:} \quad \sigma_V^2 = \sigma_{zg}^2 + \sigma_{ze}^2 + \sigma_D^2 \ . \tag{19}$$

Thus the horizontal and vertical encounter probabilities are the probabilities that Normal variates for the aircraft/vortex spacing with the above means and variances lie within $\pm (R_o - b_e/2)$ horizontally and $\pm (R_o^2 - b_e^2/4)^{\frac{1}{2}}$ of zero:

$$P_{HE} = \frac{1}{2}\left\{\text{erf}\left(\frac{W-L + (R_o - b_e/2)}{\sqrt{2}\ \sigma_H}\right) - \text{erf}\left(\frac{W-L - (R_o - b_e/2)}{\sqrt{2}\ \sigma_H}\right)\right\} ; \tag{20}$$

$$P_{VE} = \frac{1}{2}\left\{\text{erf}\left(\frac{D-G + \sqrt{R_o^2 - b_e^2/4}}{\sqrt{2}\ \sigma_V}\right) - \text{erf}\left(\frac{D-G - \sqrt{R_o^2 - b_e^2/4}}{\sqrt{2}\ \sigma_V}\right)\right\}, \tag{21}$$

For case (1), $R_o >> b_o$, the probability that the vortex-encountering aircraft is within the hazard rectangle is given directly by the product of P_{HE} and P_{VE}:

$$P_e = P_{HE}\ P_{VE} \ . \tag{22}$$

For case (2), $R_o \sim b_o$, two smaller circles of radius $R_o/\sqrt{2}$ are used to maintain equal area of the circles (and, hence, continuity of the probability) and to reflect the effect and identity of both vortices (Ref. 24). Assuming that both circles remain relatively close to the center of the vortex pair, then

$$P_e = 2\, P_{HE}\, P_{VE} \tag{23}$$

with P_{HE} and P_{VE} evaluated at the reduced radius. The size of R_o where case (1) transitions to case (2) is not unique; it is merely a mathematical technique to avoid double counting areas of overlapping hazard radii when R_o is small enough to distinguish the two vortices. The break point assumed between case (1) and case (2) in the program given in Appendix D is at R_o 50 percent above the vortex separation

$$R_o = 1.5\, b_o = \frac{3\pi}{8}\, b_g. \tag{24}$$

The probability of a hazardous vortex encounter, P_{he}, is calculated by substituting the R_o calculated [from equation (9)] for a given interaircraft spacing, d, into the above expressions for P_{HE} and P_{VE}, and integrating over all possible wind runs W:

$$P_{he} = P_h P_e = \int_{-\infty}^{\infty} P_{VE}\, P_{HE}\, p(W)\, dW. \tag{25}$$

To determine the expected encounter risk for a given approach, P_{he} should be integrated along the direction of flight from the OM to the MM. Instead, the maximum value of P_{he} for two aircraft at minimum prescribed separations is evaluated to determine the maximum potential hazard at the minimum spacing. The integration along the final is not meaningful as the two aircraft will not maintain identical speeds or spacings between the OM and MM. If the following aircraft is slower (faster) than the leading aircraft,

the separation will increase (decrease) as the aircraft proceed along the ILS. Herein, the separation is held fixed, and P_{he} is evaluated at the location between the OM and MM where P_{he} would be at a maximum at the minimum legal spacing (for all aircraft pairs P_{he} is maximized at the OM location--all calculations were done with the following aircraft at the OM, and the OM was assumed to be 7 nautical miles from the runway as this also maximizes P_{he}). This places a conservative upper bound on the encounter risk that might be experienced on final approach between the outer and middle markers.

4.2 NAVIGATION MODEL

It is assumed that the navigation deviations of the vortex-generating and vortex-encountering aircraft were Normally distributed. It is further assumed that the peaks of the lateral and vertical distributions are coincident; that is, the midpoints of the two distributions intersect on the nominal flight path.

In a study conducted for the FAA (Ref. 25), an Unusual Events Recording System was installed on a B-737 for 6 months of operation. Figures 10 and 11 show the measured standard deviations for IFR operations. (The localizer course was defined for a 10,000-foot runway). Beyond 5 nautical miles, the B-737 data indicate extreme variations as the data frequently included portions of a turn preceding the localizer intercept near the OM. Inside the OM, the lateral deviations for the B-737 IFR approaches to a number of airports are the same as for simultaneous approaches to parallel runways at Chicago's O'Hare International Airport by several aircraft types (Ref. 26). Operations in the vertical plane covered almost the entire $\pm$ 0.7-degree width of the glide-slope beam at a range of 1 to 8 nautical miles from the runway threshold. This dispersion for IFR operations was greater than expected, but was attributed to the pilot using a visual approach as soon as the airport was in sight.

The broken lines in Figures 10 and 11 are a least-squares fit to the B-737 data collected inside the OM (about 26,000 feet (4.3

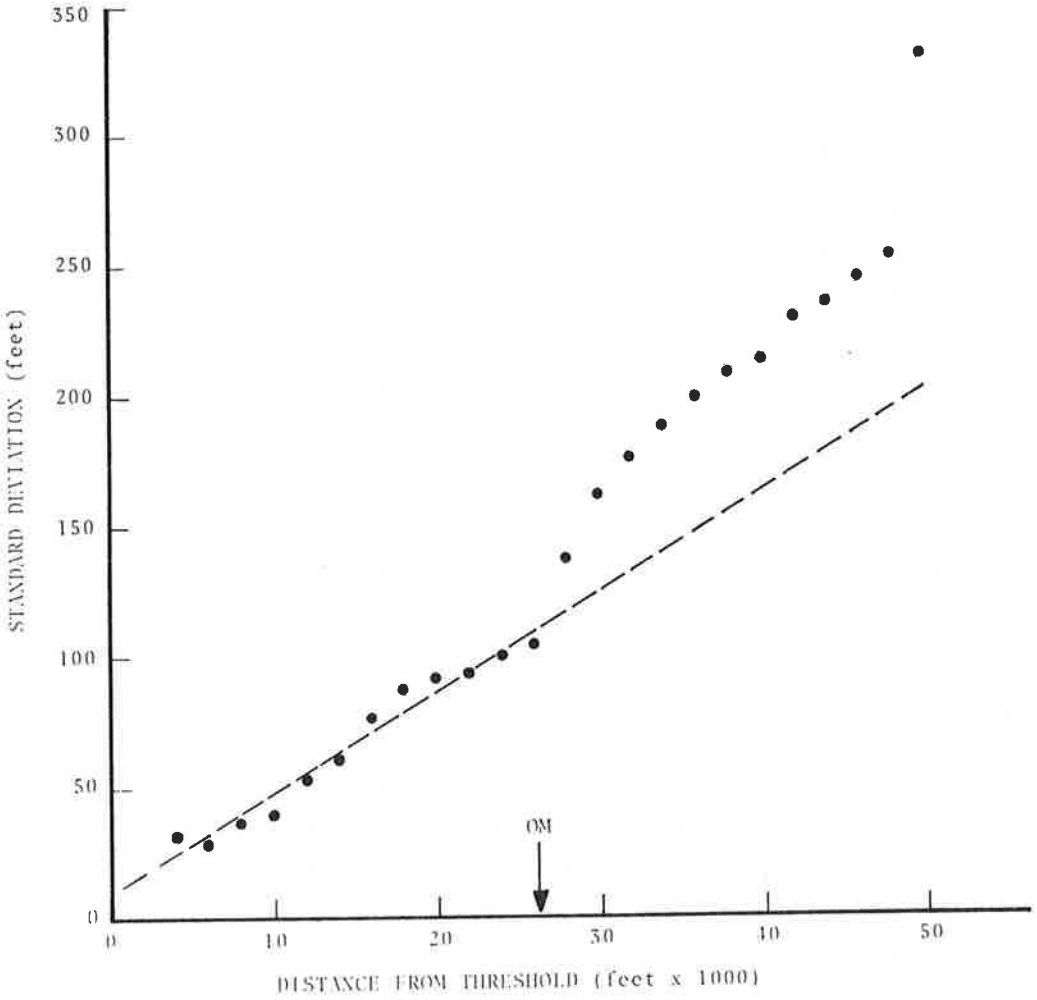

FIGURE 10. VERTICAL NAVIGATION ERRORS

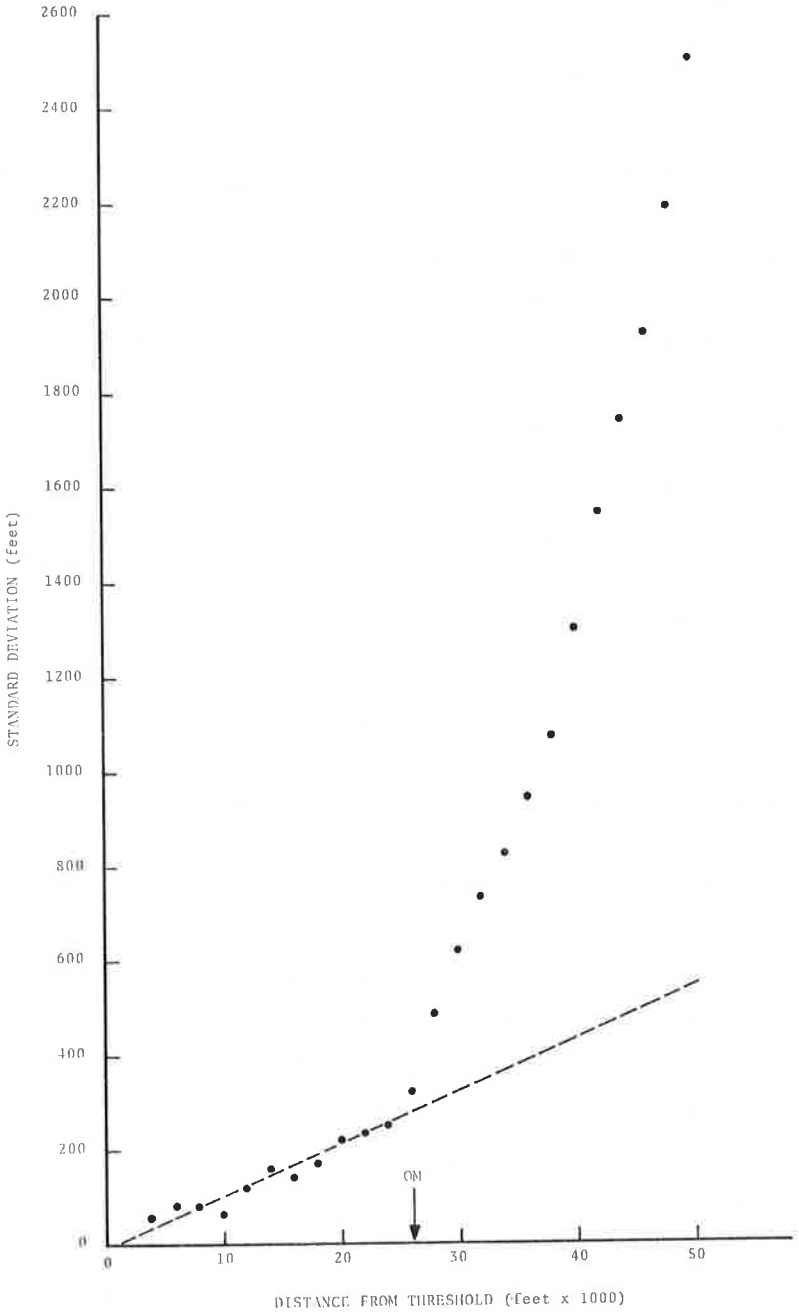

FIGURE 11. HORIZONTAL NAVIGATION ERRORS

nautical miles) from the runway threshold for the measurements). The equations for the standard deviation are:

$$\sigma_y = 0.0112L_T - 9.4206,$$
$$\sigma_z = 0.0039L_T + 9.8049, \qquad (26)$$

where L_T is the distance (in feet) from the runway threshold. The correlation coefficients of the least-squares fit to σ_y and σ_z are 0.98 and 0.96, respectively. It is assumed that equations (26) may be used for any ILS runway between the runway threshold and the OM (4 to 7 nautical miles from the runway threshold).

4.3 VORTEX-DESCENT RATE MODEL

To calculate the vertical-encounter probability (Eq. (21)), the vortex-descent distance D and the standard deviation σ_D are required. The state of knowledge on vortex-descent is oftentimes misinterpreted; Appendix B reviews the existing data.

Vortex-descent rates used herein were extracted from laser-Doppler-velocimeter measurements taken at the John F. Kennedy International Airport (Refs. 27-29). Initial descent rates were extracted from the vortex-track data given in Reference 28; only initial descent rates were extracted as the vortices entered and became dominated by ground effect within about 20 seconds. As discussed in Reference 30 and in Appendix B, the initial descent rate is a good description of the vortex descent for the first 30 to 60 seconds of the life of a vortex outside of ground effect. Catastrophic decay (leading to the early demise of a vortex) and atmospheric stability affect the descent rate, but are neglected.

Figure 12 shows B-747 initial descent rates extracted from the Kennedy data. The mean initial descent rate was found to be 6.3 ft./sec with a standard deviation of 1.9 ft/sec. (For the B-707, the mean initial descent rate was 5.2 ft/sec with a standard deviation of 1.8 ft/sec.) Although the standard deviations are relatively large, most of contribution to the large deviations came

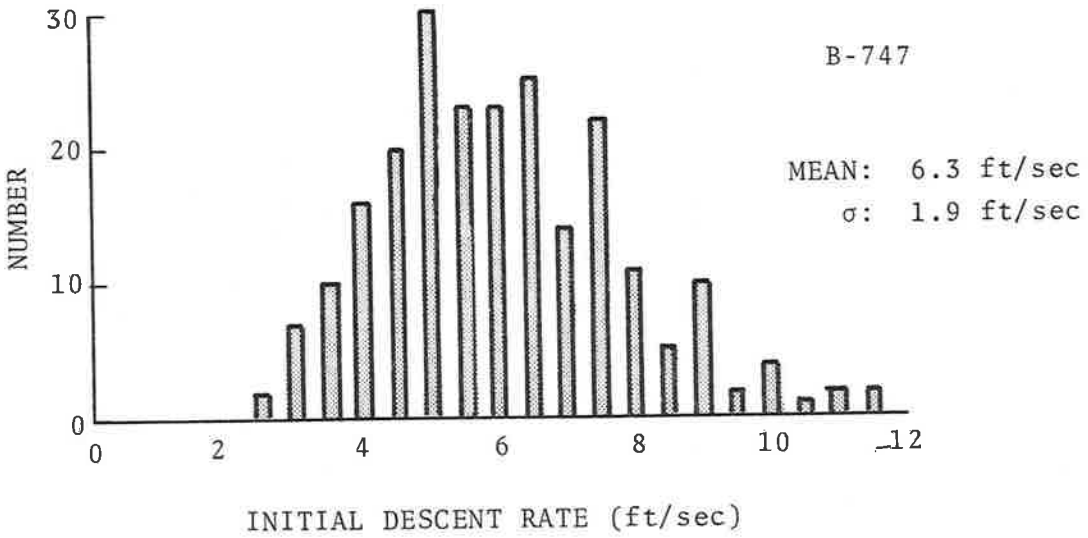

FIGURE 12. INITIAL DESCENT RATE OF B-747 VORTICES

from the relatively large number of cases with high descent rates.

It was not possible to justify extracting initial descent rates for other aircraft types using the Kennedy data as there were too few cases (there were at least 100 cases each of the B-707 and B-747). Assuming elliptic wing loading, the initial vortex circulation is given by (Ref. 2):

$$\Gamma_o = \frac{4\ W_t}{\pi \rho V b_g}\ , \tag{27}$$

where W_t is the gross weight of the aircraft, and ρ is the density of the air. The theoretical initial descent speed is then given by:

$$V_D = \frac{\Gamma_o}{2\pi b_o} = \frac{8\ W_t}{\pi^3 \rho V b_g^{\ 2}} \tag{28}$$

($b_o = \frac{\pi}{4}\ b_g$, with elliptic loading). With $\rho = 2.34 \times 10^{-3}$ slug/ft^3, the calculated initial descent rates are 5.3 and 6.8 ft/sec for the B-707 and B-747, respectively. (The values of the parameters used are given in Tables 2 and 5. The weights are the maximum landing weights.) The calculated and measured initial descent rates agree quite well: 5.3 and 5.2 ft/sec for the B-707; 6.8 and 6.3 ft/sec for the B-747. Thus, initial descent rates for other aircraft types were calculated using the assumption of elliptic wing loading, and standard deviations were selected based on the magnitude of the initial descent rates (see Table 5).

4.4 CROSS-WIND MODEL

Winds are three-dimensional motions of the air, and consist of very large to very small scale temporal and spatial variations. The variability of the wind is caused and governed by the rotation of the earth (Coriolis force), geographic characteristics (such as orographic effects), and the available solar energy reaching the

TABLE 5. VORTEX-DESCENT PARAMETERS

Aircraft Model	Maximum Landing Weight	Initial Descent Velocity	σ_D
	(lb)	(ft/sec)	(ft/sec)
B-707/120B	190,000	5.3(5.2*)	1.8*
B-707/320B	247,000	5.5	1.8
B-727/100	142,500	6.6	1.9
B-737/100	101,000	6.5	1.9
B-747/200B	564,000	6.8(6.3*)	1.9*
DC-8/20	199,500	4.9	1.8
DC-8/62	240,000	5.7	1.8
DC-9/20	93,400	6.2	1.9
DC-10/30	403,000	7.0	1.9
L-1011/200	368,000	7.0	1.9
PA-28-180	3,600	4.0	1.7
Learjet-25	13,300	7.5	1.9

*Measured values.

earth's atmosphere and surface which is further a function of the time of day. Other dominating factors causing wind variability are land-sea influences, terrain type, elevation, available water, vegetation, and many additional natural and artificial constituents.

Constructing a wind model, especially one which implies a correlation between surface-wind measurements and the winds at altitudes above ground level in excess of 1000 feet, is difficult. Adequate wind models exist for the planetary boundary layer (between the ground and about 500 feet in altitude) as the turning of the wind with height is relatively small. Above the planetary boundary layer, little is known about how to relate the winds with surface measurements. However, the analysis of the VAS does not require a complete wind model, only one which probabilistically relates winds at the surface in "green light" conditions to the winds aloft.

Cross winds play a role in preventing vortex encounters during approaches to landing. The larger the cross-wind component, the less likely that a vortex encounter can occur. For small or zero cross-wind components, vortex encounters are prevented by the dissipation of the vortices, by the vertical displacement of the vortices, and by the relative flight paths of the aircraft.

The analytical model discussed in Section 4.1 requires a cross-wind p.d.f. to calculate the probability of a hazardous-vortex encounter. The cross-wind model is presented in Appendix C and is summarized below. Justification, if any, for the model awaits the collection of wind data (Volume II of this report). Existing data (discussed in Appendix C) do support the model even though the derivation of the model contains some inconsistencies.

The cross-wind model was formulated using winds measured by aerovanes mounted on a 1500-foot tower (Ref. 31). The cross-wind p.d.f., $p_c(w_c)$, in terms of the mean wind speed aloft μ may be written (Appendix C):

$$p_c(w_c) = \frac{1}{\mu} e^{-\pi w_c^2/4\mu^2}$$

for $w_c \geq 0$. Using μ=18.6 knots (one of the observed values in Ref. 31),

$$p_c(w_c) = 0.0538e^{-0.00227w_c^2}. \quad (29)$$

The VAS measures wind velocity 50 feet above the ground at the approach end of the active runway. The algorithm for determining "vortex safe" or "green light" conditions in the MM to runway threshold region relies on the one-minute average wind vector observation lying outside an ellipse (Fig. 5) that is aligned with the runway coordinate system. The calculation of surface cross-wind probability density is straightforward, involving the development of a conditional surface wind rose (based on the wind vector not being inside the VAS ellipse), and then, performing the variable transformation on the conditional surface wind rose.

The procedure is less clear for inferring a cross-wind p.d.f. aloft given a "red light/green light" observation of surface winds. Little information exists that can be brought to bear on this problem. Generalizations can be made: steering or veering of the wind occurs with increasing altitude, and wind speed increases with altitude. Specific data that could be used to define an analog to the surface ellipse for use at altitude do not appear to exist.

In the absence of such specific detail, a simple statement is postulated: if the VAS registers a "green light," the winds aloft are also outside of the VAS ellipse. There are several questions and additional assumptions implicit in the use of this postulate (discussed at length in Appendix C). However, limited data collected at O'Hare appear to be in agreement with the postulate. The verification of this correspondence is one of the subjects of Volume II. Figure 13 shows the two p.d.f.'s: $p_c(w_c)$ (equation (29)) for the cross-wind magnitude with no wind information from the VAS, and $p_c(w_c/GL\alpha)$ for the cross-wind magnitude when the VAS registers a "green light."

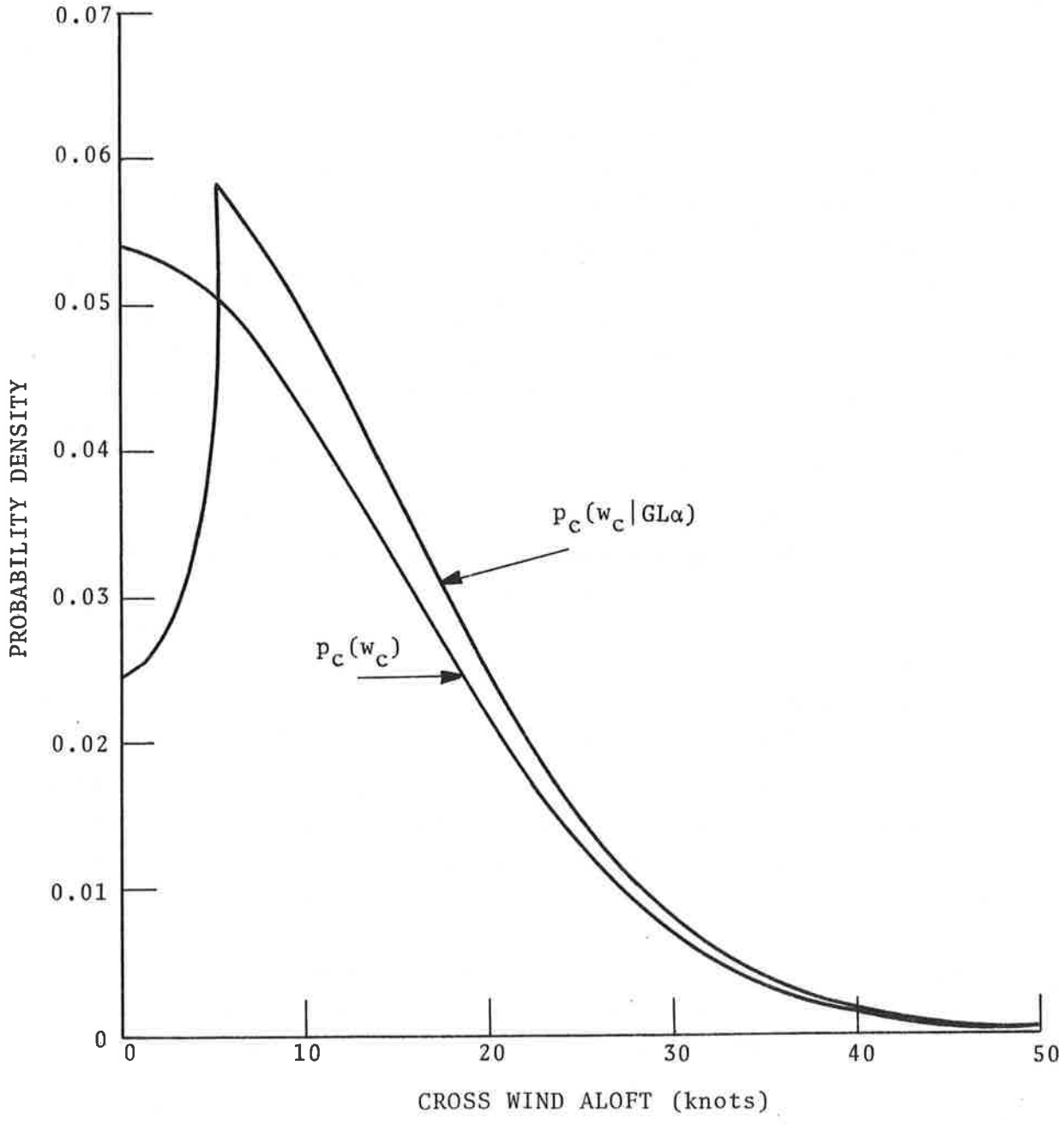

FIGURE 13. CROSS-WIND PROBABILITY DENSITY FUNCTIONS WITHOUT ($p_c(w_c)$) AND WITH ($p_c(w_c/GL\alpha)$) VAS INFORMATION

4.5 ANALYTIC MODEL

Sections 4.1 through 4.4 describe an analytic model for calculating the probability of a hazardous-vortex encounter. A computer routine for doing the calculations is given in Appendix D. The steps in the calculations are summarized below.

The initial vortex strength is calculated from:

$$\Gamma_o = mb_e + \Gamma_{int},$$

where b_e is the wingspan of the vortex-encountering aircraft. The decay of the vortex strength is given by (equation (8))

$$\frac{\Gamma}{\Gamma_o} = 9.58 \left(\frac{d}{b_g} \frac{C}{A} L\right)^{-1}$$

for $d > 47.9\ b_g$. The hazard radius is then calculated:

$$R_o = \frac{\Gamma}{2\pi f p U} .$$

If $R_o \geq b_e/2$, then a hazardous-vortex encounter is possible depending on the location of the following aircraft with respect to the vortices. The horizontal encounter probability is (equation (20))

$$P_{HE} = \frac{1}{2}\left\{ \operatorname{erf}\left(\frac{W-L + (R_o - b_e/2)}{\sqrt{2}\,\sigma_H}\right) - \operatorname{erf}\left(\frac{W-L - (R_o - b_e/2)}{\sqrt{2}\,\sigma_H}\right)\right\},$$

the vertical encounter probability is (equation (21))

$$P_{VE} = \frac{1}{2}\left\{ \operatorname{erf}\left(\frac{D-G + \sqrt{R_o^2 - b_e^2/4}}{\sqrt{2}\,\sigma_V}\right) - \operatorname{erf}\left(\frac{D-G - \sqrt{R_o^2 - b_e^2/4}}{\sqrt{2}\,\sigma_V}\right)\right\},$$

so that the probability that the vortex-encountering aircraft is within the hazardous-vortex encounter cross section is:

$$P_e = \int_{-\infty}^{\infty} P_{HE}\, P_{VE}\, p_w(w)\, dw,$$

where $p_w(w)$ is the p.d.f. for the wind. The probability of a hazardous-vortex encounter is:

$$P_{he} = P_h P_e = \begin{cases} 0 & d > d_o, \\ P_e & d \leq d_o, \end{cases}$$

where (equation (14)):

$$d_o = \frac{15.2}{f\hat{p}U} \frac{b_g}{b_e} (mb_e + \Gamma_{int}), \qquad \frac{dC_L}{b_g A} \geq 9.58.$$

5. RESULTS OF SAFETY ANALYSIS FOR ALL AIRCRAFT

In this section, the results of the VAS safety analysis are presented. The analytical process consists of seven fundamental steps:

1. Calculation of the ordinary risks accepted in the present system using 3/4/5-nautical-mile spacings.
2. Establishment of a baseline probability as a maximum acceptable risk.
3. Calculation of the new risks to be expected when using 3-nautical-mile spacings during VAS green-light conditions.
4. Formulation of operational guidelines to maintain the risks with VAS-reduced spacings at or below the baseline risk.
5. Sensitivity analysis on the conclusions to determine if the conclusions are adversely affected by potential errors in the models and/or parameters.
6. Comparison of the conclusions to the available body of physical evidence of risk and acceptability.
7. Formulation of a refined set of operational guidelines and recommended actions.

The model presented in Section 4 is used for the calculations. The fraction f of the roll-control capability (Section 4.1.2) is taken as 0.378.

5.1 RISKS IN PRESENT SYSTEM

In any probability analysis dealing with small numbers, it is important to interpret the results in a meaningful way. Because of the many conservative assumptions enacted in defining the model and its parameters, the absolute probabilities themselves have limited meaning. Comparison among the various probabilities are expected to be meaningful however (possible exception is discussed in Sec. 5.2).

The largest probability for a hazardous-vortex encounter at the current separations occurs for the PA-28 following 3 nautical miles behind the DC-8. Table 4 shows that the hazard radius shrinks

to zero at a separation of 6 nautical miles. (Note that this discussion refers to the region near the OM where the separation standard is 3 nautical miles; the separation standard calls for 4 nautical miles near the MM due to the possibility of a vortex stalling in ground effect.) All probabilities will be compared with the DC-8/PA-28 probability of a hazardous-vortex encounter.

Table 6 shows the risks at the OM for the various aircraft pairs at the current 3/4/5 separations relative to the risk for the DC-8/PA-28 pair. Most of the entries are zero. According to the model, the risk of a hazardous-vortex encounter is zero for the airliners following other airliners at the current separations and nonzero only for the Small category of aircraft following certain airliners. However, no accident is known to have been caused by vortices when any of the respective aircraft were separated by the appropriate 3, 4 or 5 nautical miles.

5.2 BASELINE PROBABILITY

The situations represented by the nonzero probabilities in Table 6 (the PA-28 5 nautical miles behind a B-747, DC-10, L-1011, DC-8H, or B-707H; the Learjet 5 nautical miles behind a B-747; the PA-28 3 nautical miles behind a DC-8, B-707, or B-727; and the Learjet 3 nautical miles behind a DC-8 or B-707) occur frequently in the vicinity of the OM. Since these situations occur frequently (particularly in VFR conditions) and with nonzero probability of a vortex hazard, these risks are considered to be acceptable as no hazardous-vortex encounters are known to have occurred. Reference 1 (and Section 2) examined these situations in great detail, and found no apparent hazard.

The baseline probability, N, is defined as the largest of the nonzero probabilities (DC-8/PA-28). If the probability of a vortex encounter for any leader/follower pair is found to be less than or equal to N, the situation will be assumed to be safe. If the probability of a hazardous-vortex encounter were greater than N, it would not necessarily mean that a hazardous condition existed--it would mean, however, that a vortex encounter might occur, and

TABLE 6. RISKS FOR THE CURRENT 3/4/5 SEPARATIONS RELATIVE TO THE DC-8/PA-28 PAIR

Lead Aircraft	Trail Aircraft											
	B-747	DC-10	L-1011	DC-8H	B-707H	DC-8	B-707	B-727	DC-9	B-737	Learjet	PA-28
B-747	0.0	0.0	0.0	0.0	0.0	0.0	0.0	0.0	0.0	0.0	0.003	0.058
DC-10	0.0	0.0	0.0	0.0	0.0	0.0	0.0	0.0	0.0	0.0	0.0	0.004
L-1011	0.0	0.0	0.0	0.0	0.0	0.0	0.0	0.0	0.0	0.0	0.0	0.002
DC-8H	0.0	0.0	0.0	0.0	0.0	0.0	0.0	0.0	0.0	0.0	0.0	0.002
B-707H	0.0	0.0	0.0	0.0	0.0	0.0	0.0	0.0	0.0	0.0	0.0	0.002
DC-8	0.0	0.0	0.0	0.0	0.0	0.0	0.0	0.0	0.0	0.0	0.163	1.0
B-707	0.0	0.0	0.0	0.0	0.0	0.0	0.0	0.0	0.0	0.0	0.007	0.454
B-727	0.0	0.0	0.0	0.0	0.0	0.0	0.0	0.0	0.0	0.0	0.0	0.053
DC-9	0.0	0.0	0.0	0.0	0.0	0.0	0.0	0.0	0.0	0.0	0.0	0.0
B-737	0.0	0.0	0.0	0.0	0.0	0.0	0.0	0.0	0.0	0.0	0.0	0.0
Learjet	0.0	0.0	0.0	0.0	0.0	0.0	0.0	0.0	0.0	0.0	0.0	0.0
PA-28	0.0	0.0	0.0	0.0	0.0	0.0	0.0	0.0	0.0	0.0	0.0	0.0

the degree of hazard could depend on how much larger the probability was compared with N (and to the actual roll recovery capability of the following aircraft). Also, it does not mean that 1 in N^{-1} landings of a PA-28 behind a DC-8 will result in a hazardous-vortex encounter; the model and its parameters have been purposely chosen to be conservative.

There is, however, a possible problem with comparing two conservative estimates. Absolute conservatism of estimates of two elements does not necessarily imply conservation in their comparisons. For example, see Fig. 14. Consider a proposed case where reduction to 3 nautical miles under VAS-green conditions is recommended. Both the estimated baseline and the estimated proposed probabilities of a hazardous vortex encounter are conservative estimates of the actual baseline and proposed probabilities. Based on these estimates one would claim that the hazard associated with the proposed case is below that associated with the baseline case (because proposed/estimated < baseline/estimated) and hence the proposed case is acceptable. However, it is possible that the actual probability of the proposed case is greater than the actual probability of the baseline case (as is shown in Fig. 14), and hence the situation represented by the proposed case is more hazardous than the baseline case. To determine the consequences (if any) of the situation just described requires detailed analysis and is deferred to Volume III.

If the reader is concerned about the possible problem and its consequences, the analysis in Section 6 avoids the problem by introducing a VAS which excludes reduced separations for the Small-category aircraft. The remainder of Section 5 assumes that the problem is resolved in favor of the analytical approach used herein. Even if the problem of comparing conservative estimates does apply in this analysis, most of the results in this section will not be altered.

5.3 RISKS WITH VAS

The probabilities of a hazardous-vortex encounter are shown

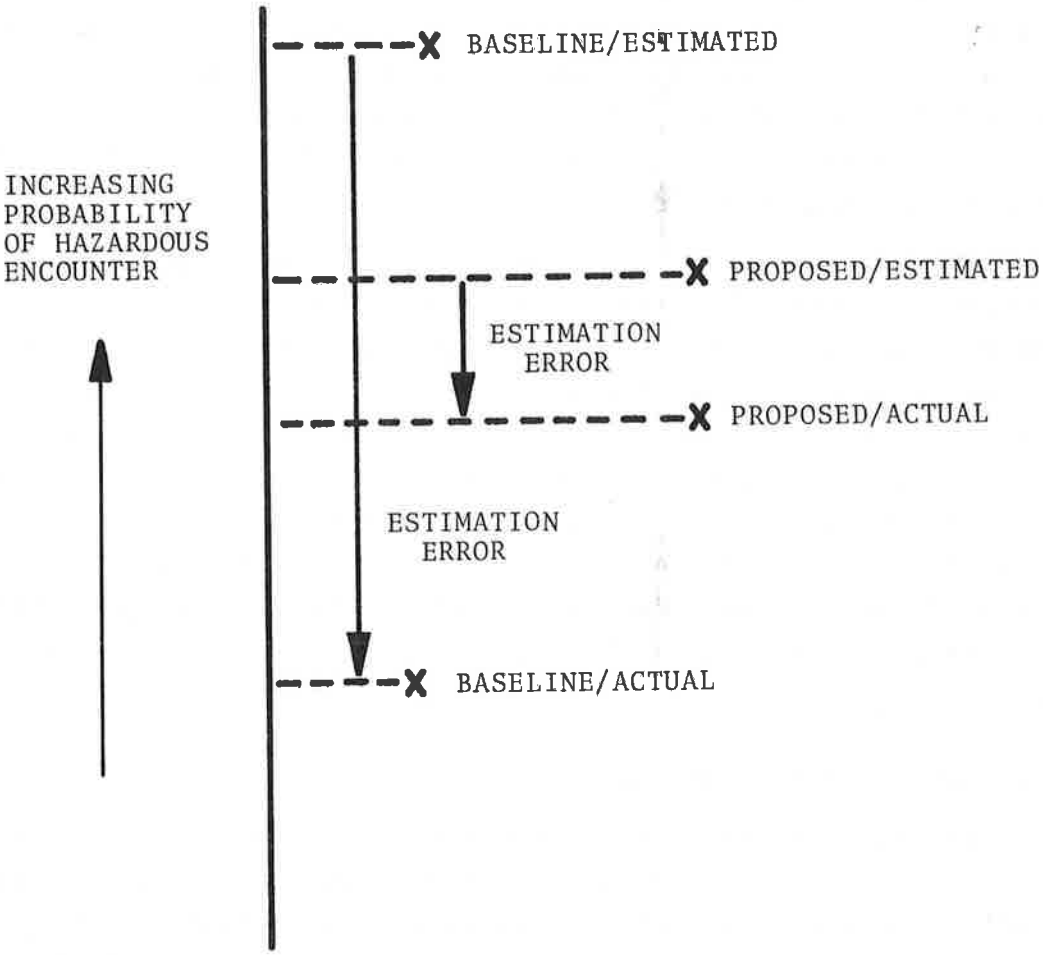

FIGURE 14. ILLUSTRATION OF POSSIBLE PROBLEM OF COMPARING TWO CONSERVATIVE ESTIMATES

in Table 7 for VAS-green conditions. Here, all the aircraft are spaced at 3 nautical miles, and the probabilities are given relative to N, the baseline value. Only one entry exceeds the baseline probability; a value of 1.8N is found for the PA-28, 3 nautical miles behind the B-747. This probability reduces to 1.0N for a separation of 3.5 nautical miles. Figure 15 shows how the probability (in units of N) varies as a function of the distance of the PA-28 from the runway threshold, given that the PA-28 is 3 nautical miles behind the B-747 in VAS-green conditions. If the OM is more than 29,000 feet (4.7 nautical miles) from the runway threshold, then the probabilities can exceed the baseline value.

It is important to reiterate that decreased separations will be permitted only when the VAS displays a green light. During VAS-red conditions, the model indicates probabilities of a hazardous vortex encounter in excess of N. Because of the difference in flight speeds, it is unlikely that many of the aircraft pairs can maintain a 3-nautical-mile separation (e.g., B-747/PA-28). The uniform 3-nautical-mile separation is intended only inside the OM. In most situations the aircraft are in trail with the present standards well before reaching the OM so the minimum separations obtainable using VAS will be approximately 3, 3½, and 4½ nautical miles.

5.4 OPERATIONAL GUIDELINES

To maintain the risks with VAS-reduced spacings at or below the baseline risk N, certain operational guidelines are required. Table 7 shows that nonzero probabilities are obtained for the Small category of aircraft following most of the airliners. Reduced separations are permissible during VAS-green conditions as the vortices of the preceding aircraft are descending and/or translating out of the path of the following aircraft. There may be problems if these Small aircraft (as well as the B-727, DC-9, and B-737 behind a B-747) are turned on at, or allowed to descend to, lower altitudes than the leading aircraft. During the trails of the VAS, the Small category of aircraft should be positioned at 3

TABLE 7. RELATIVE RISKS FOR THREE-NAUTICAL-MILE SEPARATIONS DURING VAS-GREEN CONDITIONS

Lead Aircraft	Trail Aircraft											
	B-747	DC-10	L-1011	DC-8H	B-707H	DC-8	B-707	B-727	DC-9	B-737	Learjet	PA-28
B-747	0.0	0.0	0.0	0.0	0.0	0.0	0.0	0.104	0.545	0.380	0.664	1.826
DC-10	0.0	0.0	0.0	0.0	0.0	0.0	0.0	0.0	0.0	0.0	0.087	0.450
L-1011	0.0	0.0	0.0	0.0	0.0	0.0	0.0	0.0	0.0	0.0	0.057	0.402
DC-8H	0.0	0.0	0.0	0.0	0.0	0.0	0.0	0.0	0.0	0.0	0.045	0.401
B-707H	0.0	0.0	0.0	0.0	0.0	0.0	0.0	0.0	0.0	0.0	0.046	0.528
DC-8	0.0	0.0	0.0	0.0	0.0	0.0	0.0	0.0	0.0	0.0	0.149	0.914
B-707	0.0	0.0	0.0	0.0	0.0	0.0	0.0	0.0	0.0	0.0	0.006	0.415
B-727	0.0	0.0	0.0	0.0	0.0	0.0	0.0	0.0	0.0	0.0	0.0	0.049
DC-9	0.0	0.0	0.0	0.0	0.0	0.0	0.0	0.0	0.0	0.0	0.0	0.0
B-737	0.0	0.0	0.0	0.0	0.0	0.0	0.0	0.0	0.0	0.0	0.0	0.0
Learjet	0.0	0.0	0.0	0.0	0.0	0.0	0.0	0.0	0.0	0.0	0.0	0.0
PA-28	0.0	0.0	0.0	0.0	0.0	0.0	0.0	0.0	0.0	0.0	0.0	0.0

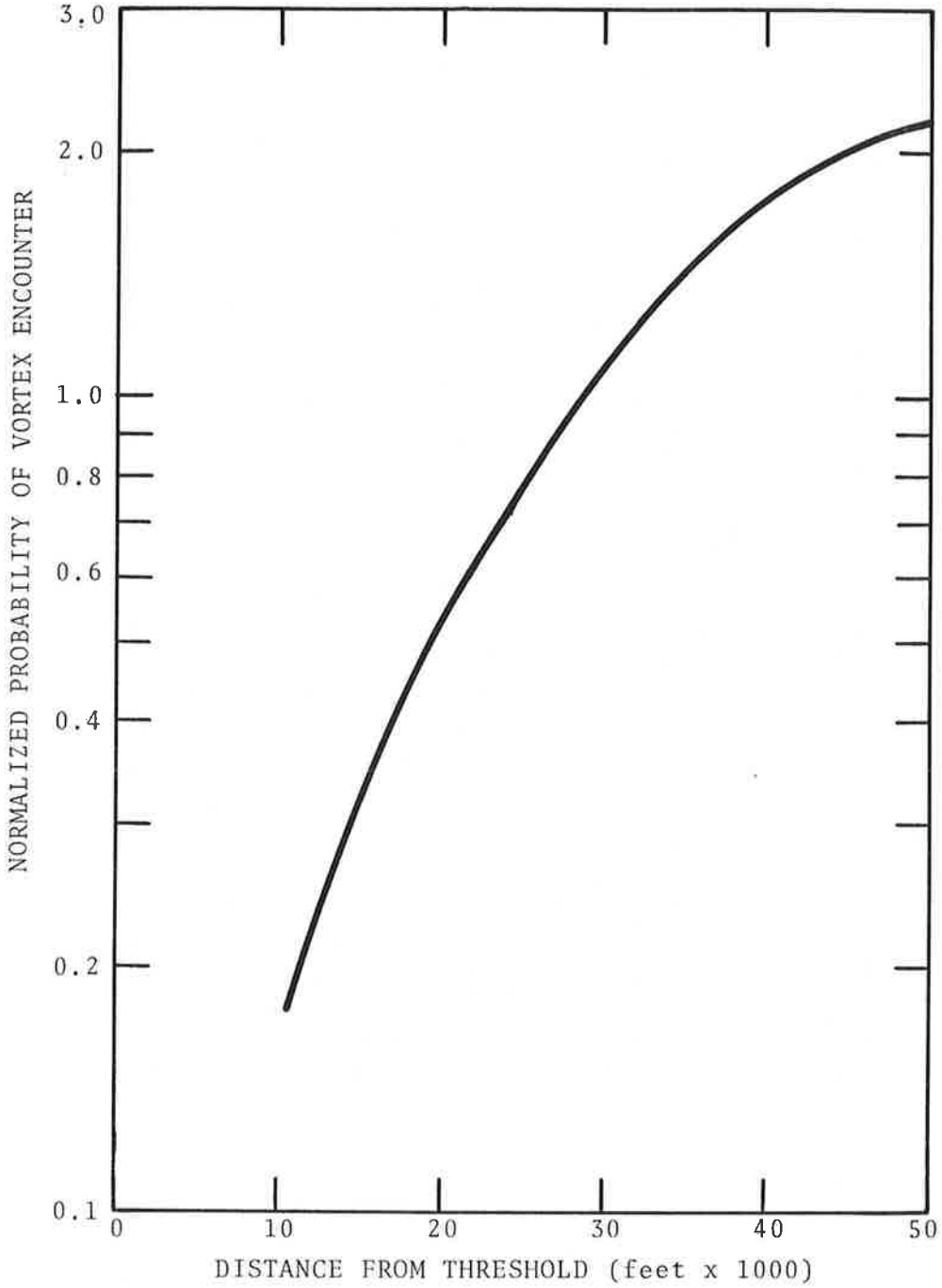

FIGURE 15. NORMALIZED PROBABILITY OF VORTEX ENCOUNTER FOR A PA-28 THREE NAUTICAL MILES BEHIND A B-747 UNDER VAS-GREEN CONDITIONS AS A FUNCTION OF THE DISTANCE OF THE PA-28 FROM THE RUNWAY THRESHOLD

nautical miles behind other categories only if both aircraft are turned on the ILS at or beyond the OM, and both are making precision (i.e., localizer and glide slope) approaches. Because of the generally slower speeds of the Small aircraft, prohibiting short finals will cause the 3-nautical-mile separation at the OM to increase gradually to 4 nautical miles at the MM.

Although the probability of a vortex encounter for the B-747/PA-28 pair at 3 nautical miles is found to be in excess of the baseline probability N, the conservative assumptions throughout the analysis should preclude the necessity for segregating the PA-28 (and other civil single-engine or light-twin aircraft) from following the B-747 at 3 nautical miles. The problem (if, indeed, there is a problem) exists only in the vicinity of the OM where the PA-28 will have ample room to maneuver.

5.5 SENSITIVITY ANALYSIS

A sensitivity analysis has been done to determine the effect on the normalized encounter probability and f of possible errors in the models and/or parameters. Details are presented in Appendix E. Although the probability values do change depending on the details of the wind, navigation, vortex-descent, vortex decay, and roll-recovery capability models, the results and conclusions concerning the safety of the VAS, however, do not appear to require alteration. All the calculations were done with the following aircraft at the OM as this is the location at which the encounter probability is maximized. The OM was assumed to be 7 nautical miles from the runway as this also maximizes the probability.

5.6 OTHER EVIDENCE

Other evidence was examined to look for support or contradiction of the conclusions of the safety analysis. Three independent observations lend credence to the analytic results: wake vortex incident reports analyzed by the British Civil Aviation Authority, accident data, and VFR spacings.

The Civil Aviation Authority of Great Britain has been

analyzing wake vortex incidents (no accidents) reported in the United Kingdom since 1972 (Refs. 6-8 and Section 3.1). Through September 1977, 353 incidents have been tabulated. When the documented (73) incidents occurring between runway threshold and an altitude of 1000 feet above ground level were correlated with the wind measured at a height of 30 feet (the centerfield sensor at the London Heathrow International Airport), only 3 incidents were found when the winds exceeded the VAS wind criterion in Figure 5 (Refs. 7 and 8). All severe incidents (reported bank angles in excess of 30 degrees) occurred in wind conditions well inside the ellipse (VAS-red conditions). The three incidents which occurred in wind conditions outside the ellipse (VAS-green conditions) were within 2 knots of the wind criterion. The 2 incidents farthest outside the ellipse occurred at an altitude of 1000 feet (one had a reported bank angle between 10 and 30 degrees, and the other less than 10 degrees). The third incident occurred with centerfield winds just outside the ellipse (less than 0.25 knots from the boundary) and reported a roll excursion of less than 10 degrees. The Heathrow centerfield winds were averaged over a 10-minute period and the results do not contradict the VAS concept and the safety analysis. The VAS, however, uses 1-minute-averaged winds.

An analysis of vortex-caused accidents (Ref. 1 and Section 2.2.1) noted that those accidents which occurred between the MM and OM have distinct characteristics. The vortex encounters seemed to be random, and occurred only because the Small aircraft were approaching at a low altitude with poor lateral navigation. These aircraft apparently would not have encountered vortices if the aircraft were on a precision approach.

The chance of a vortex encounter increases as interarrival aircraft separations decrease. VFR operations oftentimes are conducted with interarrival separations which are less than the IFR minimum separations. But these smaller spacings are flown safely in VFR. Of course, VFR and IFR operations are not the same; in VFR the pilot accepts more risk as he is more aware of his environment. The VAS proposes a 3-nautical-mile minimum and only

during specific wind conditions.

5.7 CONCLUSIONS AND RECOMMENDED ACTIONS

The VAS as described herein is intended for independent single-runway landings. Closely spaced parallel runways and runway intersections will require a case-by-case examination to determine how VAS should operate. For example, an 8-knot cross wind indicates VAS-green conditions, and separations may be reduced to a uniform 3 nautical miles. However, if the vortices are blown toward a closely spaced parallel runway, the wind criterion that insures vortices cannot pose a threat to an aircraft landing on the same runway may not insure that the threat is nonexistent for an aircraft landing on a downwind parallel runway. Either the wind criterion will need to be modified or operational restrictions will need to be enforced to prevent a hazardous condition.

The analysis has not considered other than straight-in approaches that might occur under IFR (e.g., sidestep or circling approaches). These other approaches are not necessarily unsafe with the VAS; indeed, such extensions need to be done at some future time, but the analysis herein addressed only straight-in IFR approaches.

The results of the analysis show that, subject to verification of several assumptions, uniform 3-nautical-mile separations between the runway threshold and the outer marker may be used safely when: (1) the VAS registers a green light, and (2) all aircraft are restricted to an ILS approach between the OM and touch down. Short finals and VOR or localizer approaches with reduced separations should not be permitted (short finals are precluded in IFR); the flight paths of these non-precision approaches act to increase the probability of a vortex hazard. The normal vortex descent and translation with the wind which decrease the hazard probability for precision approaches can move the vortices into the path of an aircraft on a short final or on a VOR or localizer approach. Extensive data have demonstrated the safety in the threshold to middle marker region; probability analysis

based on state-of-the-art knowledge of vortex behavior extends the safe region from middle to outer marker. For many of the aircraft pairs a simplified analysis is appropriate that avoids the use of unverified assumptions (see Section 6).

The results herein are derived from an analytical model. A data-collection program is underway to verify the mathematical analysis. Appendix F describes the data-collection effort at O'Hare. Until the confirmation tests are completed, the analysis is only as good as the model. However, the model is conservative and has been shown to be relatively insensitive to the assumed parameters.

When the VAS indicates reduced separations may be used, the state of knowledge of vortex behavior is consistent with safely applying the reduced separations out to the outer marker. If the tests at O'Hare confirm the model predictions, the FAA should be justified in commissioning the VAS as a tool for decreasing delays at the major airports.

6. SAFETY ANALYSIS FOR HEAVY/HEAVY AND HEAVY/LARGE

The two main unresolved issues of the approach presented in Sections 4 and 5 were the wind model (Section 4.4 and Appendix C) and the potential problem related to the comparison of two conservative estimates (Section 5.2). If, however, the VAS were to be used to reduce only the Heavy/Heavy and Heavy/Large standards (omitting the Heavy/Small and Large/Small cases), then the two unresolved issues will not be considered in the safety analysis as will be shown in this section. The discussion below addresses the safety of 3-nautical-mile separations for jetliners during VAS-green conditions, and then expands the analysis to include all Large aircraft.

6.1 HAZARD MODEL

In Section 4.1.1, it was argued that a potentially hazardous-vortex encounter can occur only if $R_o \geq b_e/2$ and if a following aircraft were fully located within the circle defined by the hazard radius R_o. The probability of a hazard is defined as zero when

$$R_o < b_e/2.$$

If one accepts this definition, then for all those pairs of aircraft with $R_o < b_e/2$ at 3 nautical miles, the standards can be reduced. The two unresolved issues do not apply to these cases. Using $f = 0.378$ (one-half the maximum roll authority required safely to fly the current separation standards at the assumed speeds) and equation (14) (or equation (12) if necessary), the distances at which R_o becomes smaller than $b_e/2$ are calculated and presented in Table 4. Most of the calculated distances are less than 3 nautical miles; for these aircraft pairs, the model indicates that the separation standards can be set at 3 nautical miles between the outer and middle marker with or without the VAS. The VAS will be required to indicate when 3 nautical miles may be used between the middle marker and the runway threshold however. The Small-category aircraft following Heavy-and Large-category

aircraft and the B-727, B-737, and DC-9 following the B-747 have yielded calculated distances in excess of 3 nautical miles. It will be shown that the condition of $R_o < b_e/2$ can be expanded to embrace the B-727, B-737, and DC-9 following the B-747, and that the VAS can be applied to the operations of Heavy/Heavy and Heavy/Large combinations of aircraft.

Recalling equations (5) and (8), the hazard radius is

$$R_o = \frac{\Gamma}{2\pi f \hat{p}\ U} \qquad (5)$$

$$= \frac{9.58\ \Gamma_o}{2\pi f \hat{p}\ U}\left(\frac{d}{b_g}\frac{C_L}{A}\right) - 1 \quad \text{for } dC_L/b_g A \geq 9.58.$$

Introducing equation (13) and rearranging,

$$R_o = \frac{9.58\ (A/C_L)}{f \hat{p}\ U}\ \frac{\left(mb_e + \Gamma_{int}\right) b_g}{2\pi d} \ .$$

The following relationships can be inferred from the above equation:

a. R_o increases if f, $\hat{p}$, or U decreases.
b. R_o increases if A/C_L or the estimate of vortex decay (indicated by 9.58, the breakpoint of the decay curve--Fig. 6) increases.

For a given aircraft pair, b_g, b_e, and d are constants. Since m and Γ_{int} are selected as ultimate or maximum values (Appendix A), they may be considered constants. A $\hat{p}$ of 0.06 (airliners) or 0.08 (general-aviation aircraft) is a lower bound (Section 4.1.1), so that it also may be considered a constant. The 9.58 value is an upper limit on the decay parameter (Fig. 6) except, possibly, for the B-727. For the calculations to follow, 12.0 is used for the B-727 decay parameter (the suspect B-727 data in Fig. 6 are included), and 9.58 is used for all other vortex-generating or lead aircraft.

Thus the vortex decay parameter may also be considered a constant.

Setting R_o equal to $b_e/2$,

$$f = \frac{(A/C_L)}{U} \frac{\left(mb_e + \Gamma_{int}\right)b_g}{\pi \hat{p}\, db_e} \quad (9.58) \quad .$$

Table 3 is obtained by setting d equal to the current separation standards; Table 8 is obtained by setting d equal to 3 nautical miles--many of the entries are the same as in Table 3.

The largest f value in Table 8 is 0.458 for the B-747/DC-9 pair. If this f value is acceptable (i.e., assuming the aircraft ever finds itself in a vortex, it will require no more than 46 percent of an aircraft's roll-control authority to counteract the rolling motion of a vortex), then the 3-nautical-mile standard can be applied under the assumption that $R_o < b_e/2$ implies no vortex hazard. It is noted (see Table 3) that, according to the hazard model f values greater than 0.458 are required now at the current separation standards and assumed speeds for the DC-8/Learjet and for the general-aviation-type aircraft following Heavy and Large aircraft.

6.2 SENSITIVITY ANALYSIS

The purpose of this section is to examine the sensitivity of the parameters in the expression

$$f = \frac{(A/C_L)}{U} \frac{\left(\bar{m}b_e + \Gamma_{int}\right)b_g}{\pi \hat{p}\, db_e} \quad (9.58) \quad .$$

As indicated for R_o in Section 6.1, the elements of importance are (A/C_L) and U. Differentiating

$$\Delta f = \frac{\partial f}{\partial (A/C_L)} \Delta (A/C_L) + \frac{\partial f}{\partial U} \Delta U$$

TABLE 8. MAXIMUM FRACTION OF ROLL-CONTROL AUTHORITY REQUIRED TO REDUCE THE PROBABILITY OF A HAZARDOUS VORTEX ENCOUNTER TO ZERO WITH THREE-NAUTICAL-MILE SEPARATIONS

Lead Aircraft	Trail Aircraft									
	B-747	DC-10	L-1011	DC-8H	B-707H	DC-8	B-707	B-727	DC-9	B-737
B-747	0.292	0.312	0.305	0.355	0.323	0.342	0.333	0.400	0.458	0.442
DC-10	0.200	0.213	0.209	0.244	0.223	0.235	0.230	0.278	0.320	0.308
L-1011	0.193	0.207	0.203	0.235	0.213	0.227	0.220	0.265	0.303	0.293
DC-8H	0.184	0.196	0.192	0.224	0.204	0.215	0.210	0.253	0.290	0.280
B-707H	0.171	0.184	0.180	0.209	0.191	0.202	0.198	0.238	0.275	0.265
DC-8	0.167	0.181	0.179	0.208	0.190	0.201	0.198	0.244	0.284	0.275
B-707	0.174	0.185	0.181	0.210	0.191	0.202	0.197	0.235	0.268	0.259
B-727	0.178	0.189	0.185	0.215	0.195	0.207	0.202	0.241	0.274	0.264
DC-9	0.091	0.097	0.095	0.111	0.101	0.109	0.105	0.127	0.146	0.141
B-737	0.079	0.084	0.083	0.096	0.087	0.092	0.090	0.108	0.124	0.119

$$\Delta f = \frac{f}{(A/C_L)} \Delta(A/C_L) - \frac{f}{U} \Delta U \ . \qquad (30)$$

6.2.1 B-747/DC-9

Consider first the B-747/DC-9 combination as it gives the largest f value for the airliners at 3-nautical-mile separation. The maximum non-dimensional roll rate, $\hat{p}$, is assumed to be 0.06 as this is the minimum value for airliners. However, the DC-9 has considerably more lateral roll power. Reference 32 indicates that in landing configuration with rudder-fixed $\hat{p}$ varies from about 0.07 at 100 knots to 0.25 at 180 knots; with the outboard spoiler inoperative the value at 180 knots falls to 0.16. At the speed assumed in the calculations for Table 8, $\hat{p}$ is about 0.12. Thus, a more realistic value of f will be (0.458)(0.06)/(0.12) = 0.229, and the B-747/DC-9 combination no longer represents the worst-case situation (even with different speeds).

6.2.2 B-747/B-737

The B-747/B-737 pairing has yielded the second largest f value in Table 8. Aerodynamic coefficients in Ref. 33 indicate that $\hat{p}$ is about 0.10 for the B-737. Thus, a more realistic value of f is 0.265, and now the B-747/B-737 combination no longer represents a worst-case situation.

6.2.3 B-747/B-727

Since the B-747/DC-9 and B-747/B-737 pairings have been eliminated as contenders for the worst-case situation, the B-747/B-727 is next in line. The pertinent aerodynamic coefficients for determining $\hat{p}$ for the B-727 could not be obtained. Thus, f = 0.400 is taken to be the largest f value required by an airliner to fly safely 3-nautical-mile spacings between the outer and middle marker. This figure is less than some f values calculated using today's separation standards (see Table 3).

An upper bound on the uncertainty in f is found by evaluating equation (30) using the largest positive deviation in A/C_L and the

largest negative deviation in U. A/C_L is approximated by 5.0 in all calculations. A more precise value for the B-747 is 5.1 (C_L is about 1.4 for a landing B-747 (Ref. 21) and A is the wingspan divided by the mean aerodynamic chord, 195.7/27.3 = 7.2). The approach speed for the B-727 varies between about 105 and 130 knots for landing weights from operational empty weight plus reserves to maximum landing weight. Using the slowest speed,

$$\Delta f = \frac{0.400}{5.0} (5.1 - 5.0) - \frac{0.400}{205.8} (177.2 - 205.8)$$

$$= 0.008 + 0.056$$

$$= 0.064.$$

The maximum f required for 3-nautical-mile separations is f + Δf or 0.464, less than half the available roll-control power. However, f values greater than 0.464 are found for some aircraft pairs using today's standards (Table 3). This suggests that VAS-reduced separations for jetliners are safe.

6.2.4 Other Aircraft Pairs

Similarly, the remaining leader/follower combinations can be examined. However, the B-747/B-727 case discussed above leads to the largest value of f + Δf.

The argument presented herein cannot be used with following Small aircraft. The PA-28 would require f values in excess of 1.0 following the B-747, DC-8, and B-707 at 3 nautical miles as may be seen by appropriately scaling the entries in Table 3.

6.3 VAS FOR HEAVY AND LARGE AIRCRAFT

In Section 6.2, it is shown that the decay of vortices alone will permit 3-nautical-mile separations between the outer and middle markers for the airliners or transport-category jet aircraft. Using VAS-reduced spacings for a Heavy or a Large airliner following a Heavy probably can be implemented, but effectively introduces a new category for air traffic controllers to contend with (Heavy,

Large, and Small versus Heavy, Large jetliners, other Large, and Small). Although the "other Large" category aircraft operate less frequently into the large airports, it will obviously be easier for the controllers if all Large aircraft use VAS-reduced spacings. In this section, it is shown that VAS-reduced separations may be used safely by Heavy/Heavy and Heavy/Large combinations; the analysis does not depend on the unresolved issues in Section 5; namely, the wind model and the possible problem with comparing conservative probability estimates.

Given an acceptable f value, the minimum approach speeds consistent with a safe vortex encounter ($P_h = 0$) can be calculated for the various Large aircraft. However, what is an acceptable value of f? Table 3 shows that the maximum f required for the current separation standards is 0.756 for the PA-28 3 nautical miles behind a DC-8. To be conservative, a slow speed is used in those calculations for the PA-28; a more typical PA-28 speed at the outer marker is about 95 knots. Using 95 knots, f reduces to 0.519. For the purposes of this analysis, 0.519 will be used for today's separations, rather than the more conservative 0.758. Using

$$f = \frac{(A/C_L)}{U} \frac{\left(mb_e + \Gamma_{int}\right) b_g \ (9.58)}{\pi \hat{p} \ db_e} \ ,$$

a parametric equation can be found for determining the minimum flight speed U required to give f = 0.519 for the various Large aircraft. The worst-case situation is when a B-747 is the vortex-generating or lead aircraft. Selecting the B-747 specifies m, Γ_{int}, b_g, and A/C_L. With some rearranging of terms, the above equation becomes

$$U = \frac{(5.1)(9.58)(195.7)(19.56\ b_e + 1148.6)}{\pi \hat{p}(3)(60.76)(0.519) b_e}$$

$$= 0.322 \ \frac{\left(19.56\ b_e + 1148.6\right)}{\hat{p}\ b_e} \ .$$

Figure 16 shows U versus b_e for f = 0.519. The two curves are for $\hat{p}$ = 0.06 and 0.08. For a specific aircarft (e.g., b_e and $\hat{p}$), the curves show the minimum speed required to give f = 0.519; higher speeds lead to lower values of f. For those aircraft for which aerodynamic coefficients are available, the X's mark the calculated minimum U. For these aircraft, as long as the speed U is greater than or equal to the plotted value, f will be less than or equal to 0.519. The interpretation of Fig. 16 is as follows. The model (Section 4.1.1 and 4.1.2) gives a zero probability of a hazardous-vortex encounter at VAS-reduced spacings and an assumed safe f = 0.519 if, for instance, the Learjet-25 passes the outer marker with a speed of at least 90 knots and the DC-9 at least 50 knots (since DC-9s require a speed in excess of 50 knots to fly, they certainly pass the outer marker with a speed of at least 50 knots).

For those aircraft where $\hat{p}$ is not available, the minimum flight speed at the outer marker required to give P_h = 0 may be read from the appropriate curves in Fig. 16. Excluding military aircraft (fighters are designed to achieve at least $\hat{p}$ = 0.09), all the Large aircraft can be checked to find the largest minimum U. For example, after the Learjet models, the next larger wingspans are 42.3 feet for the Aerospatiale Corvette and 42.9 feet for the Dassault Falcon-10. These aircraft have a $\hat{p}$ of at least 0.08, and thus, lead to a minimum U of 111 and 110 knots, respectively. Similarly, checking each of the Large aircraft and using the appropriate $\hat{p}$ leads to a largest minimum U of 111 knots.

The calculations above have shown that VAS-reduced spacings are safe between the outer and middle marker for the airliners and for the non-airliner Large aircraft if their speeds at the OM are at least 111 knots. Since approach speeds are usually in excess of 120 knots at the outer marker, the use of VAS-reduced spacings may be applied for Heavy/Heavy and Heavy/Large combinations.

If a maximum f of 0.519 is acceptable (recall that some of today's standards reflect larger f values--Table 3), the VAS can be used to permit 3-nautical-mile separations in VAS-green conditions for Heavy and Large aircraft following a Heavy. It must be

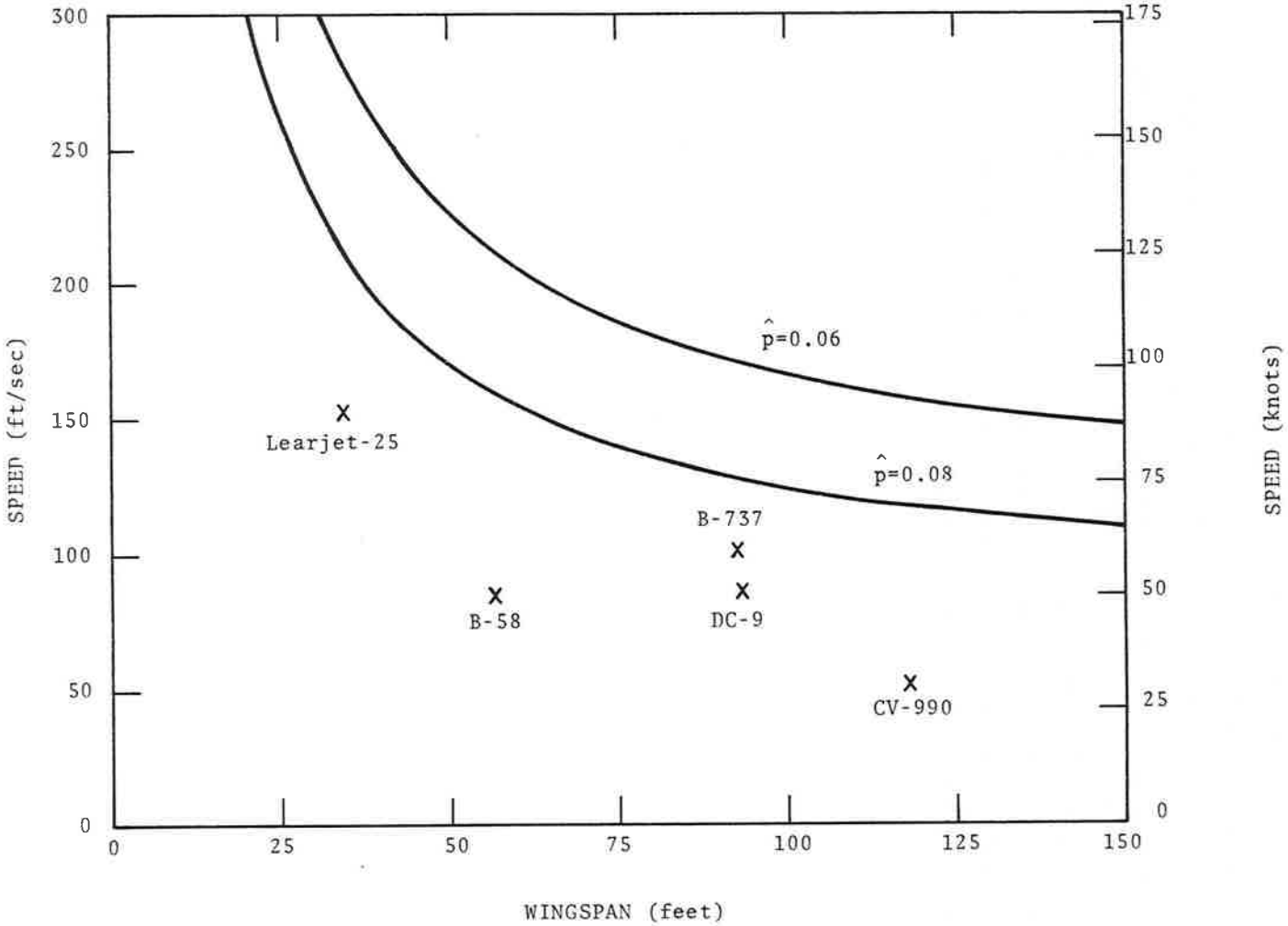

FIGURE 16. MINIMUM SPEED THAT WILL REDUCE PROBABILITY OF A VORTEX HAZARD TO ZERO ASSUMING F = 0.519. $\hat{}$ The X's indicate the minimum speed calculated using the actual p for the aircraft.

noted that a maximum f of 0.519 does not mean for instance, that every aircraft following 3 nautical miles behind a B-747 will require the use of half its roll-control power to conduct its approach. According to the model, if an aircraft ever finds itself in the vortex of a B-747 3 nautical miles ahead, the extreme upper theoretical limit on the f required will be about 0.5, within the control capability of aircraft. Pending further analyses and data collection (Volumes III and II, respectively), the Small-category aircraft, if this restricted VAS is adopted, retain their present separation standards regardless of the VAS condition.

7. SUMMARY

The discussions in Sections 5 and 6 have presented alternative safety analyses of the VAS. Both analyses used the same model of a vortex hazard (Sections 4.1.1 and 4.1.2). At this point, the two analyses follow different arguments. The restricted VAS in Section 6 notes that vortex decay is the primary mechanism outside the middle marker for avoiding hazardous-vortex encounters by Heavy and Large aircraft following 3 nautical miles behind Heavy aircraft. The probability of a hazardous-vortex encounter is zero if the parameter f, the fraction of the roll-control authority required to counter the rolling motion imposed by a vortex, is about 0.5. If this value of f is acceptable (higher values are accepted, or appear to be accepted, with today's safe separation standards), then the VAS may be used to reduce Heavy/Heavy and Heavy/Large IFR standards to 3 nautical miles between the outer marker and touchdown during VAS-green conditions.

The analysis of the safety of 3-nautical-mile separations under VAS-green conditions for all aircraft required a more detailed model. To calculate the probability of a hazardous-vortex encounter by a Small aircraft behind a Heavy or Large aircraft, decay alone was not sufficient. It was necessary to introduce a cross-wind-aloft model which contains acknowledged mathematical inconsistencies but yet seemed to correlate with limited data. The analysis also required comparing conservative estimates of hazard probabilities; a possible problem with this method was indicated. Assuming the results of the data collection (Volume II) and the detailed analysis of the use of conservative estimates (Volume III) validate the calculations in Section 5, the VAS may be safely used to reduce separations between the outer marker and touchdown for all aircraft during VAS-green conditions.

APPENDIX A

INITIAL VORTEX STRENGTH

The strength Γ of the vortices shed by the lead aircraft parameterizes the degree of hazard to the following vortex-encountering aircraft. The strength or circulation of a vortex may be used to determine quantitatively roll moments and rates an aircraft would experience if inadvertently caught in a vortex.

A Monostatic Acoustic Vortex-Sensing System (MAVSS) (Refs. 9 and 10)has been place at Chicago O'Hare on the approach to runways 14R and 32L since the summer of 1976. The function of the MAVSS is to measure a vertical profile of the vertical component of the wind. Since the vertical component of the ambient wind is zero at the ground, the vortex winds are measured with little interference from the ambient wind. A single MAVSS antenna measures the velocity profile of a vortex as it drifts over the antenna; an array of antennas samples the vortex at different times, and thereby, measures vortex decay.

The measured vertical velocity distributions are used to calculate an "effective strength" --the strength of a line vortex which will produce the same torque on an aircraft as the measured velocities will produce. In other words, the first moment of the measured vertical velocity distribution is defined to be equal to the first moment of a potential or line vortex (Ref.10):

$$\int_{-b_e/2}^{b_e/2} V_{\text{line vortex}}\, r\, dr = \int_{-b_e/2}^{b_e/2} V_{\text{Doppler}}\, r\, dr,$$

$$\int_{-b_e/2}^{b_e/2} \frac{\Gamma'}{2\pi r}\, r\, dr = \int_{-b_e/2}^{b_e/2} V_{\text{Doppler}}\, r\, dr,$$

$$\Gamma' = \frac{2\pi}{b_e} \int_{-b_e/2}^{b_e/2} V_{\text{Doppler}}\, r\, dr. \qquad (31)$$

Γ' is the "effective strength," b_e the wingspan of the vortex-encountering aircraft, and $V_{Doppler}$ are the measured vertical velocities.

At Chicago, $V_{Doppler}$ data have been collected for 1398 B-707s, 6511B-727s, 758 B-737s, 495 B-747s, 744 DC-8s, 2797 DC-9s, 1073 DC-10s, 391 L-1011s, 223 B-707Hs, 204 DC-8Hs, 356 small propeller-driven aircraft, and 68 Learjets. The reduced data consist of four values of Γ'-- Γ' evaluated for semispans ($b_e/2$) of 16.5 feet (5 meters), 33 feet (10 meters), 66 feet (20 meters), and 100 feet (30 meters).

To determine Γ_o, the initial vortex strength required in the analytic model, the maximum values of Γ' for each aircraft type and for each semispan were retrieved from the MAVSS data. The maximum values were used as the stronger the vortex, the greater the hazard posed by that vortex. By using the largest observed values of Γ', the model is using the "worst case" in the sense of safety. A linear least-squares fit to the four Γ' values (see Fig. 17) for each aircraft type was made yielding an expression of the form,

$$\Gamma_o = m\, b_e + \Gamma_{int},$$

where m is the slope, and Γ_{int} is the intercept of the Γ_o line with the Γ' axis. Note that there are many data points not shown below those plotted in Fig. 17; for example, there are 1397 data points below each of the values plotted for the B-707--only the largest Γ' value was plotted. Thus, the initial value of the vortex strength is a function of the wingspan of the vortex-encountering aircraft. The parameters are listed in Table 9 along with the correlation coefficient for the linear regression.

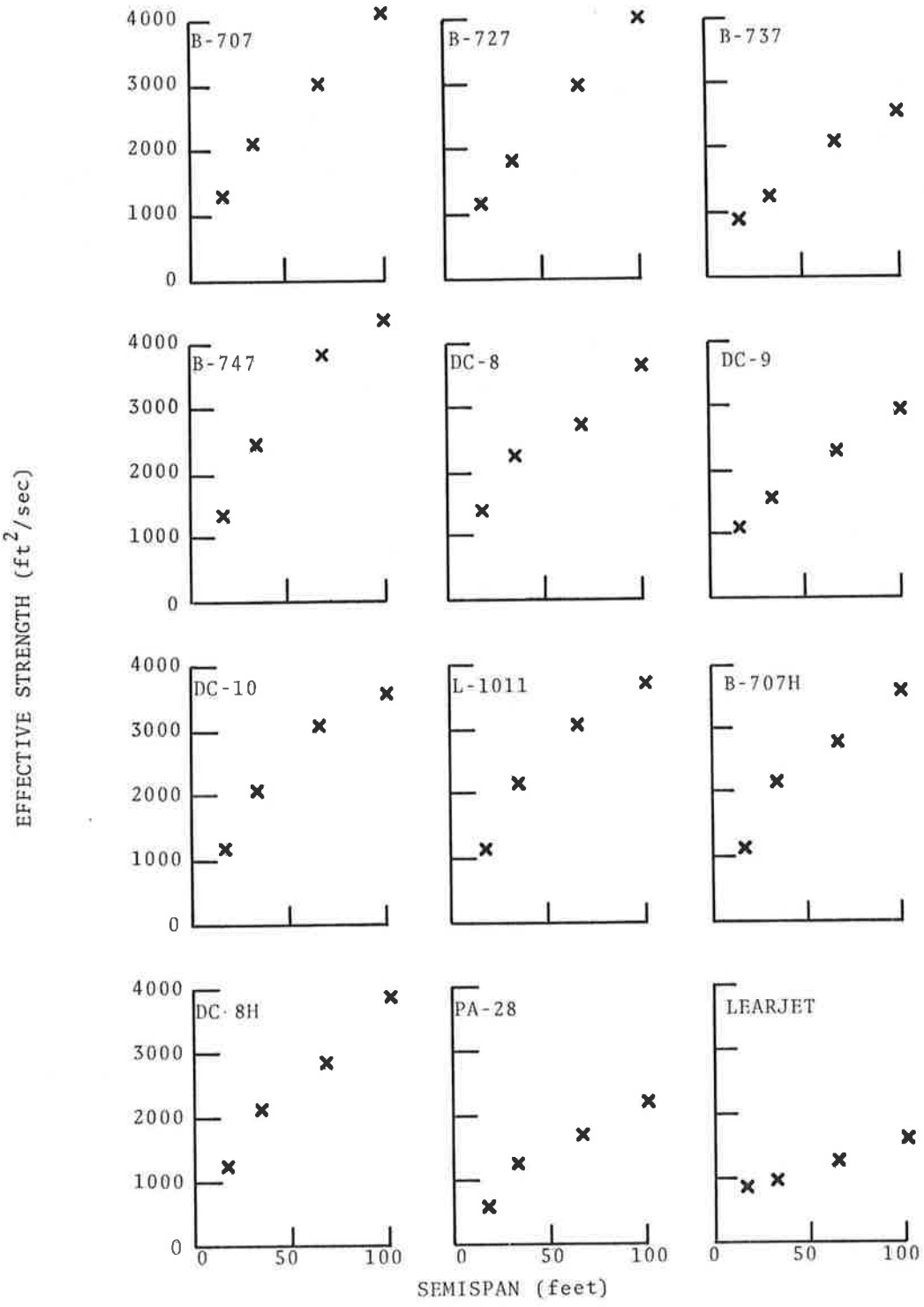

FIGURE 17. MAXIMUM Γ' VALUES

TABLE 9. PARAMETERS FOR Γ_o

Aircraft Type	Slope (ft/sec)	Intercept (ft^2/sec)	Correlation Coefficient
B-707	18.02	920.6	0.996
B-727	17.95	895.4	0.993
B-737	11.23	642.9	0.993
B-747	19.56	1148.6	0.968
DC-8	13.52	1270.5	0.977
DC-9	12.29	837.0	0.998
DC-10	15.46	1010.3	0.969
L-1011	16.35	958.5	0.977
B-707H	14.88	1007.4	0.966
DC-8H	16.13	982.2	0.990
PA-28	9.54	521.8	0.971
Learjet-25	5.20	715.2	0.999

APPENDIX B

VORTEX DESCENT

The purpose herein is to review the mechanisms governing vortex descent. The material follows closely the discussion of vortex transport in Reference 2.

B.1 VORTEX DESCENT OUT OF GROUND EFFECT

For vortex-transport calculations, the Rankine vortex model is usually used:

$$v(r) = \frac{\Gamma r}{2\pi r_c^2} \quad , \tag{32}$$

for $r < r_c$, and

$$v(r) = \frac{\Gamma}{2\pi r} \quad , \tag{33}$$

for $r \geq r_c$. Γ is the strength or circulation of the vortex, and r_c is the radius of the core. The basic assumption of vortex transport is that the transport velocity of each vortex is the velocity of the surrounding velocity field evaluated at the centroid of each vortex. The velocity field is composed of the ambient wind and the velocity imposed by other vortices. Equation (33) can be used to calculate the mutual induction of vortices upon each other if r_c is less than the separation distance between the vortices (b_o).

After the wing-vortex sheet has rolled up, the trailing system consists of a pair of vortices of finite rotational core area with a core radius a relatively small fraction of the vortex span. If the vortex pair is immersed in a "still," homogeneous inviscid flow, the pair is convected downward at a velocity $\Gamma/2\pi b_o$. The classical analysis (Ref. 2) shows that there is a closed recirculating mass of air, of roughly oval proportions, associated with

the concentrated vortex pair, and that the cell is convected downward at a uniform speed. Flow exterior to the cell never enters it. Thus, a long vortex pair, which may be regarded as substantially two-dimensional, will move downward in an unbounded fluid with constant velocity for all times.

In real flows, this situation does not persist indefinitely, and most experiments show the rate of descent decreases, and finally, approaches zero. This is caused by diffusion of core vorticity by some combination of laminar and turbulent viscosity, and it will occur even in homogeneous (unstratified) flows. Much effort has gone into explaining and quantifying the effect, but the subject still remains controversial. A rational interpretation of the effect, coupled with careful observations, which greatly assists explanation of the effect, has been put forward by Maxworthy (Ref. 34).

Maxworthy conducted experiments with vortex rings in water, using various visualization techniques to identify where the flow went. When the vorticity was relatively well distributed in the ring, he observed that the outer flow was entrained into the back of the cell, causing an increase in the cell volume. At the same time, a portion of the cell vorticity was shed into the wake, removing both vorticity and momentum from the cell. The combined effect was to increase the cell size and to reduce its propagation velocity.

The mechanism of mass entrainment is important for further development of vortex transport. Figure 18 is a sketch of the vortex flow field, in coordinates fixed at the core centers, so that the outer flow is represented by a uniform and unsteady flow from below. The cell has a well defined stagnation point, A, and over the front portion, a well defined cell boundary, A-B. Across this boundary, the pressure and velocity fields of inner and outer flows are continuous, the only discontinuity being between the inner vortical fluid and the outer irrotational flow. Because of both laminar and turbulent effects, the vorticity of the inner vortical flow is transferred to the outer flow, and as a

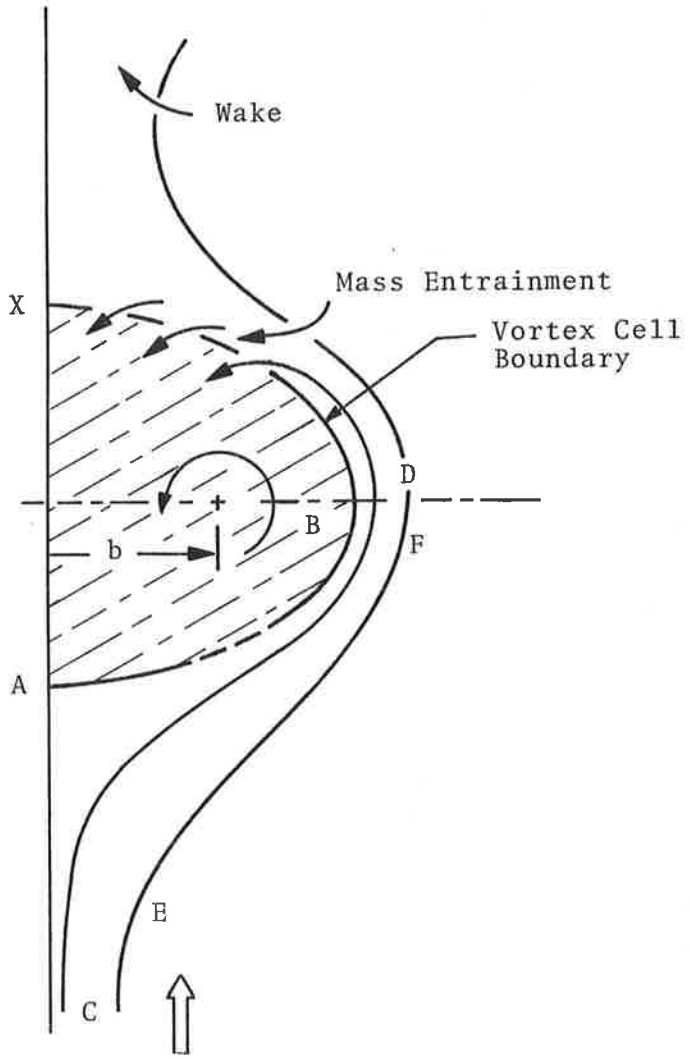

FIGURE 18. VISCOUS EFFECTS ON VORTEX CELL

consequence, the total pressure of the flow is reduced. After passing the maximum-velocity point near B, the outer flow, contained approximately by the stream tube DC, is unable to recover sufficient velocity to rejoin the outer flow at the rear, and remains as part of the stationary cell. Thus, the cell size is increased. At the same time, a neighboring stream tube EF acquires a smaller amount of vorticity, and suffers less pressure reduction, so that it does depart from the cell at the rear, but at a lower than free-stream total pressure. This portion develops into a wake behind the cell.

The same process causes entrainment of the outer flow into the cell and a detrainment (removal) of some of the cell vorticity and momentum. A further process occurs on the centerline of the cell, AX. Here, vorticity is annihilated by diffusion from the left- and right-hand cells. Thus, three vorticity transfer mechanisms occur, and the overall effect controls the cell dynamics.

Maxworthy (Ref. 34) showed that initially the vortex-shedding to form the wake was extremely weak since the cell vorticity at the boundary was quite weak. Thus, although the cell grew in size, it did not lose momentum, and the impulse was conserved. In these circumstances, the main vorticity loss occurred along the centerline and was small, and there was minimal wake-momentum loss. During the later stages in growth, when more vorticity was present near the boundary between the inner and outer flows, the wake developed. Vorticity and momentum were shed from the cell, and thus, the momentum in the cell decreased while the cell size increases. Both of these effects contributed to the reduction in descent speed and the final complete annihilation of the cell momentum for the two-dimensional vortex observed by Maxworthy. It is noted that for a three-dimensional vortex pair such as an aircraft wake, vortex annihilation caused by three-dimensional effects (sinuous instability and core-bursting), almost always precedes the two-dimensional vortex annihilation.

It must be noted that Maxworthy's experiments were conducted with vortex rings at extremely low Reynolds numbers for which the

flow was certainly laminar. However, flow-visualization tests with finite wings also exhibited a detrained wake. These experiments were also performed at very low Reynolds numbers. It is possible that during the later stages of development of an aircraft-trailing vortex system that similar processes of mass entrainment and momentum detrainment occur. For laminar transfer, the time scales would be too long to be of interest, but if the transfer were assumed to be turbulent, it might be possible to account for some of the observed effects. Thus, it appears very probable that the later development of a vortex pair follows qualitatively the stages described by Maxworthy with an additional initial stage. The three stages are postulated as shown in Figure 19.

Stage I -- The Inviscid Cell: Here, the vorticity is confined to well within the cell boundary. The cell boundary is defined as the streamline between the flow which remains with the vortex pair and that which remains with the ambient air. On the boundary itself, there will be no laminar mass or momentum transfer (since there is no distortion), and turbulent transfer will have no net effect since both inner and outer flow have the same total pressure. In these circumstances, the core size is less than the cell size, and the inviscid cell model will be a good representation of the dynamics. The time rates of change of cell size and vortex strength are zero; the descent velocity is constant.

Stage II -- The Entraining Cell: As the core vorticity diffuses and approaches the cell boundary, the first process (of mass entrainment) occurs, and the cell grows; $\dot{\Gamma} = 0$. The descent velocity reduces slightly from the inviscid value because of greater vortex separation resulting from cell growth.

Stage III -- The Decaying Cell: During the later stages, substantial mass entrainment and momentum and vorticity shedding occur, causing a wake to develop behind the vortex pair. Thus, various catastrophic instabilities usually develop before the complete decay has occurred.

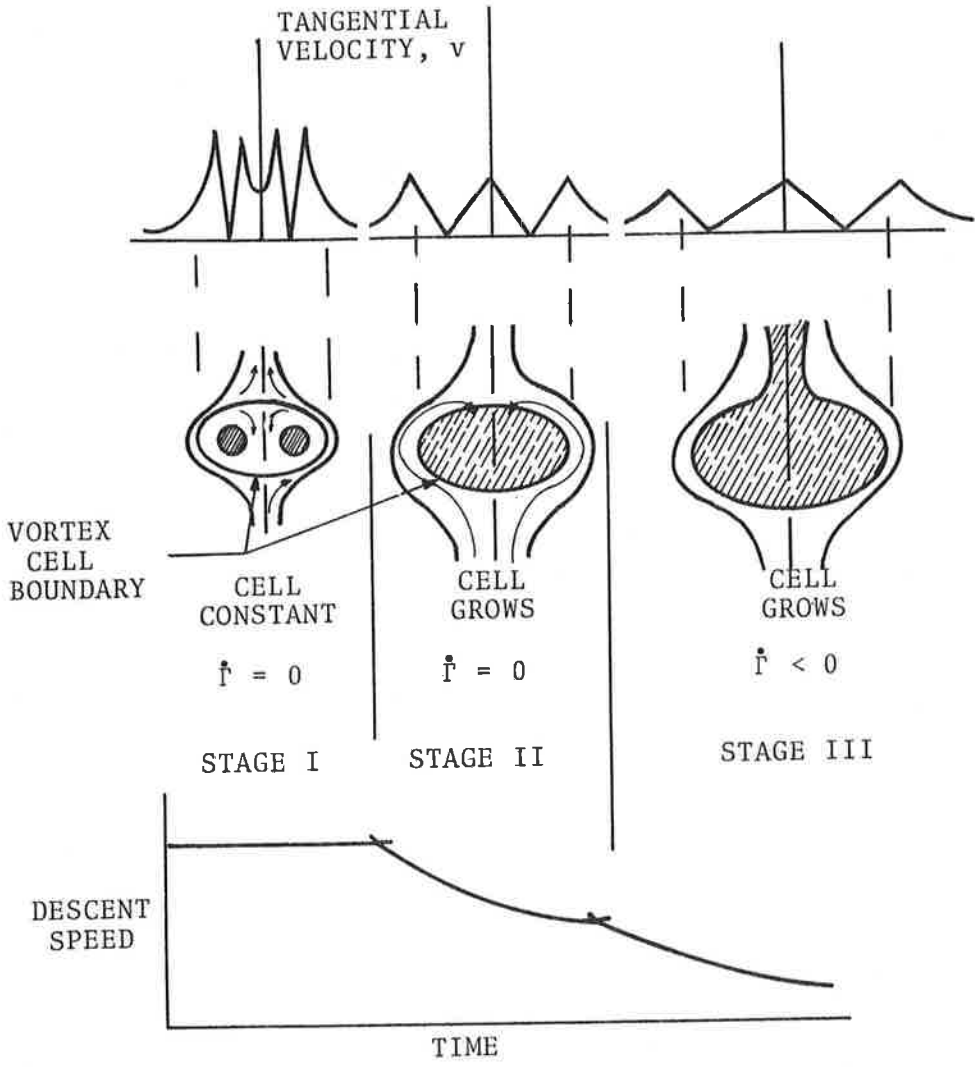

FIGURE 19. VORTEX CELL STAGES

B.2 VORTEX BUOYANCY

Vortex buoyancy is the aerostatic force imposed on the vortex by virtue of the difference in density between the air contained within the vortex and the surrounding ambient air. There are three sources of this density difference: The first is a result of the static underpressure of the vortex. The second is the result of entrainment of hot exhaust gases from the engines. The third is the result of descent through a nonadiabatic atmosphere. The first two effects give the vortex a positive (upward) buoyancy force. The third may give a positive or negative force depending on the temperature-lapse rate of the surrounding atmosphere. The magnitude of these effects on vortex motion is small compared with mutual induction.

For the first effect, the momentum equation for cylindrical flow gives

$$\frac{dp}{dr} = \frac{\rho v^2}{r} = \frac{\rho \Gamma^2}{4\pi^2 r^3}, \tag{34}$$

where the second part of the equation is valid outside the core for the Rankine vortex. Assuming adiabatic conditions in the core,

$$p\rho^{-k} = p_\infty \rho_\infty^{-k} = \text{constant}, \tag{35}$$

where k is the ratio of specific heats, and the subscript ∞ refers to ambient conditions. Equations (34) and (35) may be used to find $d\rho/dr$:

$$\frac{kp_\infty \rho^{k-1}}{\rho_\infty^{k}} d\rho = \frac{\rho \Gamma^2}{4\pi^2 r^3} dr. \tag{36}$$

Integrating between the limits of infinity and r,

$$\rho(r) = \left[\rho_\infty^{k-1} - \frac{k-1}{k}\,\frac{\rho_\infty^{k}}{p_\infty}\,\frac{\Gamma^2}{8\pi^2 r^2}\right]^{\frac{1}{k-1}}. \qquad (37)$$

As an example of the magnitude of the effect, for the flight conditions for a landing B-727 and an assumed core radius of 2 feet, the density is 0.00138 slugs/ft^3 compared with an ambient density of 0.00235 slugs/ft^3. The upward buoyant force is

$$F = 2\pi g \int_0^\infty (\rho_\infty - \rho\,(r))\; r\,dr. \qquad (38)$$

(In practice, the integral would be taken from the core radius, r_c, because the equation is based upon the Rankine vortex assumption, and is only valid for $r \geq r_c$.)

Engine-exhaust extrainment is another aircraft variable which can affect the vortex-transport process through variations in the vortex buoyancy. The density variation caused by exhaust entrainment is

$$\rho = \rho_\infty\, T_\infty/T, \qquad (39)$$

where T is the temperature of the air in the core of the vortex, and T_∞ is the ambient air temperature.

The third cause of buoyancy is vortex descent through a non-adiabatic atmosphere. The interface between the wake fluid and the exterior atmosphere is only a dividing streamline; it does not support shear or pressure. In the presence of atmospheric turbulence or turbulence in the wake, the streamline is perturbed, and some mixing between the interior wake fluid and the exterior atmosphere occurs. When the mixing is small, as it is when the wake is young and the turbulence is low, the wake fluid retains its identity and its physical properties as it moves about through the atmosphere. One consequence is the creation of aerostatic forces

as the wake moves into regions of varied temperature and density. For example, an upward (or buoyant) force is developed on those segments of a wake descending into a stably stratified atmosphere if there is little or no mixing of the ambient air with the wake fluid. Results of experiments on wake buoyancy are presented by Tombach (Ref. 35); he showed that a wake descending into a stable atmosphere acquired buoyancy, until at some later time, turbulent mixing between the wake and the atmosphere became strong enough to erode the temperature difference between them. Increasing ambient turbulence shortened the period during which buoyancy was acquired, and as a consequence of more rapid mixing, resulted in more rapid decay of both buoyancy and vortex descent.

The aerostatic forces are a result of an increase in the temperature of the fluid in the wake oval, caused by adiabatic compression as the oval descends into a denser atmosphere. An atmospheric temperature stratification other than adiabatic (neutral) will result in a temperature difference, and hence, a density difference between the wake and the atmosphere. Buoyancy will thus be created for wakes descending into a stable atmosphere (the most common situation) with no mixing. Theoretical models with no mixing (Ref. 36) indicated that the buoyancy so acquired accelerated wake descent and decreased vortex spacing. The experimental observations discussed above indicated, however, the possibility of a retarding tendency caused by buoyancy, but might be a consequence of entrainment rather than of buoyancy.

Overall, the effects of aerostatic forces on vertical wake motions appear to be of smaller order than the dissipative mechanisms associated with turbulence, which could overwhelm the buoyancy effect, and thus, result in the difficulties experienced in properly isolating the buoyancy influence. A comprehensive discussion of both theoretical and experimental observations on the descent of a wake in a stratified fluid is given in Reference 36.

The predominant effect of atmospheric stability appears to be the indirect one associated with the vertical air currents resulting from atmospheric mixing. In a stable atmosphere, this mixing

is suppressed, resulting in reduced vertical air motions and reduced effects on vertical wake motions. In unstable conditions, vertical atmospheric activity and resulting wake motions are amplified. Such motions may be either upward or downward, thus unpredictable wake ascent or descent can result under such unstable atmospheric conditions.

The effects of atmospheric stratification on initial wake descent rates are shown schematically in Figure 20. For a stable atmosphere, the wake descends initially at a speed which is consistent with the inviscid analytical model. Random influences become more evident for less stable conditions. The figure applies only to vertical wake motion during the first few moments after the wake has been fully formed. Subsequent vertical wake motions are influenced by buoyancy, turbulence, and the continued random action of vertical air motions (which are accentuated for less stable conditions). Not all of these factors can be quantified at present.

Vertical air motions often become quite pronounced under the influence of thermal activity near the ground. Extreme vertical convolutions of wakes can occur because of convection by these air motions. Under these conditions, the vortex pair is stretched and distorted into a highly nonlinear configuration where mutual and self-induced vortex velocities act to amplify the process. Figure 21 shows such a wake generated near the ground under conditions of high atmospheric thermal activity. The impossibility of dealing with such a resultant wake structure on anything but a statistical basis is clearly evident. However, it remains to be shown that such a convoluted wake may pose a hazard in operational conditions.

All wake motions near the ground do not exhibit such extreme behavior. Under stable atmospheric conditions and reduced thermal activity, the wake and the vortex pair undergo more orderly motions which are fairly well understood and can be approximated analytically. Such conditions are also those of greatest operational interest because these same factors are conducive to wake persistence. Wakes generated or moving into ground effect are subjected

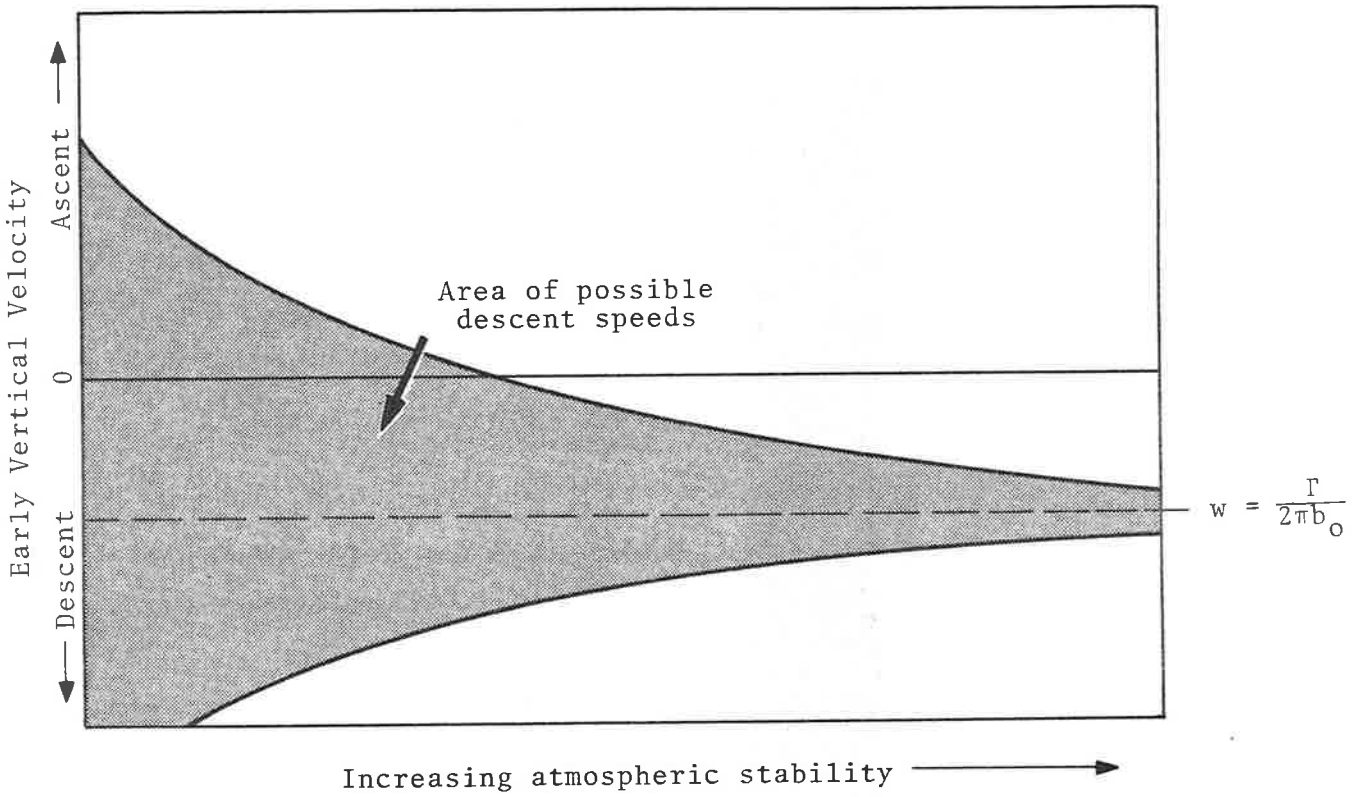

FIGURE 20. SCHEMATIC REPRESENTATION OF OBSERVED RELATIONSHIP BETWEEN ATMOSPHERIC STABILITY AND WAKE DESCENT AT EARLY TIMES. In unstable conditions, the descent is relatively indeterminate, progressively increasing stability results in descent more closely approaching the vortex-induced wake speed.

FIGURE 21. VORTICES IN GROUND EFFECT

to the influences of the induction velocities generated by the underground or image vortices. The vertical motion of the wake gradually and predictably slows and eventually stops at an altitude equal to about one-half the initial vortex spacing. The vortices then move apart.

B.3 DESCENT DATA

Tombach (Ref. 35) studied the descent of vortices shed by a light, twin-engine aircraft (AeroCommander 560F). Cameras recorded the motion and decay of smoke-marked vortices.

Descent trajectories for the AeroCommander vortices are shown in Figure 22 for unstable and neutral stratifications, and in Figure 23 for stable isothermal and inversion conditions. The solid line in the figures is the theoretical descent rate based on elliptical wing loading. The broken lines indicate other descent rates for comparison.

In Figure 22, the wakes actually rise in the two unstably stratified cases shown, probably due to being carried upward by the considerable vertical currents which accompany instability. The high turbulence which naturally occurs in such an unstable atmosphere results in very brief lives for these wakes. The wakes in a neutral atmosphere show a fairly rapid descent, with initial speeds well exceeding the theoretical descent rate. After 20 to 30 seconds, the descent has slowed, but the speeds still exceed the theoretical rate.

For the more stable atmospheres (Fig. 23), the range of initial descent speeds bracket the theoretical descent rate and are within about 25 percent of it. As before, there is often slowing down of the speed of descent after 30 to 40 seconds, with descent speeds at 50 seconds typically about 1/2 to 3/4 of their initial values.

Wakes often exhibit considerable banking or tilting of the plane containing the vortex pair. Figure 24 displays trajectories for wakes which have banked in excess of 25 degrees. Surprisingly,

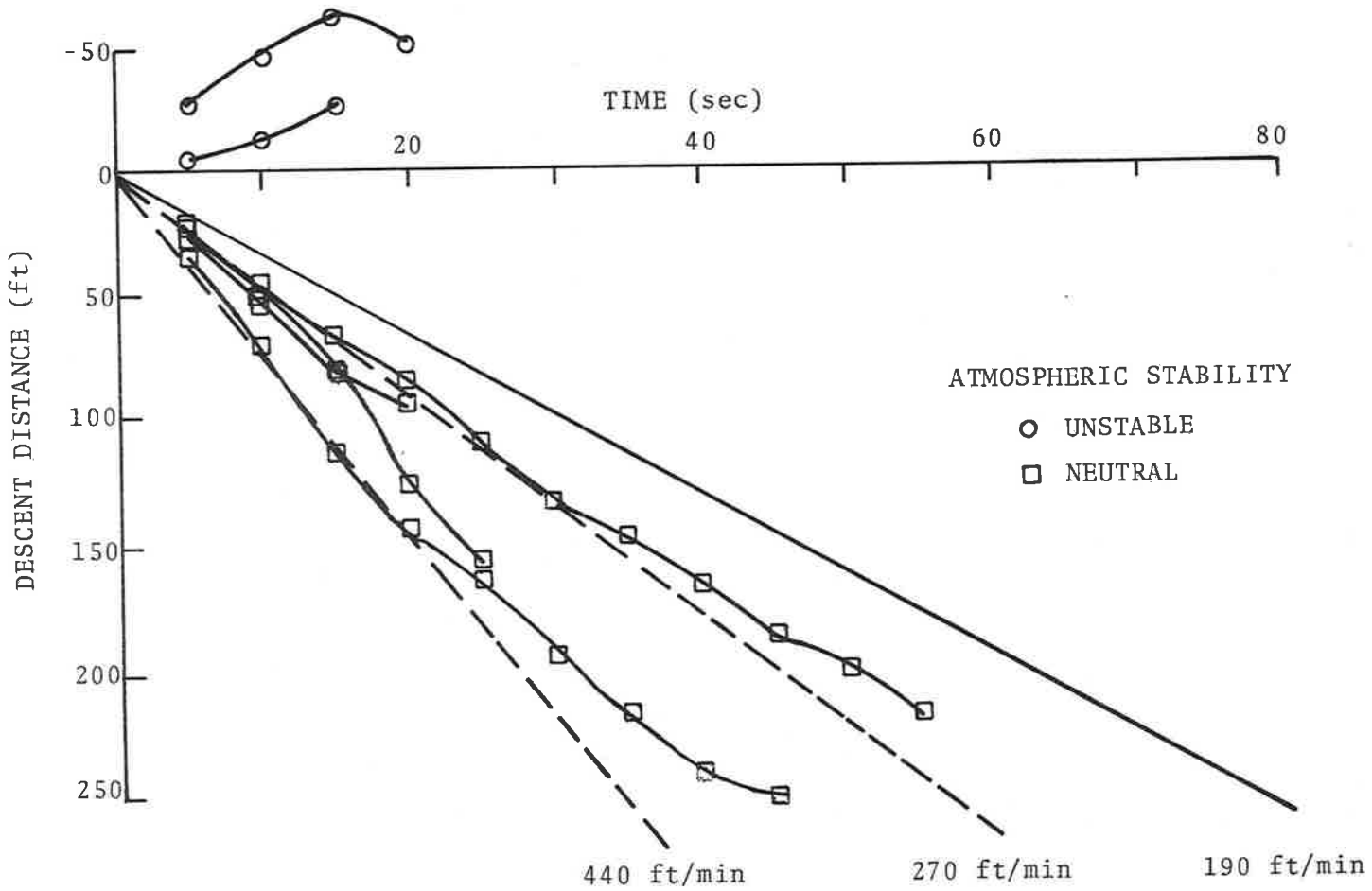

FIGURE 22. WAKE-DESCENT TRAJECTORIES UNDER UNSTABLE AND NEUTRAL ATMOSPHERIC STRATIFICATION. The calculated descent speed of 190 ft/min is represented by the heavy line; two other descent rates are indicated by the broken lines.

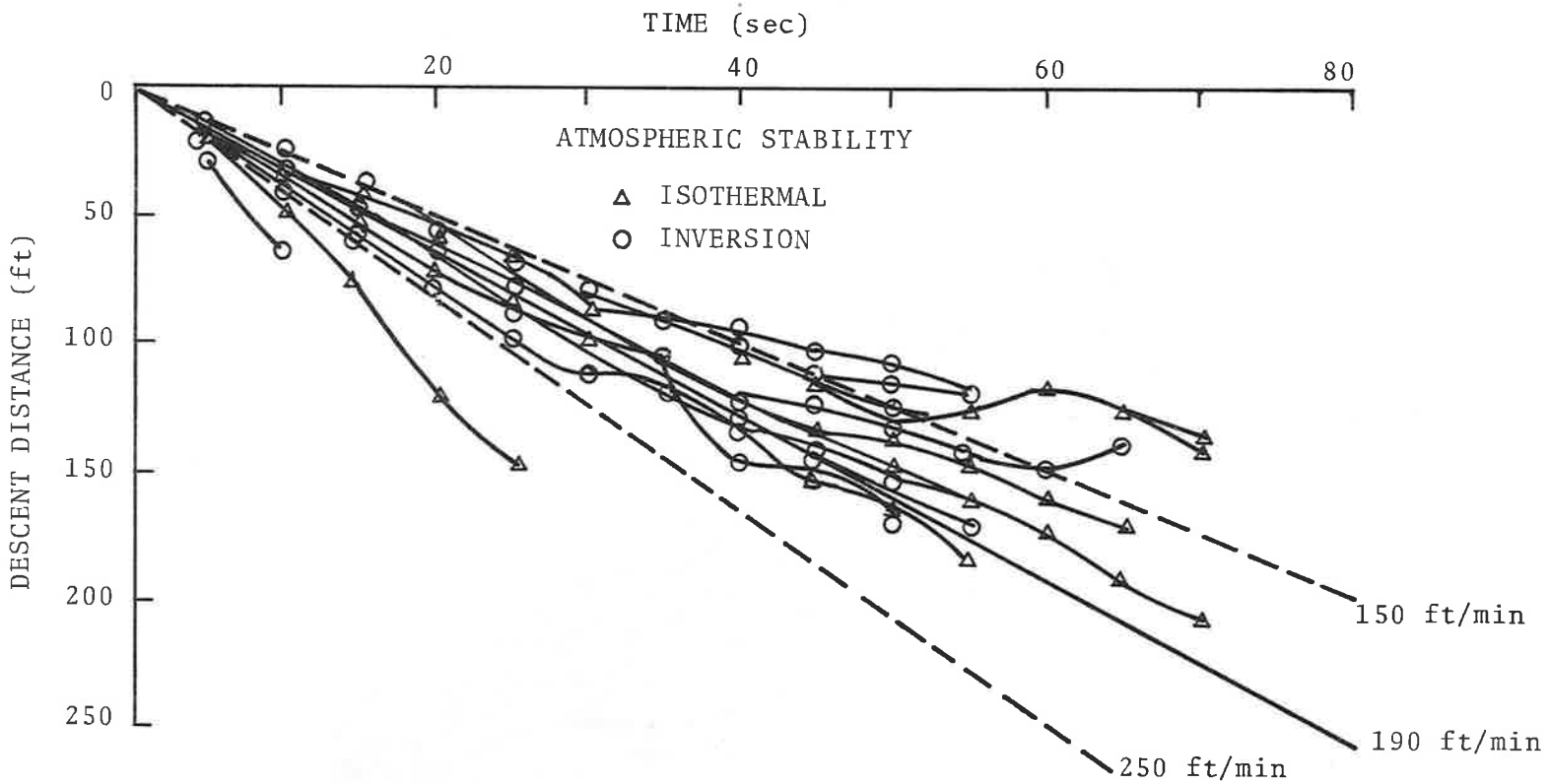

FIGURE 23. WAKE DESCENT TRAJECTORIES IN STABLE STRATIFIED ATMOSPHERES. The solid line is the descent rate calculated from the aircraft weight and initial vortex spacing; two other arbitrary rates of descent are indicated by the broken lines.

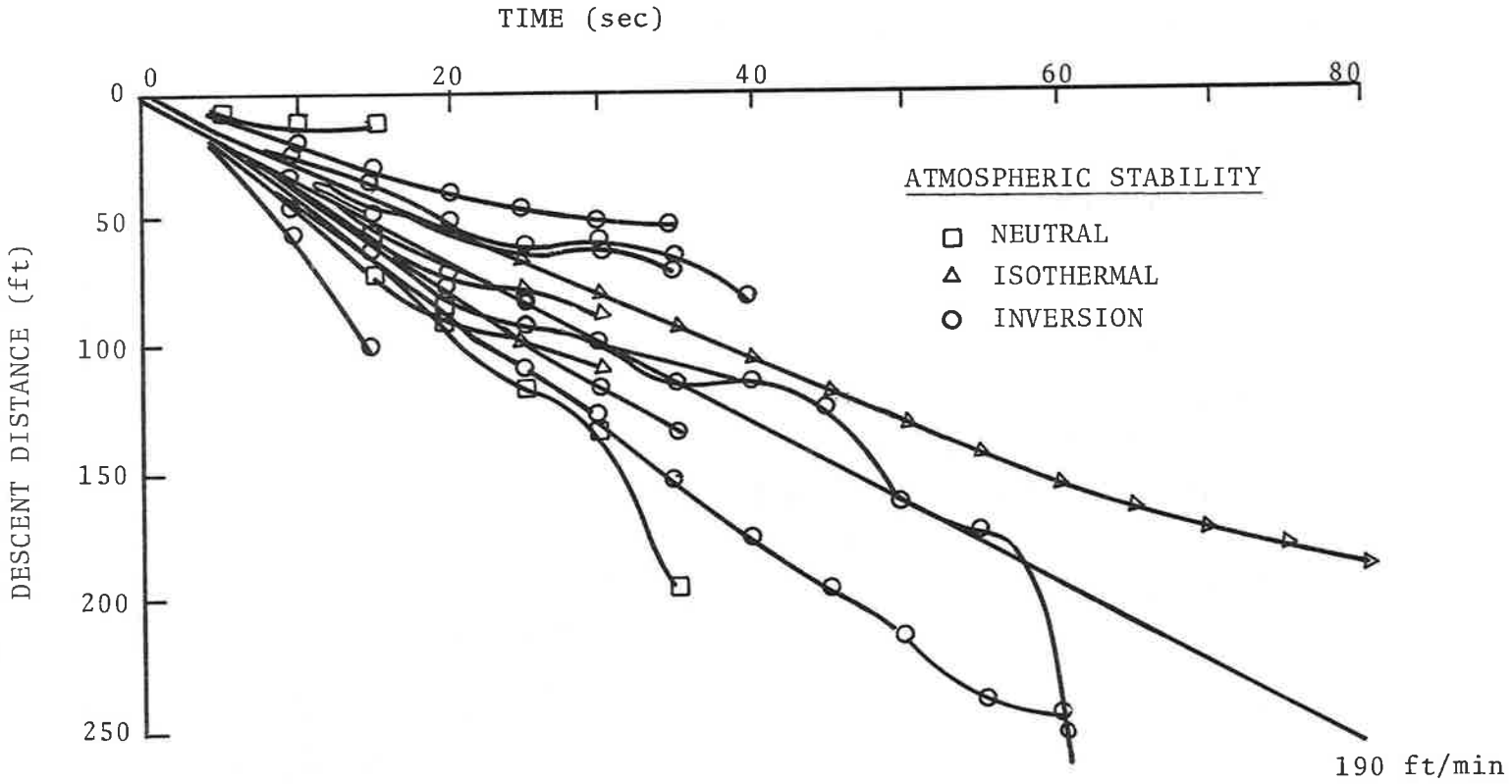

FIGURE 24. DESCENT TRAJECTORIES FOR BANKED WAKES. The theoretical descent rate for unbanked wakes is indicated by the solid line.

banking does not change the descent speeds greatly; the trajectories do not look much different than those for unbanked wakes.

The data show the effects of atmospheric stability on the descent of vortices. Slowing of descent appears to be caused by the turbulent erosion of the wake strength (with an attendant decrease in the potential hazard if the wake were encountered by an aircraft). The data are consistent with the three-stage characterization of the life of a wake discussed in Section B.1.

APPENDIX C

CROSS-WIND PROBABILITY DENSITY

C.1 GENERAL DERIVATION OF CROSS-WIND PROBABILITY DENSITY USING WIND-ROSE DATA

Wind-rose data are ordinarily presented as a polar-coordinate p.d.f. (or more usually as a discrete probability distribution) for the joint probability of a wind magnitude (r) and "from" direction (θ). Denote this wind-rose as $p_w^R(r,\theta)$.

To determine the p.d.f. for the cross wind on a given runway, consider the following transformation of variables, where α is the runway heading, and (x,y) defines a cartesian coordinate system with the positive x-axis aligned with the runway heading (Fig. 25). The transformations from the wind-rose to the runway-coordinate system are:

$$\text{head wind:} \quad w_x = r \cos(\alpha - \theta),$$

$$\text{cross wind:} \quad w_y = r \sin(\alpha - \theta),$$

and the inverse transformations are:

$$\text{magnitude:} \quad r^2 = w_x^2 + w_y^2 ,$$

$$\text{direction:} \quad \theta = \alpha - \tan^{-1}(w_y/w_x).$$

The standard formula for transforming the joint p.d.f. is

$$p_w(w_x,w_y) = |J_{xy}| \; p_w^R \left(\sqrt{w_x^2+w_y^2}, \; \alpha - \tan^{-1}(w_y/w_x)\right), \qquad (40)$$

where $|J_{xy}|$ is the absolute value of the Jacobian of the transformation:

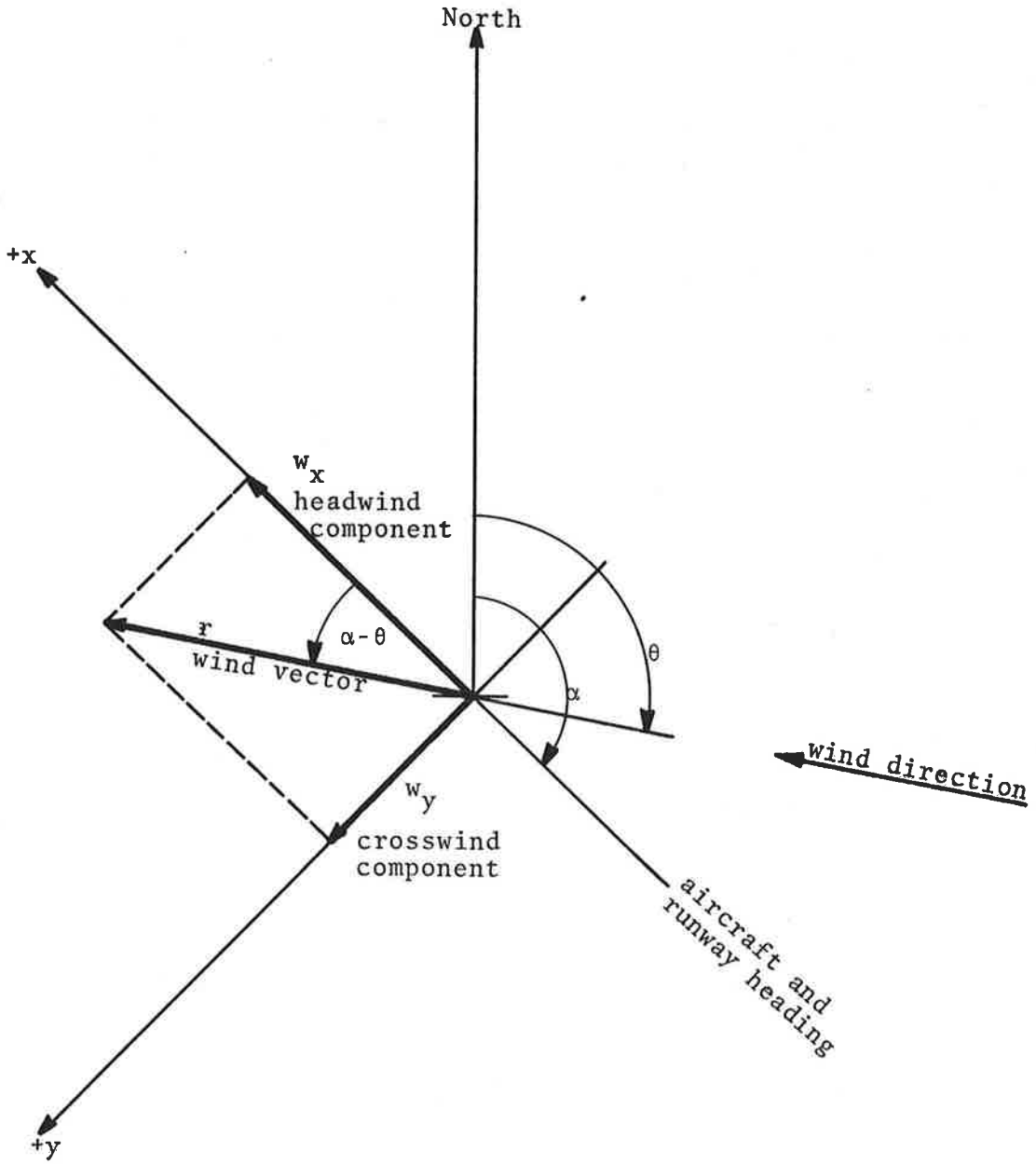

FIGURE 25. RUNWAY COORDINATE SYSTEM

$$J_{xy} = \begin{vmatrix} \frac{\partial r}{\partial w_x} & \frac{\partial r}{\partial w_y} \\ \frac{\partial \theta}{\partial w_x} & \frac{\partial \theta}{\partial w_y} \end{vmatrix} = \frac{-1}{\sqrt{w_x^2 + w_y^2}} \quad . \tag{41}$$

Thus,

$$p_w(w_x, w_y) = \frac{p_w^R(\sqrt{w_x^2 + w_y^2},\ \alpha - \tan^{-1}(w_y/w_x))}{\sqrt{w_x^2 + w_y^2}} \tag{42}$$

is the representation of the wind p.d.f. in cartesian coordinates aligned with the runway heading α.

Since the concern in vortex analysis is with the cross-wind magnitude, define $w_c = |w_y|$. The marginal p.d.f. for w_c is found by integrating out w_x at $w_y = \pm w_c$:

$$p_c(w_c) = \int_{-\infty}^{\infty} [p_w(w_x, w_c) + p_w(w_x, -w_c)]dw_x. \tag{43}$$

At this point, it is useful to make a simplifying assumption that the wind distribution is symmetric about the x-axis; i.e.,

$$p_w(w_x, w_c) = p_w(w_x, -w_c) \quad .$$

Then

$$p_c(w_c) = 2\int_{-\infty}^{\infty} p_w(w_x,w_c)\ dw_x,$$

$$= 2\int_{-\infty}^{\infty} \frac{p_w^R(\sqrt{w_x^2 + w_c^2}\ ,\ \alpha - \tan^{-1}(w_x/w_c))}{\sqrt{w_x^2 + w_c^2}}\ dw_x, \qquad (44)$$

giving the cross-wind p.d.f. from the wind rose.

Wind-rose data are a statistical representation of the probability of a particular wind vector being randomly encountered on (or above) the airport. The transformation to cross wind on a given runway is strictly speaking only valid for a randomly selected runway. Selecting a particular runway for landing is an act implying prior knowledge of the wind magnitude and direction, the usual strategy being to pick a runway heading (α) to minimize tail and cross winds. Under such conditions, limits on the allowable cross and tail winds should be imposed when defining the cross-wind p.d.f., given that runway α has been selected. For example, let L_t be the maximum allowable tail wind, and L_c the maximum cross wind, then an improved estimate of the cross-wind p.d.f. when runway α is in use would be

$$p_{c/\alpha}(w_c) = \frac{\int_{-L_t}^{\infty} p_w(w_x,w_c)\ dw_x}{\int_0^{L_c}\int_{-L_t}^{\infty} p_w(w_x,w_c)\ dw_x dw_c}. \qquad (45)$$

This will be further modified by runway usage and noise considerations.

C.2 CROSS-WIND PROBABILITY DENSITY DERIVED FROM TOWER DATA

Crawford and Hudson (Ref. 31) measured winds using aerovanes mounted on a 1500-foot tower located near Oklahoma City. Reference 31 presents annual relative frequency distributions of wind speed in 2-knot intervals for various levels on the tower. The concepts of Section C.1 will now be applied to the wind data of Crawford and Hudson to obtain a transformation to cross wind.

A number of assumptions are required to derive the cross-wind p.d.f.:

A1. The magnitude of the wind vector is as described in Reference 27.

A2. The wind direction is equally likely in any direction (i.e., random).

A3. Wind magnitude and direction are independent random variables.

A fourth assumption is implied by this approach, as discussed at the end of Section C.1;

A4. The selection of runway direction is independent of the wind behavior above the surface.

Crawford and Hudson state that the wind magnitude measured about 1,000 feet above ground could be well approximated by a form of Rayleigh distribution

$$p_r(r) = \frac{r}{\sigma^2} e^{-r^2/2\sigma^2}, \quad r \geq 0, \tag{46}$$

where σ is related to the mean observed wind speed μ by

$$\sigma = \sqrt{\frac{2}{\pi}}\ \mu . \tag{47}$$

By A1 above, this Rayleigh distribution can be taken to represent the marginal p.d.f. for the speed of winds aloft at the airport.

By A2, the marginal p.d.f. for wind direction can be written

$$p_\theta(\theta) = \frac{1}{2\pi} \quad , \tag{48}$$

for $0 \leq \theta \leq 2\pi$. Combining them with A3, the assumed wind rose for winds aloft becomes

$$p_w^R(r,\theta) = \frac{r}{2\pi\sigma^2} e^{-r^2/2\sigma^2} \quad , \tag{49}$$

for $r \geq 0$ and $0 \leq \theta \leq 2\pi$. A4 states that this wind rose holds without regard to the runway in use; without loss of generality, the runway direction may be disregarded, and α may be set equal to zero. The cross-wind p.d.f. is, then,

$$\begin{aligned} p_c(w_c) &= \frac{1}{\pi\sigma^2} \int_{-\infty}^{\infty} e^{-(w_x^2 + w_c^2)/2\sigma^2} \, dw_x \quad , \\ &= \sqrt{\frac{2}{\pi\sigma^2}} \, e^{-w_c^2/2\sigma^2} \quad , \end{aligned} \tag{50}$$

with $w_c \geq 0$. Note that this is the p.d.f. for the magnitude of a Normal random variable (i.e., w_c is distributed Normally with zero mean and variance σ^2), which is to be expected, since the Rayleigh distribution is the p.d.f. for the vector sum of two identically distributed Normal random variables. Falls and Brown (Ref. 35) substantiated that wind components may be considered bivariate Normally distributed.

The cross-wind p.d.f. may be rewritten in terms of the mean wind speed aloft (μ)

$$p_c(w_c) = \frac{1}{\mu} e^{-\pi w_c^2/4\mu^2} \quad , \quad w_c \geq 0 \tag{51}$$

and the mean cross-wind magnitude is related to the mean total wind by

$$E(w_c) = \frac{2}{\pi} \mu \ .$$

The observations reported by Reference 31 give μ = 18.6 knots at 1166 feet above ground level, with 17.2 and 18.7 knots at the next lower (873-foot) and higher (1459-foot) levels, respectively. Using the 18.6-knot value, the derived p.d.f. for cross-wind magnitude is

$$p_c(w_c) = 0.0538 \ e^{-0.00227 w_c^2} \ , \qquad (52)$$

with a mean of 11.8 knots.

If the winds of interest are correlated, even weakly, with runway selection, then factors come into play that could invalidate A2 to A4 above, and the more specific analysis must be applied. The effect of selecting a specific runway for approaches into the wind will, in general, further limit the variance of the cross wind, making low cross-wind speeds even more likely. Acknowledging this effect in the analysis could have distinct effects on the safety calculations for vortices of non-zero potential hazard since such calculations rely in the main on cross-wind transport effects for reductions in encounter probabilities.

C.3 CROSS-WIND PROBABILITY DENSITY FOR A VAS-GREEN LIGHT

The procedure is much less clear when attempting to infer a cross-wind p.d.f. aloft given a "red/green light" observation of surface winds. If there were a simple one-to-one mapping between the surface wind vector and the wind vector at altitude, then an appropriate determination of the wind rose aloft conditional on a surface "green light" could be made. However, it is not reasonable to expect that such a mapping can be established, or that any simple one-to-one correspondence should exist. In fact, it is

reasonable to expect that a statistical rather than deterministic relationship will exist--that is, any particular wind vector observed on the ground may relate probabilistically to a large set of possible wind vectors aloft (and vice versa). This makes the aloft interpretation of a "green/red light" surface observation much more cumbersome and its description dependent on observed statistical data--the measured wind rose aloft given a "green light" at the surface. The latter might indeed bear no relationship to surface winds, in which case the observation of a "green light" would convey no information of use in establishing the p.d.f. for cross winds aloft.

In the absence of specific meteorological rules, a simple assumption is postulated:

A5. If the surface wind is observed outside the VAS ellipse, then the wind vector aloft will also always lie outside of such an ellipse.

This assumption has several drawbacks and further assumptions implicit in its use: Steering of the wind vector may cause a vector nominally outside the ellipse near the MM to be inside the ellipse when applied aloft. A given surface-wind observation may yield a probability distribution aloft that is radically different from the normal wind rose; when an area (such as the "green light" region) of the surface-wind distribution is considered, the resultant conditional wind-rose p.d.f. may not be a simple scaling up of the ground-wind rose, and most certainly will not look much like a scaled surface-wind rose. Thus, caution is needed in the use of A5.

A further assumption is implicit in the application of A5:

A6. If a "green light" occurs, winds aloft maintain their normal (relative) probability relationship that was expressed by the unconditional aloft wind rose.

This results in a rather unique mapping between the surface and aloft--not quite deterministic, but extremely rigid. It implies sufficient correlation between the two wind vectors to be at

direct odds with A2-A4. This remains an unanswered contradiction to be resolved by the results of the data collection (Volume II of this report). With A5 and A6, the determination of the conditional p.d.f. for winds aloft given a "green light" at the surface is straightforward.

The VAS ellipse (E) is oriented with the runway-coordinate system; the semi-major axis a_E of the ellipse is aligned with w_x, and the semi-minor axis b_E with w_y. Define the conditional cross-wind-aloft p.d.f. given a surface "green light on runway " observation to be $p_c(w_c/GL\alpha)$. This is found (see Figure 26) by integrating the unconditional aloft p.d.f., $p_w(w_x,w_y)$, along the two lines $w_y = \pm w_c$, and then normalizing by the prior probability that the wind vector ($\vec{w}$) is outside the ellipse, $p(\vec{w}\notin E)$. (Note that this is not the a priori probability of a "green light," which is the same calculation applied to the surface wind rose. In general, when applied at altitude, the value obtained will be larger than the VAS effectiveness at the surface because of the higher wind speeds expected at altitude, some of which in fact may occur with "red light" conditions at ground level.) Thus,

$$p_c(w_c/GL\alpha) = \int_{-L_t}^{\varepsilon} [p_w(w_x,w_c) + p_w(w_x,-w_c)] \frac{dw_x}{p(\vec{w}\notin E)} + \int_{\varepsilon}^{\infty} [p_w(w_x,w_c) + p_w(w_x,-w_c)] \frac{dw_x}{p(\vec{w}\notin E)} \tag{53}$$

where

$$\varepsilon = \begin{cases} \frac{a_E}{b_E}\sqrt{b_E^2 - w_c^2} & 0 \le w_c < b_E \\ 0 & b_E \le w_c \le L_c \end{cases}.$$

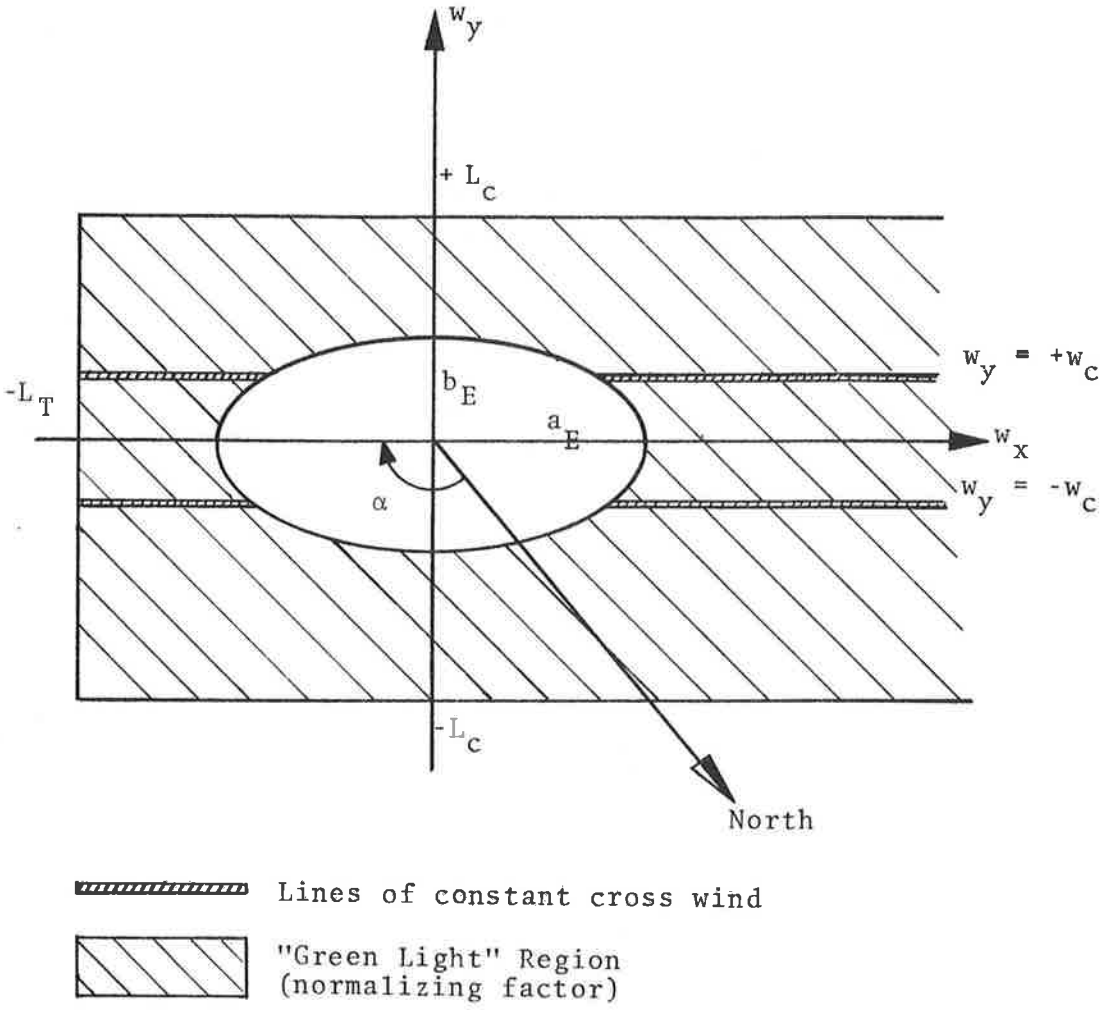

FIGURE 26. REGIONS OF INTEGRATION FOR "VAS GREEN LIGHT ON RUNWAY α"

As before, simplifications can be made regarding the symmetry of cross wind, and, when data show no prevailing winds from any direction, then head-tail-wind symmetry might be acceptable also, yielding

$$p_w(w_c/GL\alpha) = 4 \int_{\varepsilon}^{\infty} \frac{p_w^R(\sqrt{w_x^2 + w_c^2}, \alpha - \tan^{-1}(w_c/w_x))}{\sqrt{w_x^2 + w_c^2}} \frac{dw_x}{p(\bar{w} \not\in E)}, \quad (54)$$

with

$$p(w \not\in E) = 4 \int_{\circlearrowleft}^{\infty} \int_{\varepsilon}^{\infty} \frac{p_w^R(\sqrt{w_x^2 + w_c^2}, \alpha - \tan^{-1}(w_c/w_x))}{\sqrt{w_x^2 + w_c^2}} dw_x dw_c . \quad (55)$$

Since symmetry in all directions has been in effect assumed, α can be set to zero without any further loss of generality.

The assumptions in the application of $p_w(w_c/GL\alpha)$ are A5 and A6 plus any conditions that guarantee that

A7. The unconditional aloft wind rose is symmetrical with respect to the selection of runway direction.

Note that condition A7 (symmetry) is satisfied by A2 and A3 (independent, equally likely wind direction), but that the same claim of lack of surface/aloft correlation that was stated as A4 still remains at odds with the basic physical premise of using a surface observation to provide information on wind behavior aloft.

The assumed Rayleigh wind rose, converted to cartesian runway coordinates, is

$$p_w(w_x, w_y) = \frac{p_w^R(\sqrt{w_x^2 + w_y^2}, \alpha - \tan^{-1}(w_y/w_x))}{\sqrt{w_x^2 + w_y^2}},$$

$$= \frac{1}{2\pi\sigma^2} e^{-(w_x^2 + w_y^2)/2\sigma^2} \quad . \tag{56}$$

Thus, by substitution,

$$p_w(w_c/GL\alpha) = \frac{\int_\varepsilon^\infty e^{-(w_x^2 + w_c^2)/2\sigma^2} dw_x}{\int_0^\infty \int_\varepsilon^\infty e^{-(w_x^2 + w_c^2)/2\sigma^2} dw_x dw_c} ,$$

$$= \frac{Q(\varepsilon/\sigma) e^{-w_c^2/2\sigma^2}}{\int_0^\infty Q(\varepsilon/\sigma) e^{-w_c^2/2\sigma^2} dw_c} , \tag{57}$$

where

$$Q(\varepsilon/\sigma) = \int_{\varepsilon/\sigma}^\infty \frac{1}{\sqrt{2\pi}} e^{-v^2/2} dv ,$$

$$\sigma = \sqrt{\frac{2}{\pi}}\, \mu$$

(μ is the mean local wind aloft) and

$$\varepsilon = \begin{cases} \frac{a_E}{b_E} \sqrt{b_E^2 - w_c^2} & 0 \leq w_c < b_E \quad , \\ 0 & w_c \geq b_E \quad , \end{cases}$$

for the conditional p.d.f. for cross-wind magnitude aloft given as a VAS "green light on runway α" and A1 to A6 are valid

(notwithstanding the unanswered contradictions among the assumptions). Given the parameters μ= 18.6 knots, a_E = 12.5 knots, b_E = 5.5 knots, and α= any runway direction, the equation can be evaluated numerically, and is shown in Figure 13 along with the no-VAS condition. The VAS "green light" observation, as expected, implies a shift in the p.d.f. from lower to higher cross-wind values.

A more complete discussion of the material in this appendix can be found in Reference 38. In particular, the assumptions and the implications of the assumptions are discussed in detail.

C.4 DATA COLLECTION

When the surface wind is outside the VAS ellipse, does the wind vector aloft also lie outside the ellipse? This is an assumption (A5), which was invoked in the absence of any specific meteorological rules relating winds at the surface to winds along the ILS out to the OM. To test the assumption, wind data extracted from Aircraft Integrated Data System (AIDS) recordings were used.

The AIDS package consists of an onboard computer which records Inertial Navigation System data along with aircraft-control inputs (throttle, flaps, etc.). The data came from 62 KLM B-747 landings at Chicago O'Hare International Airport. The wind was determined in approximately 25-foot intervals between 50 and 1300 feet above ground level. The flights occurred between 1 July and 23 October 1976.

Whenever the wind exceeded 10 knots at the surface, little turning or change in wind direction was noted among the various altitudes (usually less than 20 degrees). Between 6 and 10 knots, the wind direction varied up to 40 degrees. Below 6 knots, large variations in wind direction were noted (sometimes exceeding 100 degrees). Fifty of the 62 approaches occurred during "VAS-green" conditions. For the 50 approaches, the winds aloft were in agreement with A5 for 48 approaches (96 percent). One of the two approaches not conforming to A5 yielded a discontinuous, and hence, suspect wind profile, whereas the other case may have occurred in

"VAS-red" conditions as the surface wind was on the edge of the VAS ellipse (a 5.5-knot cross wind). However, it does appear that A5 is warranted.

It is acknowledged that the AIDS data are restrictive as the B-747 landings occurred at about the same time each day (approximately 1600 Local Standard Time). Until the completion of the data collection discussed in Appendix F (the analysis will be contained in Volume II of this report), the AIDS data are the only relevant data available; they don't contradict A5 or the cross-wind aloft model.

APPENDIX D

LISTING OF COMPUTER PROGRAM

The encounter-probability model described in Section 4 was coded in FORTRAN for running on the TSC DECsystem-10. Figure 27 is a listing of the routine. Many comments have been inserted to permit identifying the corresponding equations of the probability model. Lower case letters cannot be used in programming the DEC system-10. Usually the notation used in the program is a straightforward interpretation of the parameter in the text (e.g., F for f, SIGD for σ_D, T or TT for t, etc.). Examples where the program notation may be confusingly inconsistent with the text are listed below:

TEXT	PROGRAM
b_e	BF
b_g	B
b_o	BG
D	DHAZ0
L_T	EL
$p_c(w_c)$	PCW
R_o	RR or R
σ_w	SIGWD

```
C...   ENCOUNTER PROBABILITY ANALYSIS
C...    DOT/TSC B.WINSTON CODE 521
        COMMON/PCWIND/PCW(51,2)
      DIMENSION KLOOP(2),IVAS(2)
      DIMENSION PDESUM(6),TT(6),PDE(6),RR(6),DD(6),PDEW(6)
      DIMENSION SIGDD(6)
C...    NO VAS , VAS CROSSWIND
        DATA IVAS/'   NO',' WITH'/
        DATA KLOOP/1,1/
         OPEN(UNIT=5,DEVICE='LPT',ACCESS='SEQOUT',MODE='ASCII',
        1 FILE='ENCTR.')
        CALL PWSET
10      CONTINUE
C...    F IS THE FRACTION OF ROLL-CONTROL AUTHORITY
        F=0.379
C***
        DO 1000 JJJ=1,13
        J=JJJ
        IF(J.EQ.13) GO TO 400
        DO 1000 JFJ=1,12
        JF=JFJ
        CALL DATFIL(J,IAC,B,V,SLOPE,BINT,VD,SIGMD)
        CALL DATFIL(JF,IACF,BF,U,SLOPEF,BINTF,VDF,SIGMDF)
C...    TIME INCREMENT (SEC/NM)
      DT=6076./V
C...    DISTANCE (FT) FROM RUNWAY THRESHOLD
      EL=34000.0
        DL=8000.0
C...    GAMMA FIT
        GAM=(SLOPE*(BF/3.28084)+BINT)*(3.28084)**2
      WRITE(5,4000) F,IAC,V,B,GAM,VD,SIGMD,SLOPE,BINT
 4000 FORMAT(1H1,' ENCOUNTER ANALYSIS',3X,'F=',F5.4/
     * ' GENERATING A/C'/1X,A5,1X,'V=',F6.1,1X,'B=',F6.1,1X,'GAMMA0 ='
     * ,F6.1,1X,'VD =', F6.2/5X,'SIGMD =',F6.2,1X,'SLOPE ='
     * ,F6.3,1X,'INTERCEPT =',F7.3/)
      WRITE(5,5000) IACF,U,BF
 5000 FORMAT(1X,'FOLLOWER A/C '/1X,A5,2X,'U =',F6.1,1X,'BF =',F6.1)
C...    PERFORM ANALYSIS FOR FOLLOWER DISTANCES UP TO
C...    6 NM AT 1-NM INCREMENTS BEHIND GENERATOR
C...
C...    CALCULATE MINIMUM DISTANCE FOR 0 PROBABILITY
        DHAZ0=((GAM*B)/(BF*U))*(26.526*9.58/6076.)/F
        IF(JF.GE.11)DHAZ0=0.75*DHAZ0
        IDHQ=0
        DDD=47.9*B/6076.0
        IF (DHAZ0.LT.DDD) IDHQ=1
        IF (DHAZ0.LT.DDD) DHAZ0=DDD
        WRITE(5,5001) DHAZ0,IDHQ
5001    FORMAT(/' MINIMUM DISTANCE FOR 0 PROBABILITY',F7.2,' NM.',I3)
        T=2.*DT
      DO 250 I=3,6
      T=T+DT
      TT(I)=T
C...    CALCULATION OF ENCOUNTER CROSS SECTION
      Q=(0.2*V*T)/B
      GAMMA=GAM
C..         GAMMA ATTENUATION AFTER BREAKPOINT
      IF(Q.GE.9.58)  GAMMA=9.58*GAMMA/Q
C...    ENCOUNTER CROSS SECTION (R)
         RR(I)=(2.653*GAMMA)/(U*F)
        IF(JF.GE.11) RR(I)=0.75*RR(I)
```

FIGURE 27. LISTING OF COMPUTER PROGRAM OF PROBABILITY MODEL

```
C...    VORTEX DESCENT PARAMETERS
        DD(I)=VD*T
        SIGDD(I)=SIGMD*T
 250    CONTINUE
          EL=EL+DL
          IF (EL.GE.50000.0) GO TO 1000
          SIGY=0.011208*EL-9.42063
          SIGZ=0.003868*EL+9.804895
          WRITE(5,9000) EL,SIGY,SIGZ
9000      FORMAT(//' L=',F8.0,' FEET',5X,'SIGMY=',F6.0,5X,'SIGMZ=',F6.0)
          DO 1500 KLI=1,2
          DO 255 I=3,6
 255      PDESUM(I)=0
          KKLI=KLOOP(KLI)
          LL=KKLI-1
        WRITE(5,6000) IVAS(KLI),LL,(I,I=3,6),(TT(I),I=3,6)
 6000 FORMAT(/A5,' VAS'/' PDESUM',I3,' - 50 KTS'/4(5X,I1,' NM',5X)/
          1 4(3X,F6.1,' SECS'))
          WRITE(5,6666) (RR(I),I=3,6)
6666     FORMAT (4(3X,F6.1,' FEET'))
C...    PERFORM ANALYSIS FOR EACH CROSS-WIND SPEED AND ACCUMULATE
C...    PROBABILITY AS A FUNCTION OF CROSS-WIND
        DO 300 K= KKLI,51
        DO 4 I=3,6
        R=RR(I)
          PDE(I)=0.
          PDEW(I)=0.
          HAZH=R-BF/2.
          IF(HAZH.LE.0.) GO TO 4
          KQ=0
          BG=3.0*(3.14159)*B/8.0
          IF (R.LT.BG) KQ=1
          IF (R.LT.BG) R=0.707*R
        D=DD(I)
        T=TT(I)
        SIGD=SIGDD(I)
C...    WIND RUN
        W=FLOAT(K-1)*1.688*T
C...  DEVIATION IN WIND RUN
            SIGWD=15.0*T*1.688
C...    HORIZONTAL DEVIATION
        SIGH=SQRT(2.0*SIGY*SIGY+SIGWD*SIGWD)
C...    VERTICAL DEVIATION
        SIGV=SQRT(2.0*SIGZ*SIGZ+SIGD*SIGD)
C...    CALCULATE HORIZONTAL ENCOUNTER PROBABILITY (PEH)
          CALL ERFUN(W,HAZH,SIGH,PEH)
C...    CALCULATE VERTICAL ENCOUNTER PROBABILITY (PEV)
          HAZV=SQRT(HAZH*(R+BF/2.))
          CALL ERFUN(D,HAZV,SIGV,PEV)
C...    PROBABILITY OF A HAZARDOUS ENCOUNTER (PDE)
          PDE(I)=PEH*PEV
C...   WHEN R LESS THAN BG BUT GREATER THAN BF/2, HAVE TO CONSIDER
C...            EACH VORTEX SEPARATELY
          IF (KQ.EQ.1) PDE(I)=2.0*PDE(I)
C...    PROBABILITY OF A HAZARDOUS ENCOUNTER GIVEN THE CROSS-WIND
        PDEW(I)=PDE(I)*PCW(K,KLI)
C...    PROBABILITY OF A HAZARDOUS ENCOUNTER ACCUMULATED UP
C...    TO A CROSS-WIND OF GIVEN MAGNITUDE
        PDESUM(I)=PDESUM(I)+PDEW(I)
 4      CONTINUE
 300    CONTINUE
```

FIGURE 27. CONTINUED

```
      WRITE(5,8000) (PDESUM(K),K=3,6)
 8000 FORMAT( 3X,4(1PE10.3,4X))
1500    CONTINUE
        GO TO 250
1000    CONTINUE
        GO TO 10
400     CONTINUE
        CLOSE(UNIT=5)
        STOP
      END


        SUBROUTINE DATFIL(J,IACO,BC,VC,SLOPEC,BINTC,VDO,SIGDO)
        DIMENSION IAC(12),B(12),V(12),SLOPE(12),BINT(12),VD(12),SIGD(12)
        DATA (IAC(L),  B(L),  V(L),SLOPE(L),BINT(L),VD(L),SIGD(L),
     1       L=1,12)/
        1    'B707 ', 130.9, 232.3, 5.491,  85.525, 5.22, 1.82,
        2    'B727 ', 108.0, 205.8, 5.471,  83.186, 6.55, 1.9 ,
        3    'B737 ',  93.0, 197.0, 3.424,  59.729, 6.54, 1.90,
        4    'B747 ', 195.7, 238.1, 5.963, 106.712, 6.32, 1.94,
        5    'DC-8 ', 142.3, 221.2, 4.122, 118.034, 4.88, 1.60,
        6    'DC-9 ',  93.3, 189.6, 3.746,  77.763, 6.24, 1.90,
        7    'DC-10', 165.3, 232.3, 4.712,  93.864, 7.00, 1.90,
        8    'L1011', 155.3, 241.1, 4.983,  89.051, 6.98, 1.90,
        9    'B707H', 145.8, 232.3, 4.536,  93.593, 5.52, 1.60,
        1    'DC-8H', 148.4, 210.2, 4.915,  91.254, 5.72, 1.80,
        1    'PA28 ',  30.0, 110.0, 2.908,  48.475, 4.00, 1.70,
        1    'LEAR ',  35.6, 154.0, 1.586,  66.441, 7.51, 1.90/
        IACO=IAC(J)
        BC=B(J)
        VC=V(J)
        SLOPEC=SLOPE(J)
        BINTC=BINT(J)
        VDC=VD(J)
        SIGDC=SIGD(J)
        RETURN
        END


      SUBROUTINE NDTR(X,P,D)
C     FOR X.GE.0, CALCULATES AREA UNDER NORMAL DISTRIBUTION CURVE
C     FOR X=X TO INFINITY
C     IBM STATICS PACKAGE FSS PAGE 78
      AX=ABS(X)
      T=1.0/(1.0+0.2316419*AX)
      D=0.3989423*EXP(-X*X/2.0)
      P=D*T*((((1.330274*T-1.821256)*T+1.781478)*T-0.3565638)*T
     * +0.3193815)
      RETURN
      END


        SUBROUTINE ERFUN(W,R,SIG,PE)
      EX=(W+R)/SIG
      EY=(W-R)/SIG
      CALL NDTR(EX,PEX,DEX)
      CALL NDTR(EY,PEY,DEY)
      IF(EY.LT.0.) GO TO 20
      PE=PEY-PEX
```

FIGURE 27. CONTINUED

```
      GO TO 21
 20   PE=1.0-(PEY+PEX)
21      RETURN
        END


        SUBROUTINE PWSET
        COMMCN/PCWIND/PCW(51,2)
        DATA A,B,EMU/12.5,5.5,18.6/
        SIG=SQRT(2./3.1415926535)*EMU
        TSIG2=SIG*SIG*2.
        B2=B*B
        ACB=A/B
        EMUI=1./EMU
        SUM=0.
        DO 2 I=1,51
        WC=I-1
        WC2=WC*WC
        EXX=EXP(-WC2/TSIG2)
        PCW(I,1)=EMUI*EXX
        Q=0.5
        IF(I.GT.6) GO TO 3
        EPS=ACB*SQRT(B2-WC2)
        CALL NDTR(EPS/SIG,Q,DUM)
3       PCW(I,2)=Q*EXX
        SUM=SUM+PCW(I,2)
2       CONTINUE
        DO 4 I=1,51
        PCW(I,2)=PCW(I,2)/SUM
4       CONTINUE
        RETURN
        END
```

FIGURE 27. CONCLUDED

APPENDIX E
SENSITIVITY ANALYSIS

In the following analyses, the calculations were done by positioning two aircraft (B-747 and DC-9) at a 3-nautical-mile separation. In addition, the following aircraft, the DC-9, was assumed to be over the OM as the probability of a vortex encounter is largest at the OM location. VAS-green conditions are assumed, and all probabilities are referenced to the baseline value N. The B-747/DC-9 pair was used as it gives the largest probabilities for the airliners.

The key variable in the conservative safety analysis is the factor f, the fraction of the roll-control authority needed to counter the swirling velocities of a vortex. In Section 4.1.2, it was argued that any value between 0.5 and 0.756 could have been selected, but one-half of 0.756 was used to be conservative. It is instructive to determine the value of f at which N, the baseline probability, is exceeded for a jetliner following another jetliner. The probability of a vortex hazard exceeds N in VAS-green conditions for a DC-9 3 nautical miles behind a B-747 only with an f less than 0.32.

The flight speed enters into the strength and hence the decay rate of the vortices shed by the lead or vortex-generating aircraft, and parameterizes the roll-rate capability of the following or vortex-encountering aircraft. Figure 28 shows how the probability of a vortex hazard (in units of N) varies with the flight speeds for the DC-9 following the B-747 at 3-nautical-mile spacings in the vicinity of the OM. The two curves were obtained by using the nominal values of all the parameters and varying just the landing speed of the B-747 to get the curve labeled B-747, or the landing speed of the DC-9 to get the curve labeled DC-9. The B-747 would need to be traveling at an inordinately high approach speed to increase the probability to N. The DC-9 would need to be flying about 10 knots less than the typical landing speed (close to stall

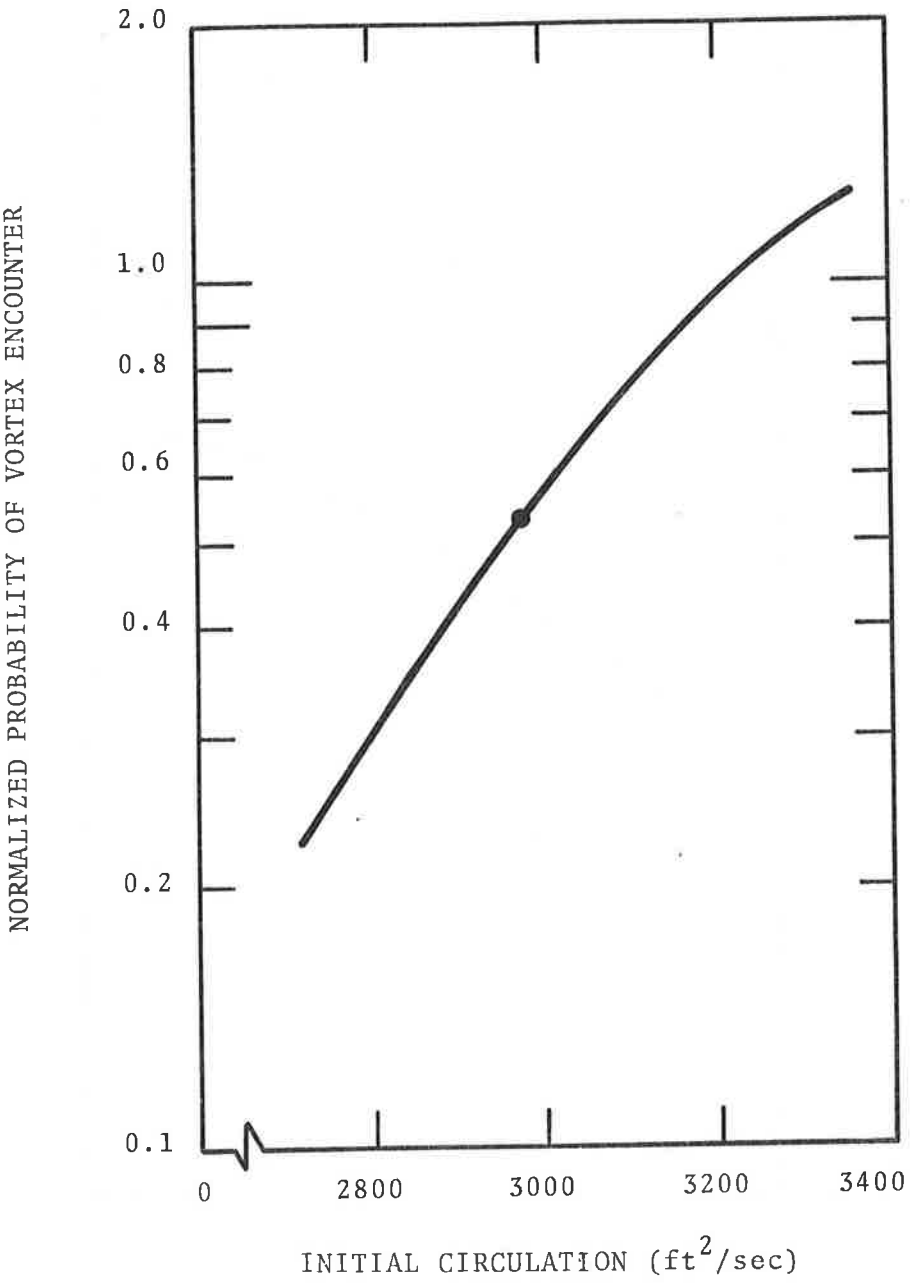

FIGURE 31. NORMALIZED PROBABILITY OF A VORTEX ENCOUNTER FOR A DC-9 THREE NAUTICAL MILES BEHIND A B-747 DURING VAS-GREEN CONDITIONS AS A FUNCTION OF THE INITIAL CIRCULATION OR STRENGTH OF THE B-747 VORTICES. The solid dot indicates the nominal value of the initial circulation.

APPENDIX F

CONFIRMATION TESTS

To verify the results of the probability analysis, a laser-Doppler velocimeter (LDV) is being used to monitor both the vortices shed by landing aircraft and the winds aloft. The vortex-descent/translation/decay models and the cross-wind aloft model are to be confirmed.

F.1 LASER-DOPPLER VELOCIMETER

There are only two practical methods for tracking vortices which are between 200 and 1000 feet above the ground: the phototheodolite tracking of smoke-marked vortices, and the use of an LDV. The former technique would involve dedicated aircraft; only those aircraft made available to the program could be investigated, and tracking would cease when the smoke detrained (not necessarily at the death of a vortex). There are technique variants, such as: using cameras with telephoto lenses, using markers other than smoke (chaff or snow would permit vortex-tracking with a microwave radar), using a tall tower to disperse the smoke, etc. An LDV, on the other hand, can be deployed at an airport on a noninterfering basis, and thus, yield data on various aircraft under operational conditions.

An LDV measures the Doppler spectrum of laser radiation back-scattered by atmospheric aerosols. The instrument incorporates means to transmit the laser radiation to the region of interest, to collect the radiation scattered from the aerosols, and to photomix on a photodetector the scattered radiation and a portion of the transmitted beam. A difference-frequency component, at the Doppler-shift frequency, is generated at the photo detector, and is translatable into an along-optic-axis wind-velocity component. For a CO_2 laser operating at a wavelength of 10.6 microns, a Doppler shift of 97.1 kHz corresponds to a 1-knot line-of-sight velocity. Details of the operation of an LDV system may be found in Ref. 27-29.

Figure 32 shows the mobile FAA/TSC LDV housed in a 24-foot, 2-1/2-ton, detachable-body truck. The system is deployed under the approach to runway 14R at Chicago's O'Hare International Airport. Initially, the LDV was deployed under the approach to runway 27R, but the lack of traffic, in particular the lack of B-747s, prompted moving the system to 14R during April 1978. The data collection and relevant analyses are described in Volume II of this report.

In the vortex mode, the LDV is used to measure the velocity field of the vortices by scanning the laser beam through various ranges and elevation angles. Doppler spectra are processed by a minicomputer system in the van; the largest Doppler shift (and hence, the largest velocity) is interpreted as the maximum vortex tangential velocity (the velocity at the core radius, v_T of equation (3)). The vortices are tracked by following the location of the largest Doppler shifts, one from each side of the vortex center. Vortex strength is calculated using the velocity field (the method is similar to that used in the MAVSS; see equation (51) in Appendix A).

In the wind mode, the LDV beam is focused at a range of interest, and scanned 360 degrees in azimuth while holding the angle from the zenith constant (typically 30 degrees). If the horizontal wind remains constant during the time of a complete rotation (approximately 2 seconds), the line-of-sight Doppler-velocity component will be a sine wave whose amplitude is a measure of the horizontal wind magnitude, whose phase is a measure of the wind, and whose average value is a measure of the vertical speed. By refocusing the LDV to a series of heights, a profile of the three wind components can be mapped.

F.2 ABBREVIATED TEST PLAN

Since the VAS equipment is in place at O'Hare, it permits correlation of high altitude (200 to 1000 feet above ground level) vortex behavior with VAS outputs. It is important to collect enough runs for the data to be statistically significant, and to experience various meteorological conditions.

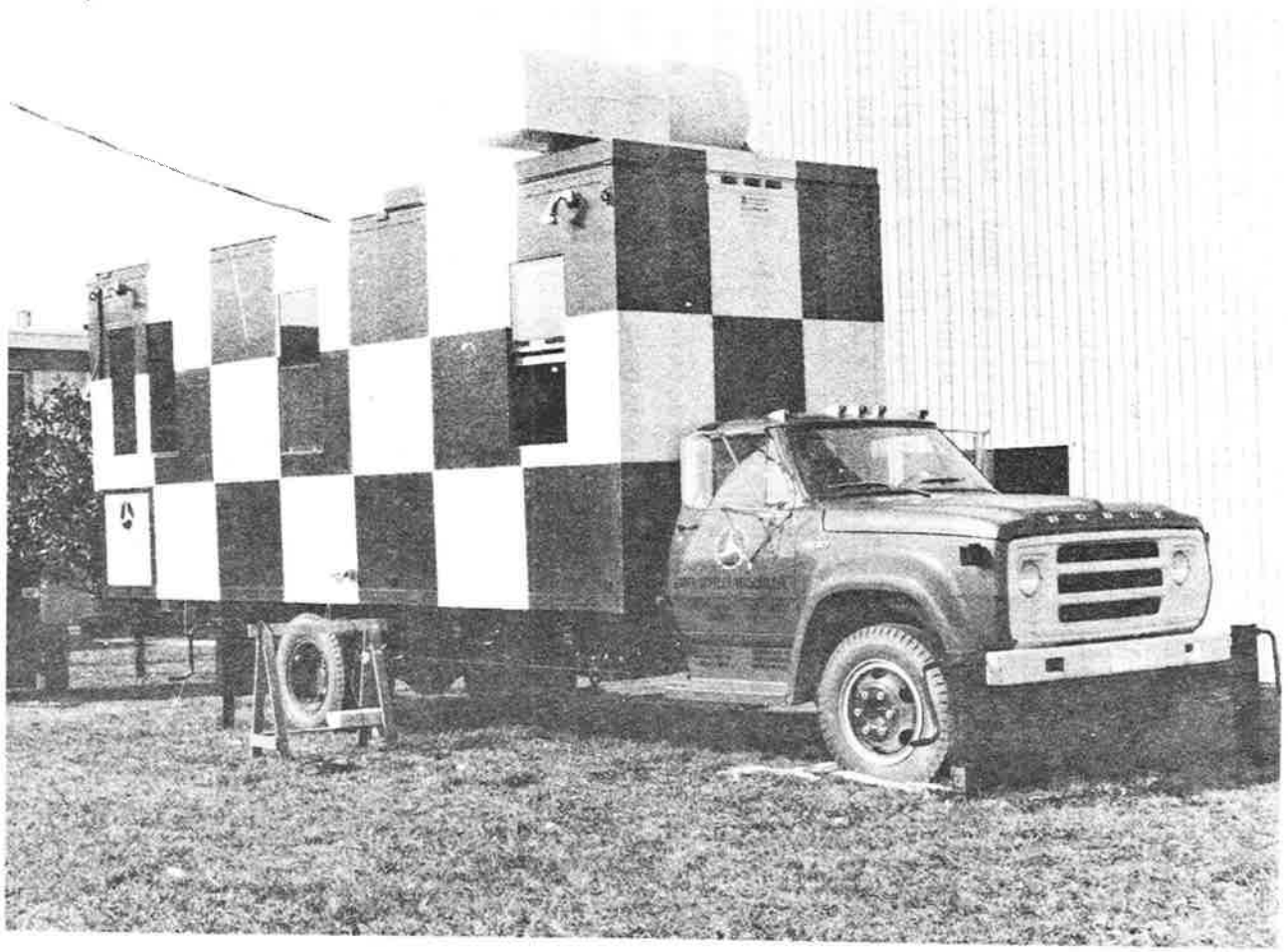

FIGURE 32. FAA/TSC MOBILE LASER-DOPPLER VELOCIMETER

The ambient wind conditions as measured by the VAS are being recorded for correlation purposes. It is expected that the conditions which indicate that reduced separations may be used (green-light conditions) are the same conditions which lead either to the quick demise of vortices aloft or to the rapid translation of vortices out of the landing corridor. Anomalous vortex behavior, if it occurs, is expected only when the VAS indicates vortex-based separations should be used (red-light conditions).

Aircraft altitude above the LDV van is being measured to determine the initial altitude of the vortices and, hence, to allow the measurement of the vortex-descent distance. A theodolite emplaced near the runway threshold, and pointed up the glide slope, is being used to measure the azimuth and elevation of the aircraft as they pass over the LDV.

To characterize the atmosphere, an acoustic sounder and a pyranograph have been deployed at O'Hare. The acoustic sounder monitors the heights of atmosphere structure fluctuations and inversion layers. The pyranograph monitors the cloud cover by measuring the solar and sky insolation; knowing the cloud cover allows an assessment of the atmospheric stability.

All the data are being compiled in a data base for analysis. For each flyby the following information is obtained: aircraft type, VAS tape and run number, LDV tape and run number, aircraft lateral position and height with respect to the LDV system, time code, VAS-averaged winds near runway threshold, VAS status (red or green light), winds aloft measured by LDV (when available), inversion height(s) (if present), pyranograph output, general weather conditions (precipitation, gustiness, etc.), position and age of each vortex detected by the LDV, strength (when possible) of the vortices, and (when known) type of operation (IFR, VFR, or visual approach).

Studies will be undertaken to identify the statistically significant correlations among the vortex behavior, ambient meteorological conditions, and VAS outputs. In particular, the

measured vortex translation, descent and decay will be compared with the respective model adopted in Section 4. If the data indicate that any of the models must be modified, the encounter probabilities will be recalculated and the consequences (if any) delineated.

The winds aloft are also measured by the LDV and compared with the VAS-measured winds. The comparison is required to verify the cross-wind model developed in Appendix C. A data base is being compiled consisting of: time code, VAS-averaged winds near the appropriate runway threshold, VAS status (red or green light), and averaged winds at various altitudes above the LDV. Cross-wind models will be derived from the data for the "no-VAS" and the "VAS-green" situations, and compared with the models in Appendix C (equations (52) and (57), respectively). If the validity of the models in Appendix C cannot be substantiated, the probability analysis will be revised using the LDV-obtained models.

APPENDIX G
REFERENCES

1. Gupta, V.P., "Vortex-related Accidents over the Ten-Year Period 1964-73," FAA-EM-75-6, Apr. 1975, Mitre Corp., McLean, VA.
2. Hallock, J.N. and Eberle, W.R. (editors), "Aircraft Wake Vortices: A State-of-the-Art Review of the United States R&D Program," FAA-RD-77-23, Feb. 1977, DOT/Transportation Systems Center, Cambridge, MA.
3. Israel, D.R., "An Overview of the Upgraded Third Generation Air Traffic Control System," EASCON-1974 Record, Oct. 1974, p. 244-249.
4. Hallock, J.N. and Wood, W.D., "Joint US/UK Vortex Tracking Program at Heathrow International Airport, Vol. I: Executive Summary," FAA-RD-76-58.I, Mar. 1976, DOT/ Transportation Systems Center, Cambridge, MA.
5. Hallock, J.N., Winston, B.P., Burnham, D.C., Sullivan, T.E., McWilliams, I.G., and Wood, W.D., "Joint US/UK Vortex Tracking Program at Heathrow International Airport, Vol. II: Data Analysis," FAA-RD-76-58.II, Sep. 1976, DOT/ Transportation Systems Center, Cambridge, MA.
6. Goldstone, L., "An Investigation into Wake Turbulence Incidents," CAA DTRD/7301, Nov. 1973, Civil Aviation Authority, London, England.
7. St. John, O.B., "Collection of Operational Data on Wake Vortex Incidents in the UK," In: Proceedings of Aircraft Wake Vortices Conference, FAA-RD-77-68, June 1977, DOT/ Transportation Systems Center, Cambridge, MA.
8. Piggot, B.A.M. and Pask, J.A., "Wake Vortex Incidents Reported in the UK 1972-1976," CAA Paper 77012, June 1977, Civil Aviation Authority, London, England.

27. Huffaker, R.M., Jeffreys, H.B., Weaver, E.A., Bilbro, J.W., Craig, G.D., George, R.W., Gleason, E.H., Marrero, P.J., Reinbolt, E.J., and Shirey, J.E., "Development of a Laser Doppler System for the Detection, Tracking, and Measurement of Aircraft Wake Vortices," FAA-RD-74-213, Mar. 1975, NASA Marshall Space Flight Center, Huntsville, AL.
28. Bilbro, J.W., Jeffreys, H.B., Weaver, E. A., Huffaker, R.M., Craig, G.D., George, R.W., and Marrero, P.J., "Laser Doppler Velocimeter Wake Vortex Tests," FAA-RD-76-11, Mar. 1976, NASA Marshall Space Flight Center, Huntsville, AL.
29. Brashears, M.R., Lawrence, T.R., and Zalay, A.D., "Mobile Laser Doppler System Checkout and Calibration," FAA-RD-77-48, I and II, June 1977, Lockheed Missiles and Space Company, Huntsville, AL.
30. Tombach, I.H., Bate, E.R., and MacCready, P.B., "Investigation of the Motion and Decay of the Vortex Wake of a Light, Twin-Engine Aircraft," AV-FR-439, Oct. 1974, AeroVironment Inc., Pasadena, CA.
31. Crawford, K.C. and Hudson, H.R., "Behavior of Winds in the Lowest 1500 Feet in Central Oklahoma: June 1966-May 1967," ESSA Tech. Memo ERLTM-NSSL-48, Aug. 1970, National Severe Storms Lab., Norman, OK.
32. Stability and Control Group, "Estimated Stability and Control Characteristics Model DC-9-30 Jet Transport," LB-32323, Dec. 1966 (revised Oct. 1968), Douglas Aircraft Company, Long Beach, CA.
33. Paulson, J.W., Jr., "Wind-Tunnel Results of the Aerodynamic Characteristics of a 1/8-Scale Model of a Twin-Engine Short-Haul Transport," NASA TM X-74011, Apr. 1977, Langley Research Center, Hampton, VA.
34. Maxworthy, T., "The Motion of Aircraft Trailing Vortices," Paper 75-APMW-58, Am. Soc. Mech. Engineers, Appl. Mech. Western Conf., Honolulu, HI, Mar. 1975.
35. Tombach, I.H., "Influence of Meteorological Factors on the Vortex Wake of a Light, Twin-Engine Aircraft," AV FR-416, Mar. 1974, AeroVironment Inc., Pasadena, CA.

36. Lissaman, P.B.S., Crow, S.C., MacCready, P.B., Tombach, I.H., and Bate, E.R., "Aircraft Vortex Wake Descent and Decay Under Real Atmospheric Effects," FAA-RD-73-120, Oct. 1973, AeroVironment Inc., Pasadena, CA.
37. Falls, L.W. and Brown, S.C., "Optimum Runway Orientation Relative to Crosswinds," NASA TN D-6930, Sep. 1972, Marshall Space Flight Center, Huntsville, AL.
38. Harris, R.M., "A Model for the Estimation of Aloft Crosswind Probability Densities on Final Approach," WP-13001, Feb. 1978, Mitre Corp., McLean, VA.

300 copies